

OPTIMIZATION OF MACROSTRUCTURE IN ALUMINIUM FOAMS

A THESIS SUBMITTED TO
THE GRADUATE SCHOOL OF NATURAL AND APPLIED SCIENCES
OF
THE MIDDLE EAST TECHNICAL UNIVERSITY

BY

SERDAR TAN

IN PARTIAL FULFILLMENT OF THE REQUIREMENTS FOR THE DEGREE OF
MASTER OF SCIENCE
IN
THE DEPARTMENT OF METALLURGICAL AND MATERIALS ENGINEERING

SEPTEMBER 2003

Approval of the Graduate School of Natural and Applied Sciences

Prof. Dr. Canan ÖZGEN
Director

I certify that this thesis satisfies all the requirements as a thesis for the degree of Master of Science.

Prof. Dr. Bilgehan Ögel
Head of Department

This is to certify that we have read this thesis and that in our opinion it is fully adequate, in scope and quality, as a thesis for the degree of Master of Science.

Prof.Dr. Tayfur Öztürk
Supervisor

Examining Committee Members

Prof. Dr. Şakir Bor

Prof.Dr.İshak Karakaya

Prof.Dr.Tayfur Öztürk

Prof.Dr. Teoman Tinçer

Assoc.Prof.Dr.Ali Kalkanlı

ABSTRACT

OPTIMIZATION OF MACROSTRUCTURE IN ALUMINIUM FOAMS

Tan, Serdar

M.S., Department of Metallurgical and Materials Engineering

Supervisor: Prof. Dr. Tayfur Öztürk

September 2003, 105 pages

Pure aluminium and aluminium-5wt % TiO₂ aluminium foams were produced by powder metallurgy technique with the use of TiH₂ as foaming agent. Two sizes of TiH₂ were used: 20µm and 3µm.

It has been confirmed that high level of compaction is the primary requirement in foaming. It was shown that hot swaging could be used as a method of compaction for foaming as it leads to values close to full density. Pure aluminium foamed at 675°C and 725°C leads to a volume expansion between 90-180 %.

A model was developed for pure aluminium to explain the pore initiation and the resultant pore size. The model predicts a critical particle size for TiH₂ below which bubbles could not form. The size appears to be in the neighborhood of 30µm for 675°C and 6µm for 725°C and is temperature dependent. Equilibrium pore size appears to be a function of TiH₂ particle size and not affected significantly by the temperature of foaming. It has also been shown that depth effect, i.e. hydrostatic pressure of liquid metal, is unimportant in foaming process and can be neglected.

According to the model, to produce pores of fine sizes, two requirements must be met: use of fine foaming agent and the use of high foaming temperature.

Al-5 wt % TiO₂ was foamed at 750°C and 800°C, i.e. at temperatures that yield viscosities similar to pure aluminium. The structure of foamed metal and level of foaming, 120-160%, was similar to pure aluminium. Unlike pure aluminium, internal reactions are dominant feature of TiO₂ stabilized systems. Solid content of the system increases as a result of internal reactions between Al-Ti and Al- TiO₂. When this change occurs, however, is not known. It is possible that the viscosity of the system may be four times of its original value.

Keywords: Aluminium foam, hot swaging, milling of TiH₂, foam stabilization, critical particle size, equilibrium pore size, TiO₂, Al-Ti intermetallics.

ÖZ

ALUMİNYUM KÖPÜKLERİN MAKROYAPISININ OPTİMİZASYONU

Tan, Serdar

Y.Lisans., Metalurji ve Malzeme Mühendisliği Bölümü

Tez Yöneticisi: Prof. Dr. Tayfur Öztürk

Eylül 2003, 105 sayfa

Köpük oluşumu, Al ve Al- % 5 TiO₂ sistemlerinde incelenmiştir. Bu amaçla toz metalurji yöntemi kullanılmış ve köpürtücü madde olarak TiH₂ ilave edilmiştir. TiH₂ % 0.6 oranında 20 µm ve 3 µm olmak üzere iki farklı boyutta kullanılmıştır. Yapılan çalışma, köpürmede sıkıştırma düzeyinin birinci derecede önemli olduğunu ve bu çalışmada kullanılan sıcak tokaçlama (400°C) yöntemi ile teorik yoğunluğa yakın değerlerin elde edilebileceğini göstermiştir. Sistemler için benzer akışkanlık değerleri hedeflenmiş ve bu amaçla saf alüminyum 675 ve 725°C , Al- %5 TiO₂ 750 ve 800°C sıcaklıklarında köpürtülmüşlerdir. Yapılan deneyler sonucunda, %180 miktarında köpürmenin mümkün olduğu gözlemlenmiştir. Al- %5 TiO₂ sisteminde katı miktarının Al-Ti ve Al-TiO₂ arasında gerçekleşen tepkimeler sonucu arttığı tespit edilmiştir.

Metal köpüklerde gözenek oluşumunu ve gözenek büyüklüğünü inceleyen bir model geliştirilmiştir. Saf alüminyum için geliştirilen model, yüzey gerilimi nedeniyle belirli boyuttan küçük TiH₂ tozlarının gözenek oluşturamayacağını öngörmektedir. 675°C ve 725°C için kritik TiH₂ büyüklüklerinin 30 µm ve 6 µm olduğu belirlenmiştir. TiH₂ boyutunun gözenek büyüklüğünü belirleyen en önemli değişken olduğu bulunmuştur. Geliştirilen model, büyüklüğü 16-50µm arasında olan TiH₂

tozlarının kullanılması ile alüminyum içerisinde 1-4 mm boyutunda gözenekler elde edilmesi gerektiğini göstermektedir. Model küçük boyutta gözenek elde edilebilmesi için ince TiH_2 tozlarının kullanılmasının ve yüksek sıcaklıklarda köpürtme yapılmasının gerekli olduğunu göstermiştir.

Anahtar Kelimeler :Alüminyum köpükler, sıcak tokaçlama, TiO_2 , Al-Ti ara bileşikleri, kritik toz boyutu, gözenek büyüklüğü.

To My Family

ACKNOWLEDGEMENTS

I gratefully thank to Prof.Dr.Tayfur Öztürk who has given advice and support throughout the entire period of the study and guidance, corrections, clarifications.

Thanks go to Prof. Dr. Vedat Akdeniz, Prof. Dr. Bilgehan Ögel, Assoc. Prof. Dr. Ali Kalkanlı and Prof. Dr. Nesrin Hasırcı for permitting the use of facilities of their laboratories.

Help of the staff of Metallurgical and Materials Engineering Department is gratefully acknowledged.

I also thank to members of Composite Materials Laboratory, especially to Ceylan Kubilay for his assistance in swaging and density measurements.

I am truly indebted to my family for their continuous patience and support. Finally, my special thanks go to Semra Can for her love, sincere help and incitement.

TABLE OF CONTENTS

ABSTRACT	iii
ÖZ	v
DEDICATION	vii
ACKNOWLEDGEMENTS	viii
TABLE OF CONTENTS	ix

CHAPTER

I.INTRODUCTION	1
II.LITERATURE REWIEV	2
2.1. Introduction	2
2.2. Foaming Processes for Aluminium	3
2.2.1. Liquid Based Foaming Techniques	4
2.2.2. Replication Techniques	9
2.2.3. Powder Metallurgy (P/M) Based Foaming Process.....	11
2.2.3.1. Process Variables in P/M Technique	13
2.2.3.2.Characteristic Properties of Al Foams Produced by P/M Technique.....	19
2.3. Fundamental Parameters in Foaming	21
2.3.1. Viscosity	22
2.3.2. Stability of Gas Bubbles in a Liquid	25
2.3.3. Surface Tension	27
2.4. Stability of Components in Al Foaming	30
2.4.1. Decomposition of TiH_2	30

2.4.2. Al-H System	33
2.4.3. Al-Ti System	38
III. EXPERIMENTAL PROCEDURE	41
3.1. Materials	41
3.2. Milling of TiH ₂	41
3.3. Mixing of Powders	45
3.4. Consolidation of Powder Mixtures	45
3.5. Foaming of Compact Systems	46
3.6. Sample Characterization	48
IV. RESULTS AND DISCUSSION.....	50
4.1. Foaming Systems	50
4.2. Characterization of Swaged Powder Compacts	50
4.3. Foaming of Pure Aluminium.....	54
4.4. A Model for Foaming of Pure Aluminium	66
4.4.1. Pore Initiation / Critical Particle Size of Foaming Agent.....	67
4.4.2. Equilibrium Pore Size.....	70
4.4.3. Comparison with Experiments.....	70
4.5. Foaming of TiO ₂ Stabilized System	76
V. CONCLUSION	87
REFERENCES	89
APPENDICES	
A. Foaming of Aluminium with and without TiO ₂ Addition	95
B. Milling and Sedimental Sieving of TiH ₂ Powders	101

CHAPTER I

INTRODUCTION

Metal foams are in the scope of the industry in last ten years. The unique combination of mechanical and physical properties makes them attractive materials for engineering applications. Low density and good mechanical properties make the aluminium primary metal to be foamed.

Liquid and powder metallurgy techniques are used to foam various aluminium systems. Although these techniques yield high amounts of foaming, they could result some foaming inhomogeneities, such as pore coalescence and liquid drainage. For this reason, processes should be improved in terms of macrostructure. As commonly mentioned in the literature, uniform macrostructure with maximum amount of foaming is the primary goal of the foaming processes.

Studies carried out in recent years indicated that properties of aluminium foams depend to a large extent on the macrostructure, i.e. amount, size, shape and distribution of the pores in the foamed matrix. It is also shown that the properties of the aluminium foams are improved if pores are small in size. However, there is no study to obtain foams with small sized pores.

In the present work, processing conditions to obtain aluminium foam with small size pores by powder metallurgy technique is investigated. A model is presented to explain the bubble formation and final pore size.

CHAPTER II

LITERATURE REVIEW

2.1. INTRODUCTION

Metallic foams are in the perspective of industry in the last 40 years. Today, many engineering problems are solved by using some cellular materials with their unique combination of properties. According to Davies et al. (1983), metallic foams can be defined as metallic cellular materials that have high porosity fraction, typically ranging from 40 % to 98 %.

Depending on the required property, material selection becomes important for foaming systems. Most commonly used metal for foaming is Al. Low density of Al with combination of its mechanical properties makes it an attractive material for structural applications. Apart from Al, there are studies concerning a variety of systems: Mg (Yamada et al., 2000), Zn (Thornton et al., 1975), Ti (Bram et al., 2000), Cu (Simone et al., 1997) and Steel (Park et al., 2001).

According to Yu et al. (1998), certain properties should be identified to define metallic foams. Determination of the cellular structure, i.e. being open cell or closed cell is the first crucial step. In an open cell structure, the pores are interconnected with each other whereas in closed cell foams, the cells are disconnected, that is separated by the matrix metal walls. For a specific production method and chemical composition, the parameters to define the cellular structure are density of foam, cell shape and their distribution. Foam cannot be identified without indicating these parameters.

Applications of the metallic foams are strongly property dependent (Degischer, 2002). While considering a specific application, a clear distinction should be drawn between open cell and closed cell metal foams. Closed cell Al foam production is primarily focused by researchers, especially for structural applications, due to its combination of low density and stiffness. These include various components designed to absorb energy under relatively low compressive loads. In the metallic foams, compressive deformation involves a plateau region after yielding at constant stress, followed by an increase resistance to further deformation (Banhart et al., 1999). According to Gibson and Ashby (1997), the relative foam density has the greatest influence on the mechanical properties. Moreover, cellular metals have good energy absorbing capacity because of the extensive plateau regime (Fuganti et al., 2000). On the other hand, Degischer (2002) states that in the existence of tensile forces, such as bending, metal foams tend to fracture readily. He also indicates that this problem can be overcome by reducing cell size, preferably to sub-mm levels. Al with low density is the primary metal to be foamed to use in the crush box and chassis.

Open cell foams are used in filters, catalyst supports (Swars, 1987), heat exchangers (Frischmann, 1995), fluid flow damping parts such as shock wave dissipation devices (Eisenmann, 1998), biomedical prostheses (Bende et al., 1992), air batteries, protective permeable membranes. Such functional components have higher benefit than those in purely structural applications as well as having higher costs. The most important characteristic of the open cell foams is the cell size, of which required value alters with the application.

2.2. FOAMING PROCESSES FOR ALUMINIUM

From the historical point of view, melting of the matrix metal was the primary importance and for this reason, the first examples of foaming were related with low melting point metals such as Al, Pb, and Mg etc. Apart from this, low density and acceptable mechanical properties made the Al systems dominant metal as the matrix material in the foaming for research as well as commercialized products.

The first attempt to foam Al was performed by Sosnik (1948) in 1943. In order to produce pores he added mercury to molten Al. In 1956, Elliot (1956) replaced the mercury by foaming agents generating gas by thermal decomposition. Since then, many processes developed for Al to obtain the required cellular structure that meets the requirements of the applications. Products of different techniques show that the architecture of the cellular structure is the result of the processing technique and material type.

Variety of Al foam production methods are given in the literature. Some of these methods were commercialized and some are still under investigation. Each production method covers a characteristic range of properties, such as density, pore size and shape, pore size distribution, product shape and size, having open pore or closed pore structure etc.

Despite the variety of techniques, there are only two strategies to generate porosity: self-formation or pre-design. Methods where the porosity is generated by gas bubbles are self-forming. In the self-formation, the porosity forms in a self-evaluation process according to physical principles. The cell structure has stochastic nature, i.e. it is not predictable within a spatial framework. In the case of pre-design techniques, the resulting structure is determined by cell forming mould, or a space holder material.

2.2.1. Liquid Based Foaming Techniques

Liquid based foaming techniques involve direct foaming of liquid metal. It should be noted that almost all techniques in this category were developed by companies; such as Alcan Corporation, Cymat Aluminium Corporation etc. The techniques differ from one another according to pore generation method.

Schematic illustration of the Al foaming by gas injection is given in Fig. 2.1 (Banhart, 2001). The technique allows production of large quantities of Al foam. Although different companies use the method, the resultant Al foam has different macrostructural properties, such as cell size, so they are commercialized with different names.

As reported by Körner (2000), starting material is Al (wrought or cast) +10-30 vol. % SiC or Al₂O₃ particles. The starting material is melted with conventional foundry equipment and transferred to a tundish where gas, typically air, is injected via small nozzles incorporated into a rotating impeller that forms a dispersion of small gas bubbles. The resultant viscous mixture of bubbles and metal float up to the surface of the liquid. This can be pulled off by a conveyor belt and is then allowed to cool down and solidify. The resultant structure is a MMC matrix with surface skin and closed pores. Fig. 2.2 shows the structure of the Cymat foam.

Information supplied by Cymat (Cymat, 2002) indicates that that density of the foams obtained by this method ranges 0.05-0.55 g/cm³. The average cell size is inversely related with the density and in the range of 3-25 mm. The density of the foam can be altered by adjusting the gas flow, the impeller speed, nozzle vibration frequency and other parameters. The resulting foam is in the shape of flat panel with close outer skin and thickness of typically 10 cm.

Banhart (2000) indicates the advantages of direct foaming process as the capability of continuous production of large volume of foam and achievement of low densities for Metal Matrix Composite (MMC) foams. On the other hand, it is mentioned that necessity of cutting the foam panel for applications opens some cells that is a disadvantageous point. Moreover, natural consequence of gravitational induced drainage causes a gradient in density, pore size and pore elongation. Apart from this, shearing forces applied by conveyor belt lead to diagonally distorted cells in the final product. At last, high amount of ceramic particles can make machining of MMC foams difficult.

Leitlmeier et al. (2002) described new Al foam, so-called METCOMB, which is obtained Al foams in melt state. They proposed this process to obtain a net -shape product with uniform pore structure in an economical way.

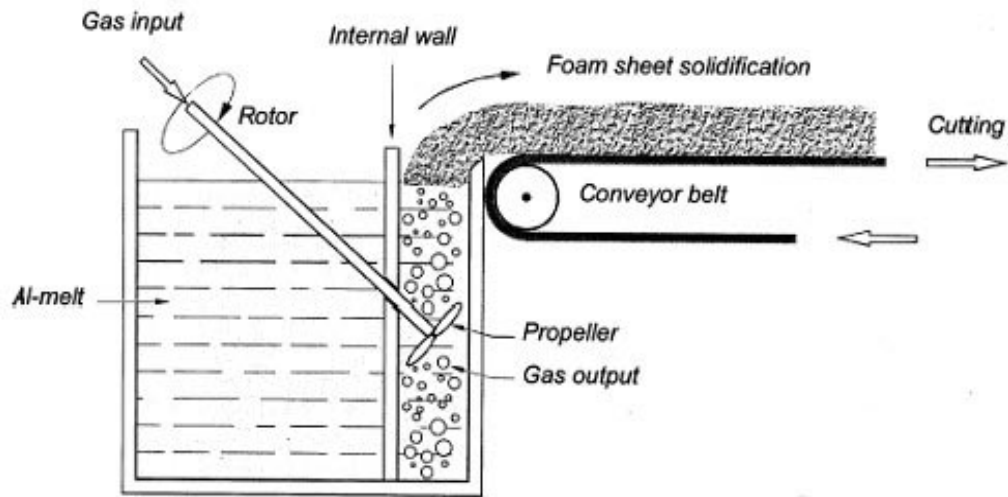


Figure 2.1. Schematic illustration of Al foaming by gas injection (Banhart, 2001)



Figure 2.2. Structure of Cymat foams produced by gas injection method (Banhart, 2001 and Körner et al. 2000)

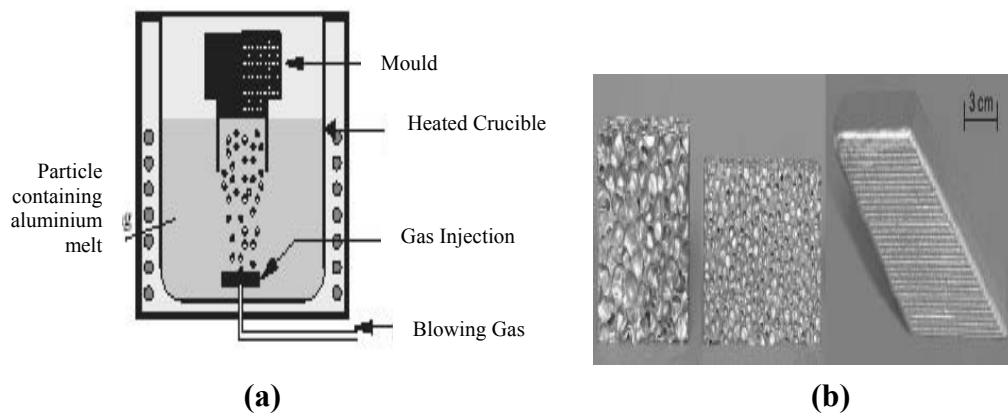


Figure 2.3. Schematic illustration of METCOMB Al foaming (a) ; and image of a product in (b) (Leitmeier, 2002)

The schematic drawing of the Al foaming by this process is given in Fig. 2.3(a). In this process, SiC or Al₂O₃ particles are distributed into Al at 700°C. Gas bubbles are formed by injecting a gas into the system and the bubbles float to surface and entrapped into the mould of required shape. The mould temperature is adjusted to allow fast cooling of the foam. It is mentioned that the bubble traveling distance, type of the foaming gas and amount of stabilizing agent are important in process variables. Near net shape products with densities down to 0.25 g/cm³ and average pore size of 5 mm can be obtained by this route.

In-situ gas generation methods are commonly applied in Al foam production with the addition of a suitable foaming agent, commonly a metal hydride: TiH₂. Decomposition of this hydride above 450°C generates hydrogen and released hydrogen forms distributed pores in the metal matrix.

Schematic illustration of the Al foaming by Shinko Wire process is given in Fig. 2.4 (Miyoshi, 2000). The resultant foam is commercialized with a trade name: Alporas Foam. To adjust the Al viscosity, 1.5 wt % Ca is added into the Al at 680°C and stirred 6 minutes in an ambient atmosphere. The addition of pure Ca and subsequent agitation facilitates the oxidation process and formation of oxides such as CaO, Al₂O₃ and CaAl₂O₄. This thickened Al is poured into a mould and 1.6 wt % TiH₂ is added as foaming agent into the molten state. Vigorous stirring and subsequent formation of H₂ by decomposition of TiH₂ causes foaming of the metal. The foamed metal is then cooled by fans. The resultant foam is a block 450 mm wide, 2050 mm long and 650 mm high. The foam has closed cell architecture. The density is 0.18 - 0.24 g/cm³ with the mean cell size of 4.5 mm and pore sizes between 1-7 mm. Fig. 2.5 shows macrostructure of Alporas foam given by Haydn (2002). The most important advantage of this process is its regular cell microstructure.

Schematic illustration of the liquid Al foaming by FORMGRIP process is given in Fig. 2.6 (Gergely, 2000). In the first stage, a pre-treated foaming agent TiH₂ is mixed with Al-12 wt % Si prealloyed powder (~150 µm) in the weight ratio 1:4.

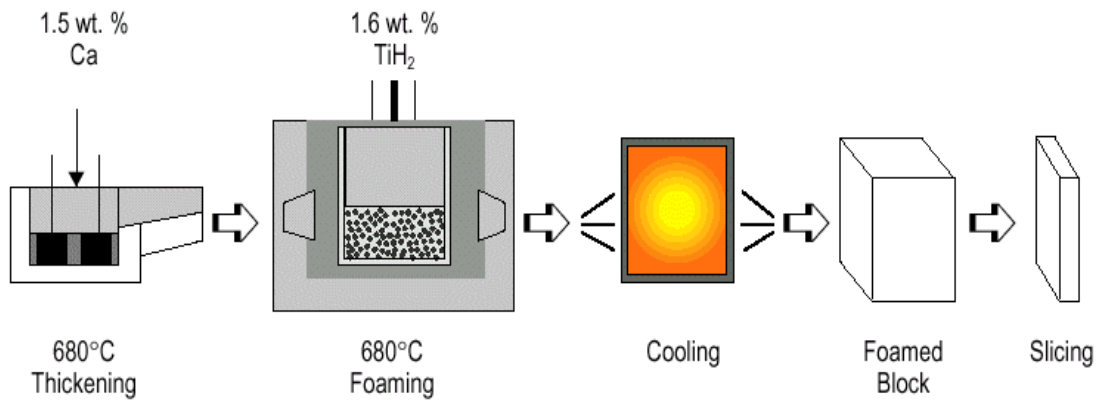


Figure 2.4. Schematic illustration of the Al foaming by Shinko Wire process (Miyoshi, 2000)

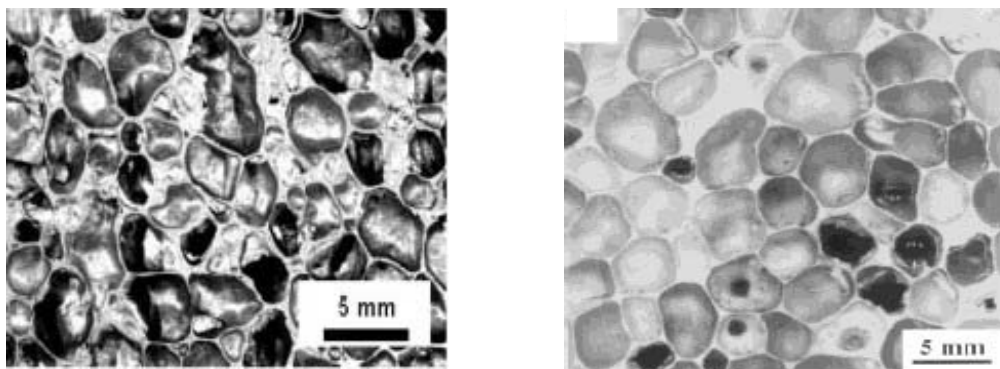


Figure 2.5. Macrostructure of Alporas foam (Haydn, 2002)

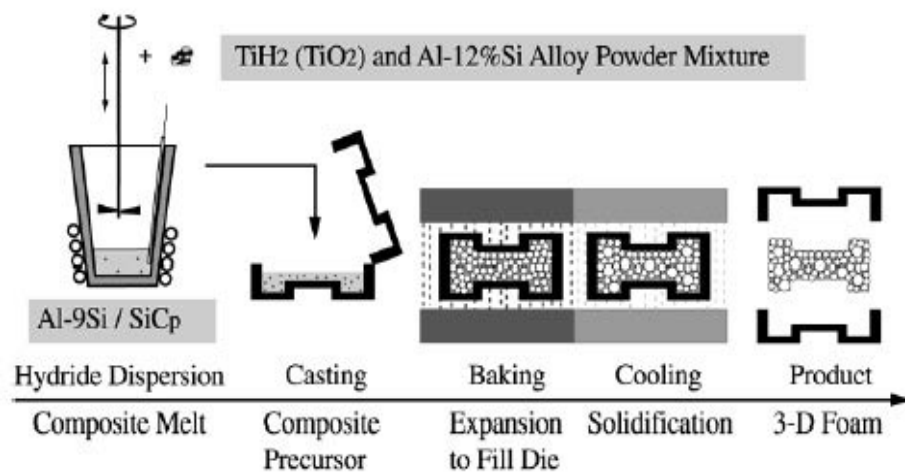


Figure 2.6. Schematic illustration of the Al foaming by FORMGRIP process (Gergely, 2000)

Then, this powder mixture is dispersed into Al- 9 wt % Si- 20 vol. % SiC melt that is at 620°C. Conventional stirring is applied at 1200 rpm for 1 minute. The mixture is poured into a mould and cooled to prevent TiH₂ decomposition. This resultant precursor has already exhibits a porosity of 14-24 % .In the second stage, the precursor is heated above the solidus temperature (675°C-725°C) and hydrogen is evolved in the structure producing a foamed structure. TiH₂ used in this process are pretreated in two steps: 400°C for 24 hours in air and then 500°C for 1 hour in air. This built up a TiO₂ barrier on the hydride, which retards the hydride dissociation. The effect of thermal treatment on the TiH₂ can be seen in Fig. 2.7. It shows that hydrogen evolution can be retarded up to 550°C in the case of applied treatment. Pore sizes of 0.8-2.4 mm and 58 % - 89 % porosity can be obtained. Fig. 2.8 shows examples of foam produced by FORMGRIP process. Degischer (2002) states that, in terms of product shape and structure control FORMGRIP is superior to Shinko Wire process. On the other hand, the economics of the process is inferior due to several process steps.

Melt routes are also suitable for using scraps of Al directly as matrix material. As Simone et al. (1998) states that these routes are very attractive since the approach allows economic handling of large quantities of materials.

2.2.2. Replication Techniques

These techniques do not involve expansion of Al, but instead they produce foams with predetermined shapes. Thus, they are grouped into pre-design strategies and produce open cell sponges of Al. The technique was first developed by ERG Inc. and named as DUOCEL foam. Schematic illustration of this process is given in Fig. 2.9 (Yamada et al., 1999). In this method, an open cell polymer foam (e.g. polyurethane) is filled with slurry of a heat resistant material (e.g. plaster). After drying the plaster, the polymer is removed by burning at 500°C and molten Al alloy (typically AA6101) is poured into the resulting porous plaster at 600°C, which corresponds to exactly the original polymer foam structure. After solidification, the mould material is removed by water spraying and mechanical action; as a result continuously connected, open-cell Al foam is obtained. Depending on the initial porosity of the polymer, various

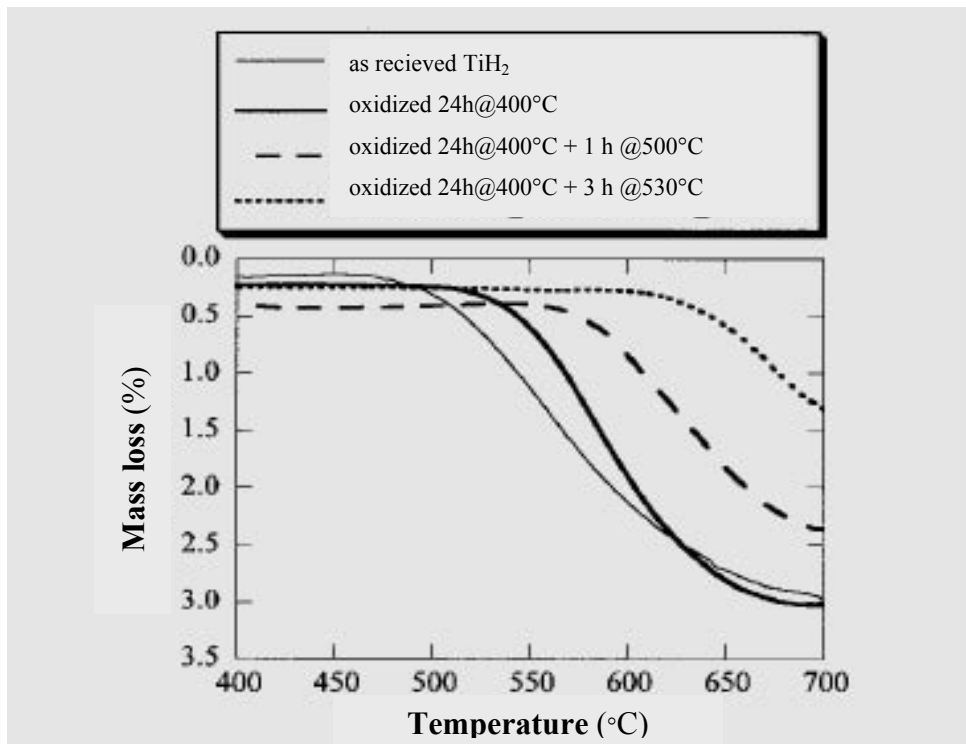


Figure 2.7. Effect of thermal treatment on desorption of TiH₂ in FORMGRIP process (Gergely, 2000)

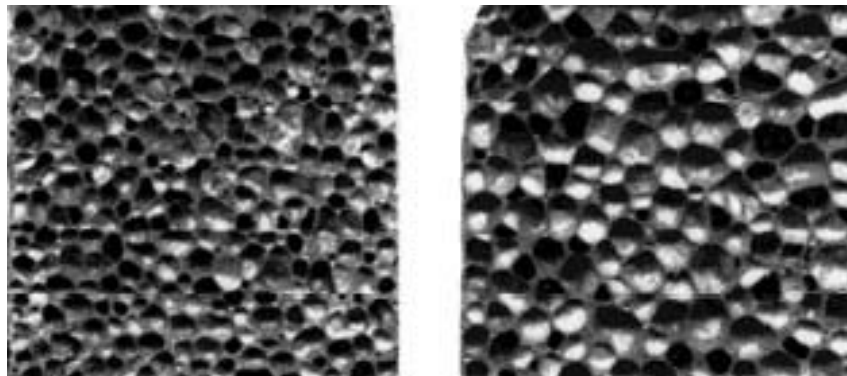


Figure 2.8. Macrostructure of FORMGRIP foam (Gergely, 2000)

ranges of densities can be obtained. Relative densities ranging from 3-50 % (i.e. 0.08 -1.35 g/cm³) can be obtained (Yamada et al., 1999; Yamada et al. 2000). Nieh (1998) reports 2.5 mm pore size for AA 6101 produced by this technique.

Ma et al. (1999) reported a high-pressure infiltration technique in which liquid Al is infiltrated into a mould containing a resin coated polystyrene preform with pressure of 460 MPa. They reported porosity in the range of 73-89 % and cell diameter in 1.2-2.9 mm.

Zhao et al. (2001) reported a novel sintering-dissolution process for manufacturing of Al foam. Schematic illustration of the process is given in Fig. 2.10. In the process, the Al powder is first mixed with NaCl powder, melting point of which 801°C, at a specific ratio. The resultant Al-NaCl powder mixture is compacted into a net-shape preform under an appropriate pressure. The preform is then sintered above a temperature in the range of 640-700°C, not less than 2 hours. The final chilled product is placed into warm water to dissolve NaCl particles. In this process, the pore size and the amount of porosity can be easily controlled by selecting the suitable powder sizes and ratios. 60-70 % of porosity can be obtained via this route.

Chou et al. (2002) proposed another approach to produce open cell Al foam. They compacted deformable soft ceramic balls, made out of Al₂O₃, with PVA binder. Then, molten Al, at 740°C, is poured onto this structure with some pressure. After solidification of the metal, ceramic balls are removed from the system by water and ultrasonic vibration. By this process, an open cell Al sponge with porosity up to 89 % is obtained.

2.2.3. Powder Metallurgy (P/M) Based Foaming Process

Schematic illustration of the Al foaming by powder-compact foaming technique is given in Fig. 2.11 (Banhart, 2001). The technique consists of mixing of Al or Al alloy powders with appropriate foaming agent, commonly TiH₂, which get entrapped by compacting to a dense product called foamable precursor material. The compaction can be achieved with a variety of techniques: hot pressing, hot or cold

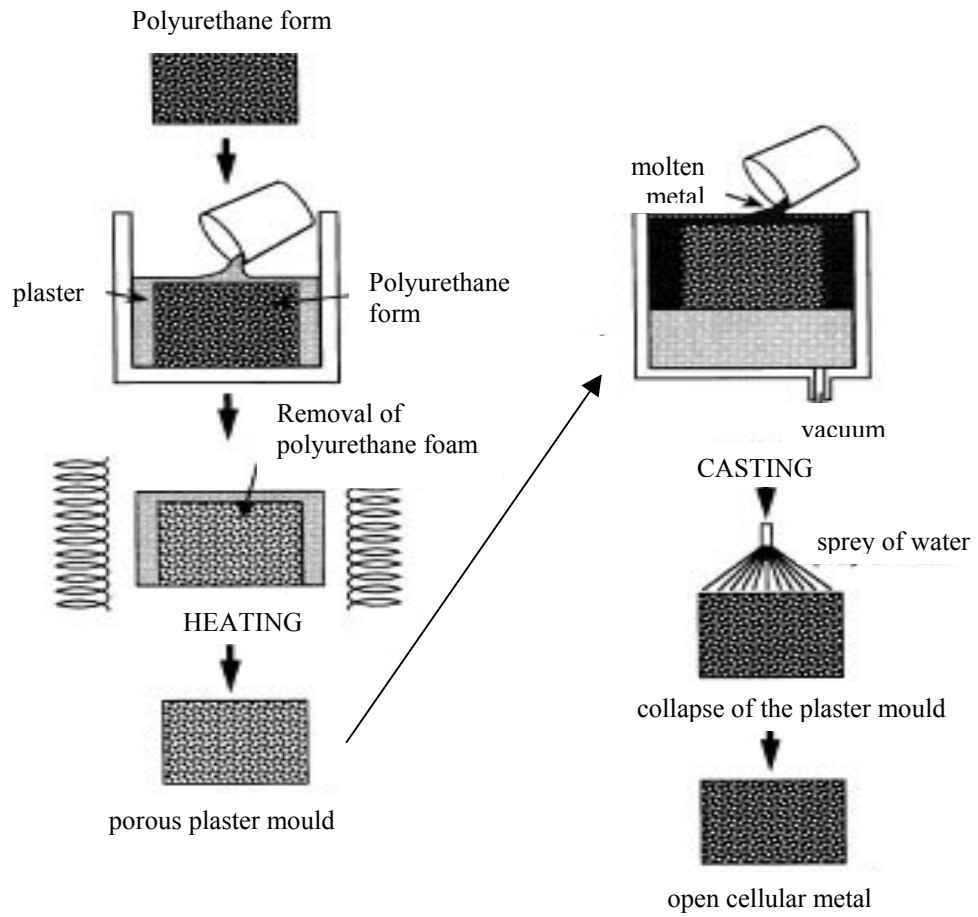


Figure 2.9. Schematic illustration of DUOCEL process (Yamada et al., 1999)

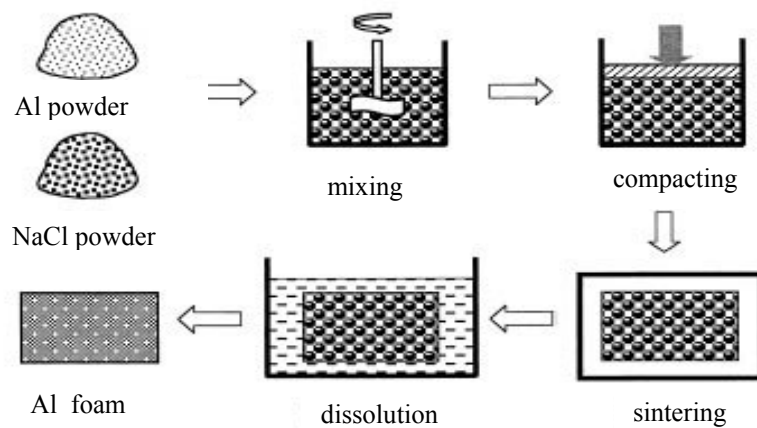


Figure 2.10. Sintering-dissolution process for manufacturing of Al foam (Zhao et al., 2001).

extrusion, rolling. By heating the compact above solidus temperature of Al alloy hydrogen gas releases from the foaming agent, TiH_2 , and bubbles form as a result of hydrogen. After cooling, low density foam with closed-cell architecture is obtained.

The technique was first proposed by Baumeister et al. (1992) for Al-TiH₂. The technique has been named by Fraunhofer-Institute for Applied Materials Research (IFAM), Germany as 'powder-compact foaming technique '.

2.2.3.1. Process Variables in P/M Technique

Similar to other foaming techniques, foaming of Al by P/M technique requires high degree of control on the process conditions. In the following sub-sections, process variables will be defined in the order of steps involved in the foam production.

Selection of Powders: Selection of powders automatically determines the system to be foamed. Banhart (2000) indicates that the appropriate selection of the raw powders in terms of purity, particle size and distribution, alloying elements and other powder properties is essential for a successful foaming.

The most important selection criterion is the composition of the foaming system. Al-Si systems are frequently used due to their low melting point and broad solidification range. AlSi7 (Yash, 2001; Duarte et al., 2000; Helfen et al., 2002), AlSi12 (Simancik et al. 1999) are the most commonly foamed systems. Al-Mg-Si (6000 series) systems are also common and selected whenever heat treatable alloys combining medium strength and moderate costs are required. Duarte et al.(2000), Lehmhus et al.(2002), Simancik et al.(1999), Baumgartner et al.(2000) used AlMg1Si0.6(Al 6061) powders for foaming. Other compositions have also been used. Banhart et al. (1998) used AlSi6Cu4; Lehmhus et al. (2002) selected AlZn5.5MgCu (Al7075) and AlZn4.5Mg1 (Al7020) alloys to examine the effect of precipitation hardening on Al foams properties. Baumeister et al. (1992) and Kennedy (2002) used pure Al for foaming whereas Elbir et al. (2001) added 10-20 wt % SiC particles to stabilize pure Al. Although there are examples, foaming of pure Al is not common due to its low viscosity. Al alloy could be pre-alloyed powder or obtained from elemental powders.

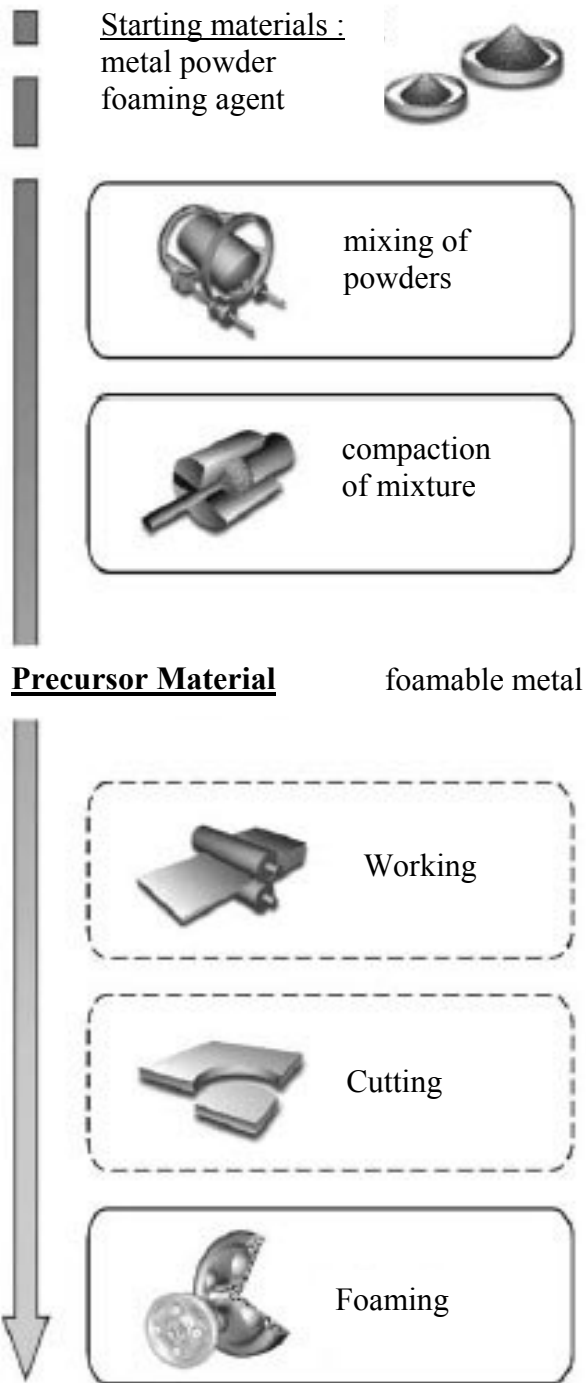


Figure 2.11. Schematic illustration of the Al foaming by powder-compact foaming technique (Banhart, 2001)

Selection of foaming agent is carried out by comparing decomposition temperature of metal hydride and melting temperature of base metal. Baumgartner et al. (2000) states that presently TiH_2 seems to be the best choice for the blowing agent for foaming of Al and Al alloys. Other hydrides, e.g. ZrH_2 and HfH_2 , have also proved to be practical, but more expensive than TiH_2 , and no technical advantage is currently known. An elementary calculation made by Baumgartner et al. (2000) show that very low content of TiH_2 is sufficient to create a high degree of porosity. In P/M technique, the amount of TiH_2 is much less than used in liquid metallurgy techniques, which is commonly 1.5-1.6 wt %. In the early studies, the amount of TiH_2 might be up to 0.8 wt % (Banhart et al., 1998). Subsequently, it has been shown that TiH_2 of 0.6 wt % is enough for foaming of Al and its alloys (Duarte et al. 2000; Baumgartner et al. 2000; Lehmus et al. 2002; Kennedy, 2002). In some research, 0.5 wt % TiH_2 was also used (Helfen et al., 2002; Elbir et al., 2001; Yash, 2001; Banhart et al., 1999).

Particle sizes, shapes and surface properties of both base metal and foaming agent can be crucial. Average particle sizes up to 160 μm were used for both prealloyed and elemental powder systems (Lehmus et al., 2002; Duarte et al., 2000). This shows that there is no limitation in the size of the matrix powder as long as it is not in the form of granules (Elbir et al., 2001). TiH_2 is mostly used in the as-received form, in which the particle size is generally less than 50 μm .

Banhart (2000) states that although it is not clearly understood, stabilization of the foams produced by P/M method can be attributed to metal-oxide layer on the Al powders. This means that amount of oxide of the Al powders may be crucial. Although it is not investigated for Al systems, Wübben et al. (2002) showed that high oxide containing Pb powders yield more stable foams.

Mixing of Powders: Homogeneity of powder mixtures is crucial to obtain homogenous pore distribution in foam product. Despite its importance, there has been no study on the effect of mixing on foaming. Banhart (2000) points that the homogenous mixture of powders should be attained to obtain high quality foams

with uniform pore distribution. Commonly, tumbling mixers are used as a method of mixing in the laboratory-scale productions (Baumgartner et al., 2000).

Compaction of Powder Mixtures: Powder consolidation can be performed using various techniques. According to Banhart (2000), to obtain high amounts of foaming, compaction should yield almost full compact structure. Duarte et al. (2000) indicates that 1% of residual porosity is tolerable. Two different routes are currently employed to obtain Al compacts. In the first method, Cold Isostatic Pressing (CIP) is applied to well mix powder system. Hot extrusion or hot rolling is subsequently applied to semi-compact structure. After the CIP, compact have 70 -80 % relative densities whereas after extrusion or rolling it approaches to theoretical value. The other route is direct powder consolidation by hot pressing. By this way, foamable tablets can be obtained directly. It should be noted that in the case of rolling, foamable sheets or sandwiches could be obtained which makes the process more flexible.

Duarte et al. (2000) carried out a detailed study on the effect of compaction on foaming. It was found that in the case of direct consolidation, the temperature of compaction is very crucial. As seen in Fig. 2.12, up to 450°C, increase in compaction temperature increases the degree of foaming. However, if compaction temperature exceeds this value, the degree of foaming decreases with temperature. It was concluded by authors that up to 450°C, the amount of compaction increases with time and hydrogen release from TiH_2 does not occur. Above this temperature, hydrogen release occurs extensively and less hydrogen remains for subsequent foaming process.

Duration of hot compaction should be long enough to achieve high compaction. The duration should be long enough to achieve high compact to let the Al atoms diffuse and result in a sintered structure. Prolonged durations may be unnecessary. In the study of Duarte et al. (2000), the duration was found to be unimportant after certain period of time. Fig. 2.13 shows this relation for AlSi7 system that shows the different compaction durations result almost same amount of foaming.

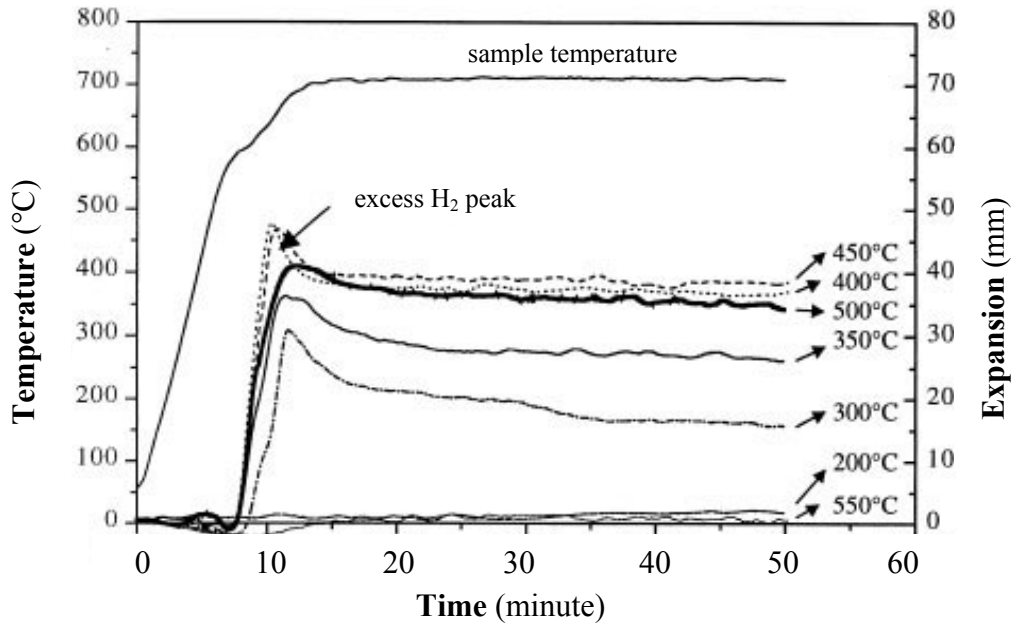


Figure 2.12. Effect of compaction temperature on Al foaming (Duarte et al., 2000)

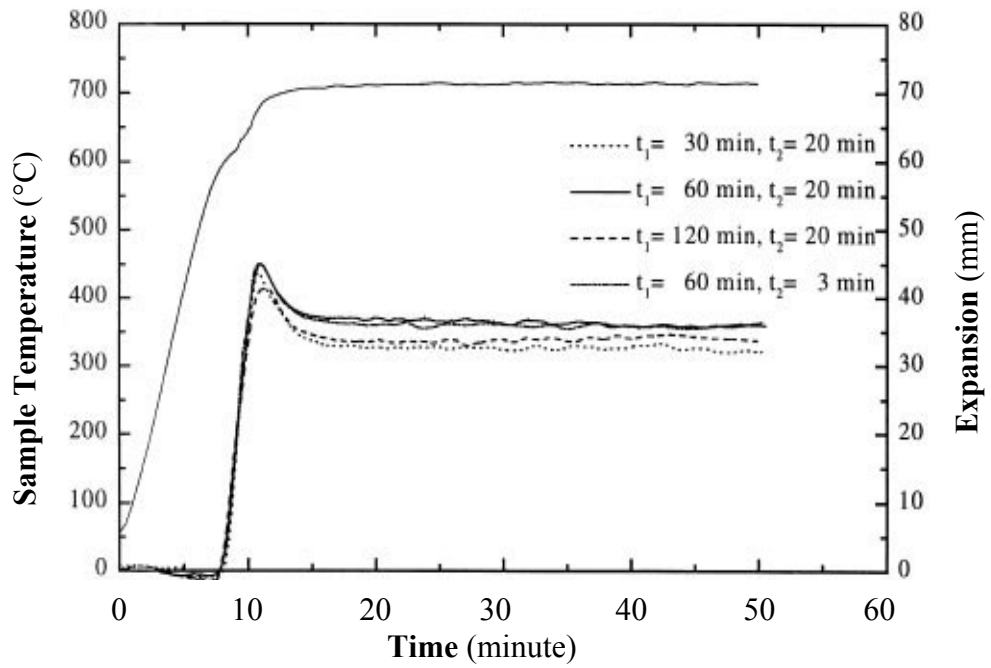


Figure 2.13. Effect of compaction parameters: temperature and time on Al foaming (Duarte et al., 2000)

Foaming of Precursor: Foaming of Al powder compacts involves several variables during the foaming process itself. Main parameters that should be considered are foaming temperature, heating and cooling rate of precursor and foaming time.

Foaming temperature should be higher than the solidus temperature of the base metal. The selected temperature should allow the flow of the metal as well as decomposition of the TiH_2 . On the other hand, viscosity is strongly temperature dependent, and for this reason, temperature should be optimized by considering foam stability in liquid phase. Table 2.1 shows the solidus, liquidus and foaming temperatures of selected Al alloys given in the literature.

It should be pointed out that in all studies samples were inserted into pre-heated moulds to increase the heating rate of the sample. Duarte et al. (2000) showed that sample temperature could be 35-50°C lower than the furnace temperature. However, it is obvious that this depends on the set-up and can be higher or smaller than the values given in the literature.

It is stated by Duarte et al. (2000) that heating and cooling rate are important to obtain high quality of Al foams. Effect of heating rate on foaming is shown in Fig. 2.14 for Al 6061 samples. Clearly, high heating rates lead to an earlier expansion because melting point is reached at an earlier time. Figure shows that heating rate down to 85°C/min yields acceptable foaming whereas the foaming decreases significantly if the rate is very slow. Duarte et al. (2000) attributes this decrease to two possible reasons: (i) by slow heating rate, TiH_2 particle release its hydrogen and gas loss occurs before melting; (ii) oxidation of Al samples at the surface for prolonged heating time may mechanically hinder the expansion of sample.

Cooling rate is also important. The foaming should be stopped at the required time. Otherwise, liquid flow due to gravitation may result drainage at the bottom of the sample. For large samples, cooling may be difficult because of low thermal conductivity of the foam. Fast cooling is mainly achieved by either air blowing or water spraying on to the mould (Banhart, 2001).

2.2.3.2. Characteristic Properties of Al Foams Produced by P/M Technique

Foams produced by P/M technique are mainly characterized according to level of expansion achieved, density, pore size and distribution. Volumetric change can be measured by either in-situ via laser expandometer (Duarte et al. 2000) or ex-situ (by removing sample from furnace) technique. Various levels of densities were reported in the literature, which are commonly in the range of $0.3\text{-}1\text{ gm/cm}^3$, including the closed skin around the foamed body (Degischer et al., 2002). Fig. 2.15 shows a typical time vs. foaming amount graph. Such graphs can be obtained by measuring the volume of the sample after a certain foaming period, by removing the sample from the furnace, i.e. an ex-situ technique.

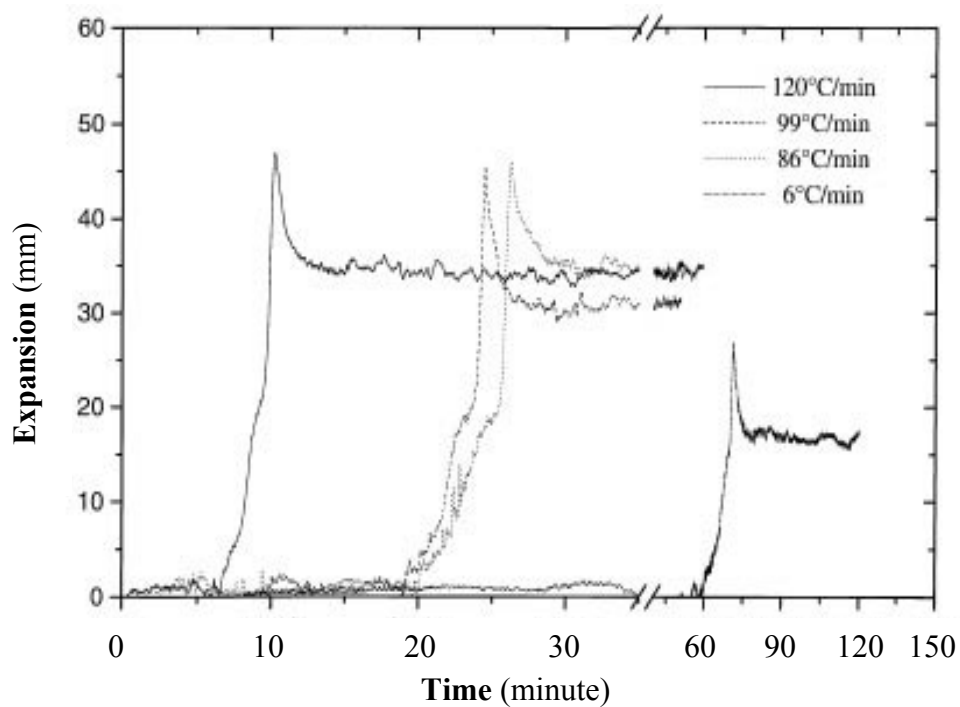


Figure 2.14. Effect of heating rate on Al foaming (Duarte et al., 2000)

By this way, volumetric change of precursor material with time in the foaming process can be monitored. In the Fig. 2.15, four stages of foaming can be observed: In the first stage, sample heats up and its volume does not change. After a certain

Table 2.1. Foaming conditions of the selected Al systems produced by P/M method

System	T_{solidus} (°C)	T_{liquidus} (°C)	T_{foaming} (°C)	t_{foaming} (min)
Al (Kennedy, 2002)	660	660	800	6-10
AlSi7 (Duarte et al.,2000)	574	623	600-800	5-50
AlSi7 (Wübben et al.,2002)	574	623	750	-
AlSi7 (Yash, 2001)	574	623	*	*
AlSi7 (Helfen et al., 2002)	574	623	600	4-7
AlSi12 (Simancik et al., 1999)	574	585	580-625	7-20
Al 6061 (Duarte et al., 1999)	580	650	650-800	5-50
Al 6061 (Lehmhus et al., 2002)	580	650	740	N.A.
Al 6082 (Lehmhus et al., 2002)	575	650	740	N.A.
Al 7075 (Lehmhus et al., 2002)	475	635	740	N.A.
Al 7020 (Lehmhus et al., 2002)	605	645	740	N.A.
Al+10 wt % SiC (Elbir et al., 2001)	660	660	750 & 800	5-25
* System was foamed via laser with spot size of 2-10 mm and at the rate of 0.4-2 mm/min				

period, an initiation occurs and sample volume increases with time (2nd stage). By reaching a maximum expansion value, amount of foaming decreases with time, which is the third stage. Finally, foaming stays constant with time in the 4th stage. Typical examples of pore structure in P/M processing are given in Fig. 2.16 (Duarte et al., 2000).

2.3. FUNDAMENTAL PARAMETERS IN FOAMING

Foaming is a process during which many thermodynamic, physical and kinetic events occur simultaneously. Creating large surface area by gas bubbles introduce an instability to the system. Especially for metal foams, opaqueness of the system makes the process more difficult to characterize. Considering the foams based on water and other liquids, viscosity, surface tension of the liquid and pressure equilibrium between pore and the surrounding media are the primary parameters during the foaming process.

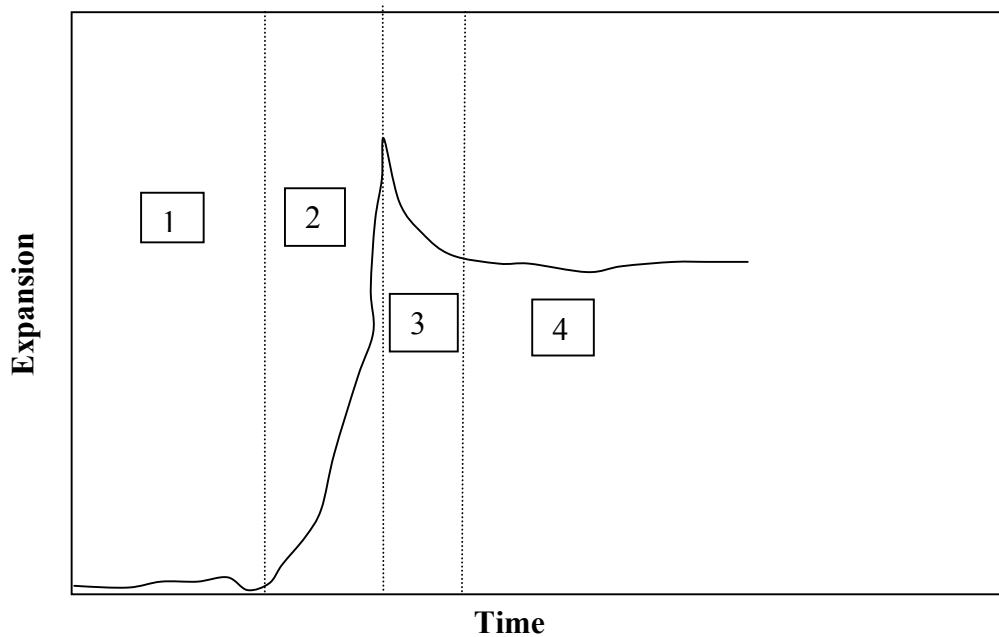


Figure 2.15. A typical time vs. amount of foaming graph

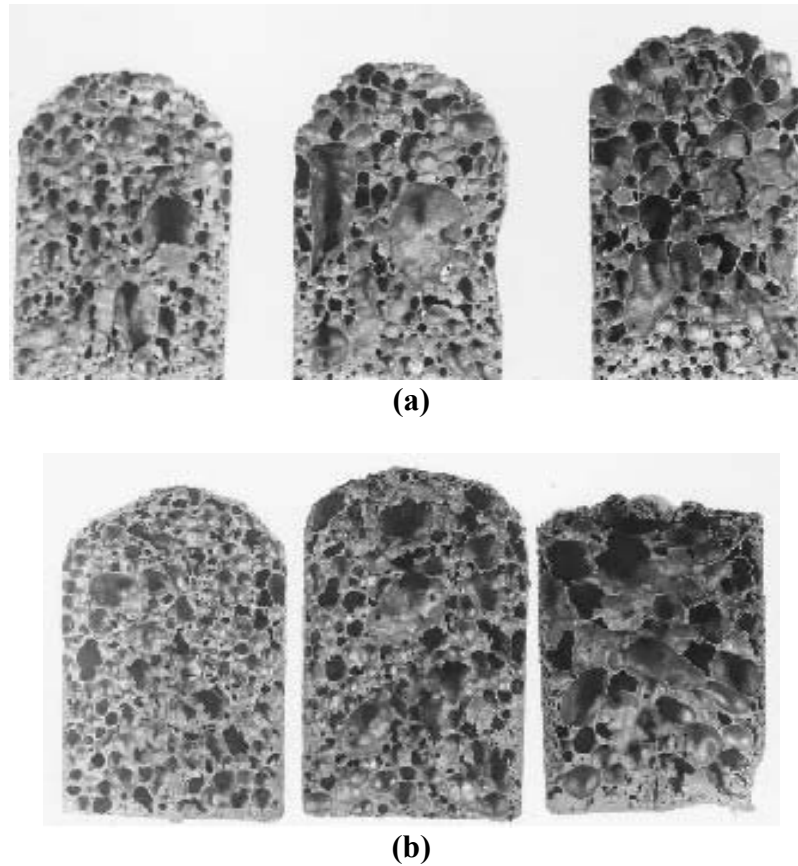


Figure 2.16. Macrostructures of foamed structures produced by P/M technique (a) for AlSi7 foamed at 750 °C and (b) for Al6061 foamed at 800° C (Duarte et al., 2000).

2.3.1. Viscosity

Viscosity affects the motion of liquid metal and additives in the molten metal. According to Park et al. (2002), a liquid's viscosity is the main factor dominating the rise of the gas bubbles. Körner et al. (2000) indicates that because of the gravity there is a pressure gradient in the melt and this deforms the bubble which makes it move. The bubble is accelerated until a stationary velocity, v , is reached where the resultant viscous force balance the buoyant force. For nearly spherical small bubbles, the rising velocity, v , can be calculated from Stokes' law for low Reynolds numbers:

$$v = \frac{2d \cdot g \cdot r^2}{9 \cdot \eta} \quad (2.1)$$

where d is the density of metal, g is gravitational acceleration, r is the radius of bubble and η is the viscosity of the metal at the specified temperature. Eq. 2.1 shows that as the viscosity of the liquid metal increases pore rising velocity decreases. By decreasing the terminal velocity of the bubbles, impact collisions of gas bubbles may be prevented that retards the pore coalescence.

In addition, many authors agree that the rate of film thinning and drainage velocity is inversely proportional to the viscosity of the liquid (Cox et al., 2001; Kumar et al., 2002; Angarska et al., 2001).

Effect of viscosity is widely investigated in liquid foaming of aluminium. Miyoshi et al. (2000) indicates that addition of Ca and subsequent stirring of molten Al increases the stirring resistance of the melt with time. Ma et al. (1998) gives the value of 6×10^{-3} Pa·s for the addition of 1.8 wt % Ca after 6 minutes of stirring which is 2×10^{-3} Pa·s without Ca addition. They also mention the minimum porosity of 1.6 mm is obtained by maximum viscosity of 7.5×10^{-3} Pa·s with 1.4 wt % TiH₂. Song et al. (2000) carried out many experiments on the effect of viscosity on foaming and concluded that too high viscosity suppresses the formation of bubbles whereas too low viscosity leads to rapid floatation of the gas bubbles. In addition, they remark that too high viscosity may lead to non-uniform distribution of foaming agent in liquid foaming techniques.

It was shown by Andrade (1934) that viscosity at melting point of a metal could be expressed by

$$\eta = 1.7 \cdot 10^{-7} \cdot (d \cdot 1000)^{\frac{2}{3}} \cdot \sqrt{T_m} \cdot (M_w \cdot 10^{-3})^{\frac{-1}{6}} \quad (2.2)$$

where, M_w is the molecular weight (g/mol), d is the density of metal (gm/cm³), T_m is the melting temperature (K) and η is the viscosity at T_m (Pa·s)

Temperature Dependency of Viscosity: Temperature dependency of viscosity of liquid alloys was investigated by Battezzati et al. (1989), Andrade et al. (1934) and Hirai et al. (1993). The authors conclude that the temperature itself is the primary variable for viscosity. For most liquid metals and alloys, above their melting temperature, the temperature dependency of the viscosity is described by Arrhenius equation:

$$\eta = \eta_c \cdot e^{-\left[\frac{2.65 (T_m)^{1.27}}{8.314 \cdot (T)} \right]} \quad (2.3)$$

$$\eta_c = \frac{\left[1.7 \cdot 10^{-7} \cdot (d \cdot 1000)^{\frac{2}{3}} \cdot \sqrt{T_m} \cdot (M_w \cdot 10^{-3})^{\frac{-1}{6}} \right]}{e^{-\left[\frac{2.65 (T_m)^{1.27}}{8.314 \cdot (T_m)} \right]}} \quad (2.4)$$

where, d is density of metal (gm/cm^3), T_m is melting temperature of the metal (K), M_w is molecular weight of the metal (g/mol), η_c is viscosity coefficient (Pa·s) and η is viscosity of the metal at temperature T (Pa·s). The viscosity of Al derived from Eq. 2.3 for 660-1100° C is given in Fig. 2.17.

Composition Dependency of Viscosity: Effect of alloying element on Al viscosity at 700°C is given in Fig. 2.18 (Gerhard et al., 1959). It can be seen that Si and Mg decrease the viscosity of Al, which makes them suitable for Al casting systems. On the other hand, Ti and Fe drastically increase the viscosity value of the Al at that temperature.

It should be noted that for a given metal, composition dependency of the melting point viscosity is less strong than the temperature dependency of the viscosity. In

general, alloys that have high melting point have higher viscosity than the alloys having low melting point.

Solid Fraction Dependency of Viscosity: Presence of a suspended solid material in the melt may seriously affect the viscosity of the overall system. Turkdoğan (1983) proposed the effective viscosity of a solid-liquid emulsion as:

$$\eta = \eta_0 \cdot (1 - 1.35 \cdot X)^{-2.5} \quad (2.5)$$

where η_0 is the virgin liquid's viscosity and η is the viscosity of this liquid with particles of concentration X .

Bretsznajder (1971) suggested a formula for the viscosity of a suspension of a solid in a liquid with the following formula:

$$\eta = \eta_0 \cdot \left[1 + \frac{2X}{\left(\frac{2}{1 - 1.2X^3} \right)^2} \right] \quad (2.6)$$

2.3.2. Stability Gas Bubble in a Liquid

When a gas phase forms in a liquid media, existence of surface tension in all directions makes the gas phase spherical in shape. This bubble has a inner pressure, P_{in} , due to existence of gas molecules. Assuming the gas in a bubble behaves in an ideal manner and the bubble has a spherical shape, P_{in} can be written as:

$$P_{in} = \frac{3n_{(H_2)} \cdot R \cdot T}{4\pi r^3} \quad (2.7)$$

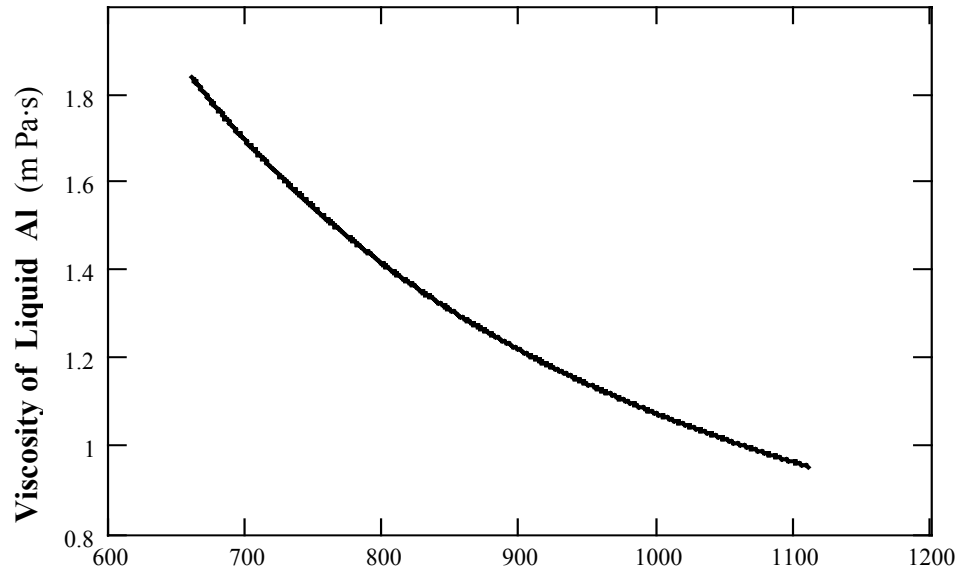


Figure 2.17. Temperature dependency of the viscosity for liquid Al (Derived from Eq. 2.3)

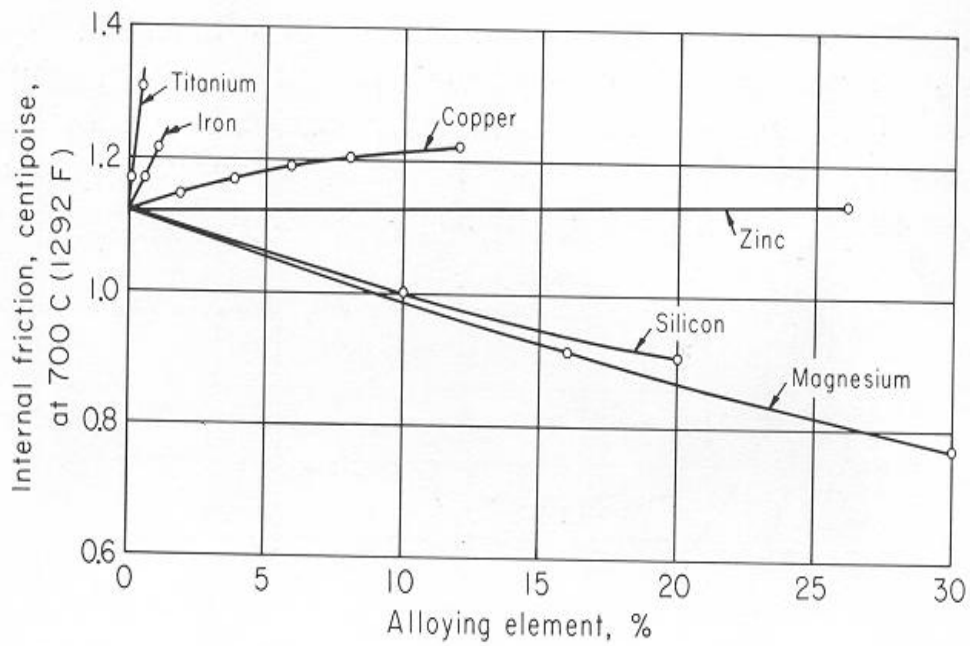


Figure 2.18. Effect of alloying element on Al viscosity at 700°C (Gebhardt et al., 1959)

where, n_{H_2} is number of moles of hydrogen in the bubble (mole), R is the universal gas constant (8.341 J/mol K), T is temperature (K) and r is the radius of the gas bubble.

Fusheng et al. (2003) points out that to form a bubble into liquid Al, gas pressure should overcome the pressure due to surface tension, P_s , atmosphere pressure, P_a , and hydrostatic pressure, P_h . Richardson (1974) and Bikerman (1973) give the pressure of a gas bubble placing in a liquid in its equilibrium condition as:

$$P_{in} = P_{ext} = P_{out} + P_s = P_a + P_h + P_s \quad (2.8)$$

where, P_{in} is pressure inside the bubble, P_a is atmospheric pressure, P_h is pressure due to weight of the liquid and P_s is pressure due to surface tension.

Pressure, P_s , due to surface tension, γ , is given by:

$$P_s = \frac{2\gamma}{r} \quad (2.9)$$

where, γ is surface tension of liquid, r is radius of the spherical gas bubble.

Hydrostatic pressure is given by :

$$P_h = \rho gh \quad (2.10)$$

where, ρ is density of the liquid, h is height of the liquid over the bubble, g is gravitational acceleration.

2.3.3. Surface Tension

As given in the Eq. 2.8 and 2.9, pressure inside a bubble is surface tension dependent. The surface tension is an intrinsic property of all liquids and is due to an incomplete coordination of atoms at the liquid-gas interface. Atoms in the bulk of the liquid are surrounded by other atoms, while those at the surface are only in contact

with the side and below. Inter-atomic attractions cause an uneven pull on the surface atoms, drawing them into the body of the liquid and resulting in a curvature of the surface as the liquid tries to assume a shape that has a minimum surface area. Thermodynamically, surface tension is defined as the surface free energy per unit area with the unit of J/m^2 . From dynamic point of view, the surface tension represents the work required to create one unit of additional surface area at constant temperature with the unit of N/m (Anson et al., 1999). Park et al. (2002) mentions that at low surface tension values it is easy to create bubbles whereas in the case of high surface tension bubble formation should be difficult.

Surface tension is a parameter in the pore formation of the liquid-gas systems as it can be seen from Eq. 2.9. According to Adamson (1976), surface tension of most liquids decreases with increasing temperature in a nearly linear fashion. Various data were tabulated by different authors for the surface tension of pure aluminium. Goumiri et al. (1982) used Sessile Drop Apparatus to measure this quantity and found 1.050 N/m for pure Al under vacuum atmosphere at 700°C . Garcia-Cordovilla et al. (1986) used maximum bubble pressure method and found the value as 1.091 N/m under argon atmosphere at 700°C . Anson et al. (1999) also used Sessile Drop Apparatus and found that oxidation of aluminium decreases the surface tension of aluminium. They found that at 680°C surface tension is 1.009 N/m if there is no visible oxide layer at the surface whereas in the existence of island of oxides the value drops to 0.845 N/m . Saravanan et al. (2001) also measured surface tension of aluminium under different atmospheres. They found that the surface tension decreases with temperature linearly. However, this linearity may be different at different temperature ranges and atmospheres. In all cases, they found that pure Al has surface tension of 0.86 N/m at 700°C . Linearity does not change for argon atmosphere (slope of $-0.15 \text{ mNm}^{-1}/\text{K}$) but varies from $0.19 \text{ mNm}^{-1}/\text{K}$ to $0.66 \text{ mNm}^{-1}/\text{K}$ at 840°C under Nitrogen atmosphere. Shimoji (1977) gives the value of surface tension as 0.914 N/m at melting point of aluminium. Korol'kov (1960) found the value as 0.860 N/m at melting point of aluminium with 0.02 variations.

Actually there is no data in the literature about the surface tension of aluminium with hydrogen. However, Saravanan's data is the one that is the most current and the graph in the Fig. 2.19 can be evaluated from his data. The best line of the graph yields the variation of surface tension of Al with temperature as:

$$\gamma \left(\frac{\text{mN}}{\text{m}} \right) = -0.1527 \cdot T(\text{K}) + 1023.2 \quad (2.11)$$

Surface tension is also composition dependent. Effect of alloying elements on the surface tension of Al is given by Horn (1967). Fig. 2.20 gives that relation under argon atmosphere. The graph indicates that Bi, Ca, Li, Mg, Sb and Sn substantially decrease the surface tension whereas Ag, Cu, Fe, Ge, Mn, Si and Zn have little effect.

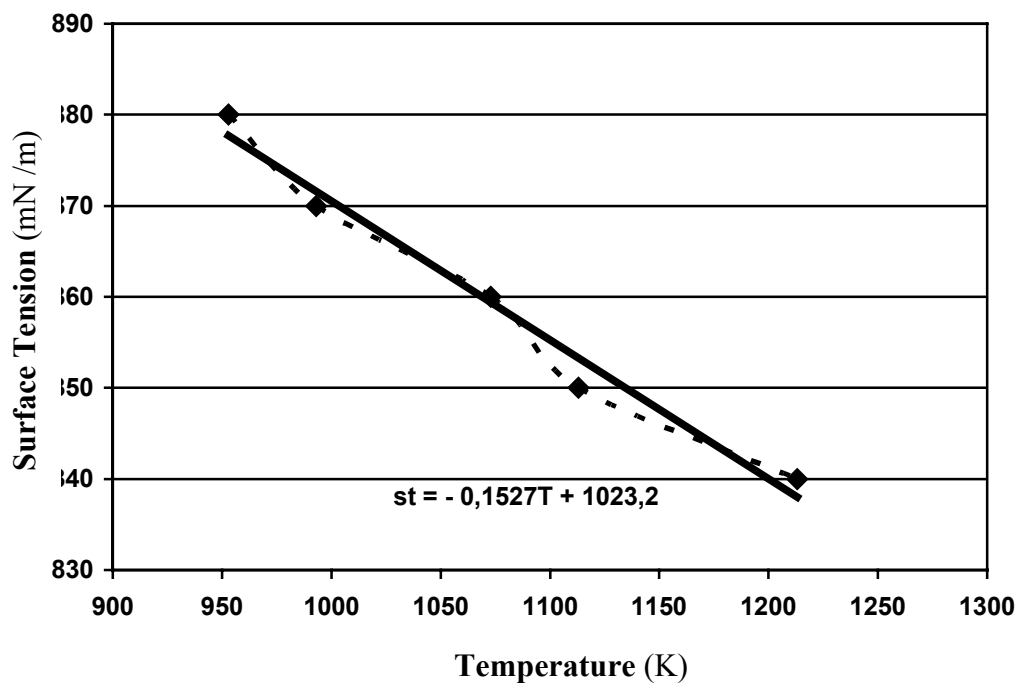


Figure 2.19. Variation of surface tension of Al with temperature. Adapted from Saravanan et al. (2001)

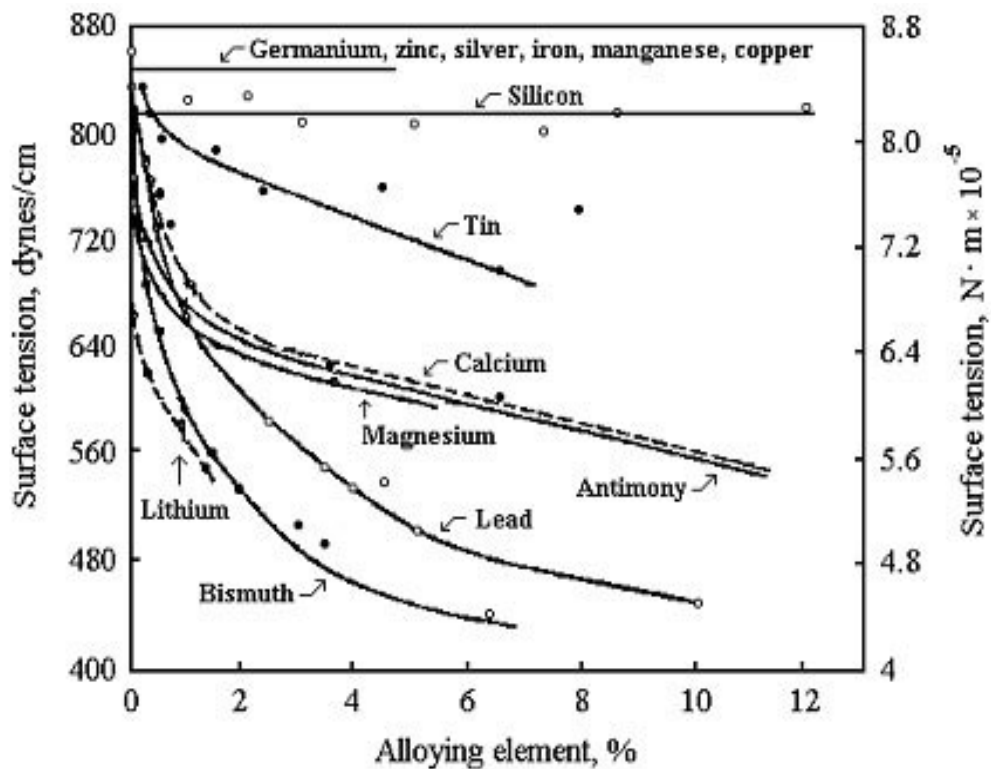


Figure 2.20. Effect of alloying elements on the surface tension of Al (Horn, 1967).

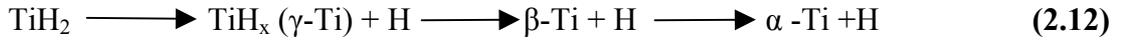
2.4. STABILITY OF COMPONENTS IN AL FOAMING

During foaming of Al, materials that exist in the foaming environment interact with each other. Some materials become unstable during the process, such as TiH_2 , whereas some others may react with each other during foaming giving reaction products, which do not exist initially.

2.4.1. Decomposition of TiH_2

Phase diagram of Ti-H system is given in Fig. 2.21. H-rich part of the Ti-H systems is point of interest for Al foaming processes. As it is mentioned, at the far end, i.e. at the 2:1 H-Ti atomic ratio, TiH_2 compound exists which is commercially produced and used in the foaming processes. Up to date, no solid hydride with H/Ti ratio greater than 2 has yet been observed (Murray, 1987).

Decomposition of TiH_2 can be represented by the following series of reactions considering the equilibrium phase diagram:



Experimental results support the sequence of decomposition. Kobzenko et al. (1995) shows that TiH_2 decomposition occurs in two stages. The first one starts at 440°C and approximately 25 % of hydrogen loss from hydride to form $\gamma\text{-TiH}_{1.5}$, which is the minimum stoichiometry for this phase. By further heating, about 550°C second transformation starts and sub-stoichiometric α and β phases form. Kennedy (2002) supports these results by DSC studies, shown in Fig. 2.22. Kennedy states that high heating rate retards the first stage of decomposition and overall hydrogen evolution starts at approximately 550°C .

XRD studies by Kennedy et al. (2003), and Fokin et al. (1995) show that heating of TiH_2 in air yields formation of oxyhydrides, i.e. TiH_xO_y , which were found to have same crystal structure with TiH_2 and difficult to distinguish by XRD. Kennedy et al. (2003) suggested that the first reaction is related with the formation of this oxyhydrides, see in Fig. 2.22. According to author, the second exothermic peak is related with the β phase's formation and further heating above 720°C yields formation of TiO_2 and Ti_3O .

Because TiH_2 is not very suitable as a hydrogen storage media, its hydrogen desorption kinetics has not been studied. It is known from other metal hydrides that mechanical milling increases the desorption kinetics of the hydride (Guvendiren et al., 2002). However, in the literature there is no a study on the desorption kinetics of the milled TiH_2 .

The most crucial parameter for TiH_2 decomposition is the pressure over the hydride. Equilibrium pressure of hydrogen over TiH_2 at different temperatures can be obtained from PCT diagram of TiH_2 given in Fig. 2.23. Plateau value of desorption PCT diagram gives the equilibrium pressure of hydrogen over TiH_2 at that

temperature. Sandrock (1999) indicates that mid-desorption plateau pressure data can be used to obtain Van't Hoff equation of TiH_2 for engineering purposes, that gives the variation of equilibrium pressure with temperature, which is actually graph of $1/T$ (K) vs. $\ln P_{eq}$ (atm):

$$\ln(P_{eq}) = \frac{\Delta H}{RT} - \frac{\Delta S}{R} \quad (2.13)$$

where ΔH and ΔS are the enthalpy and entropy changes of the dehydrating reaction, T is the absolute temperatures and R is the gas constant.

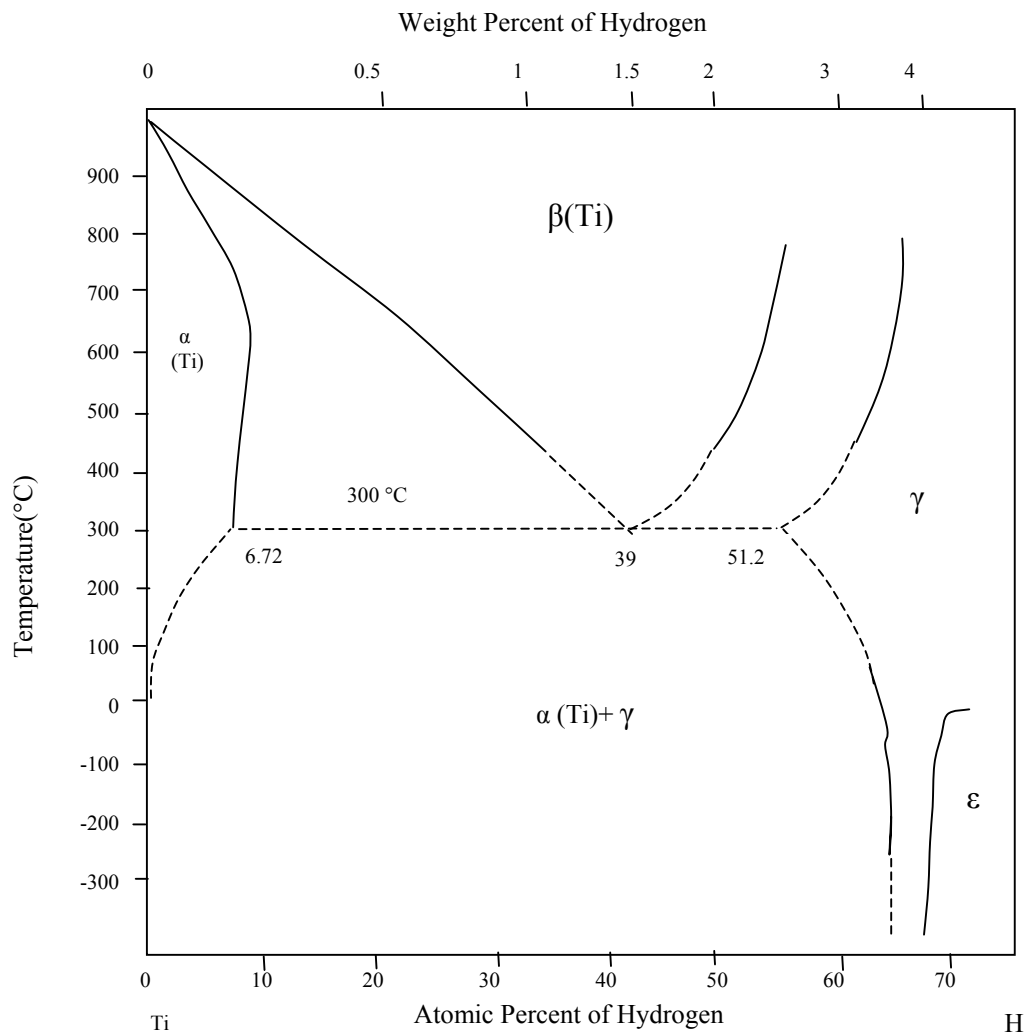


Figure 2.21. Ti-H phase diagram (Murray, 1987)

Mueller (1968) gives the plateau pressure of TiH₂ at different temperatures as follows:

Table 2.2. P_{eq} values at the specified temperatures (Mueller, 1968)

P (atm)	Temperature (°C)
0.893	636
0.197	578
0.0425	527
0.0089	477
0.0013	427

Data plotted in Fig. 2.24 is the form of Van't Hoff equation, i.e. 1/T vs. ln P. The following equation can be derived from the graph.

$$\ln P_{eq} = \frac{-19821}{T} + 21.671 \quad (2.14)$$

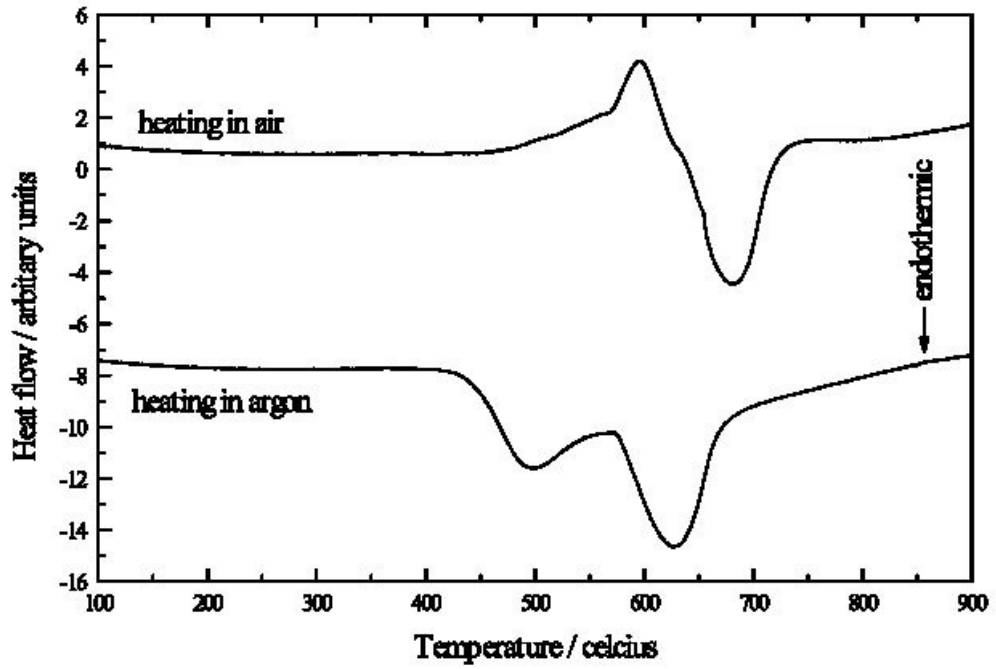
P_{eq} in this equation is the equilibrium pressure, in the units of atm above which hydrogen release stops.

2.4.2. Al-H System

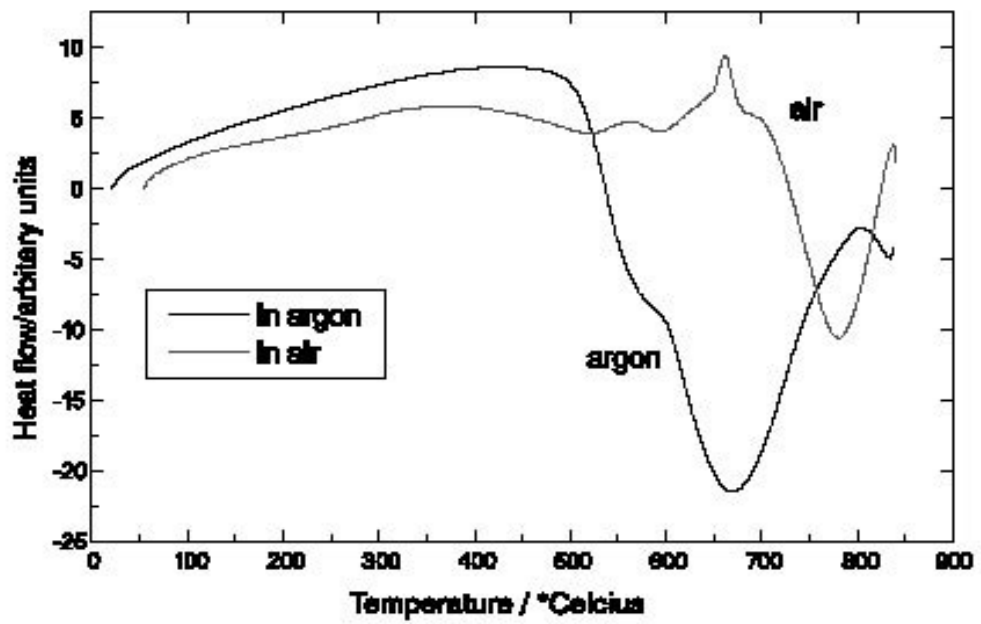
The most important point of Al-H system is the solubility of hydrogen in Al. According to Sokolskaya (1961), aluminium belongs to group of metals, which form with hydrogen true endothermic interstitial solid solution, i.e. the solubility obeys the following law:

$$S = m\sqrt{P} \cdot e^{\frac{-E_s}{2RT}} \quad (2.15)$$

where S is the solubility of the diatomic gas into metal, P is the partial pressure of the gas, T is the absolute temperature, E_s is the heat of solution, m, and R are constants.



(a)



(b)

Figure 2.22. DSC graphs of the TiH₂ at different heating rates (a) for 20 K/min and (b) 90 K/min (Kennedy, 2002 and Kennedy et al., 2003).

True dissolution is an endothermic process, and therefore the solubility of hydrogen in Al increases with increasing temperature. The process of dissolution is reversible and on cooling the gas is given off.

Eichenauer and co-workers (1961) have reported values of hydrogen solubility in solid aluminium. They proposed the following equation for hydrogen solubility in solid Al:

$$\log (S) = \frac{-2080}{T} + \frac{1}{2} \cdot \log (P) - 0.652 \quad (2.16)$$

where S is the solubility (cm³) of hydrogen in 100 gm of solid Al, P is the partial pressure of the hydrogen (mm Hg) and T is the absolute temperature.

Ransley and Neufeld (1947/1948) expressed the solubility of hydrogen in liquid Al with the following equation:

$$\log (S) = \frac{-2760}{T} + \frac{1}{2} \cdot \log (P) + 1.356 \quad (2.17)$$

where S is the solubility (cm³) of hydrogen in 100 gm of liquid Al, P is the partial pressure of the hydrogen (mm Hg) and T is the absolute temperature. The graph of the solubility of hydrogen in solid and liquid Al, obtained from Eq. 2.16 and 2.17, is given in Fig.2.25. It can be seen that hydrogen solubility can be as high as 0.2 gm /100 gm of Al. As Van Lender (1967) says, hydrogen dissolved in the molten Al is supersaturated solid solution on freezing. He adds that the porosity occurs as soon as the threshold value (0.1-0.15 cm³/100 gm of Al) is reached.

According to Sokolskaya (1961), before diffusion of hydrogen through an aluminium media (sheet or liquid), dissociation of molecular hydrogen occurs as:



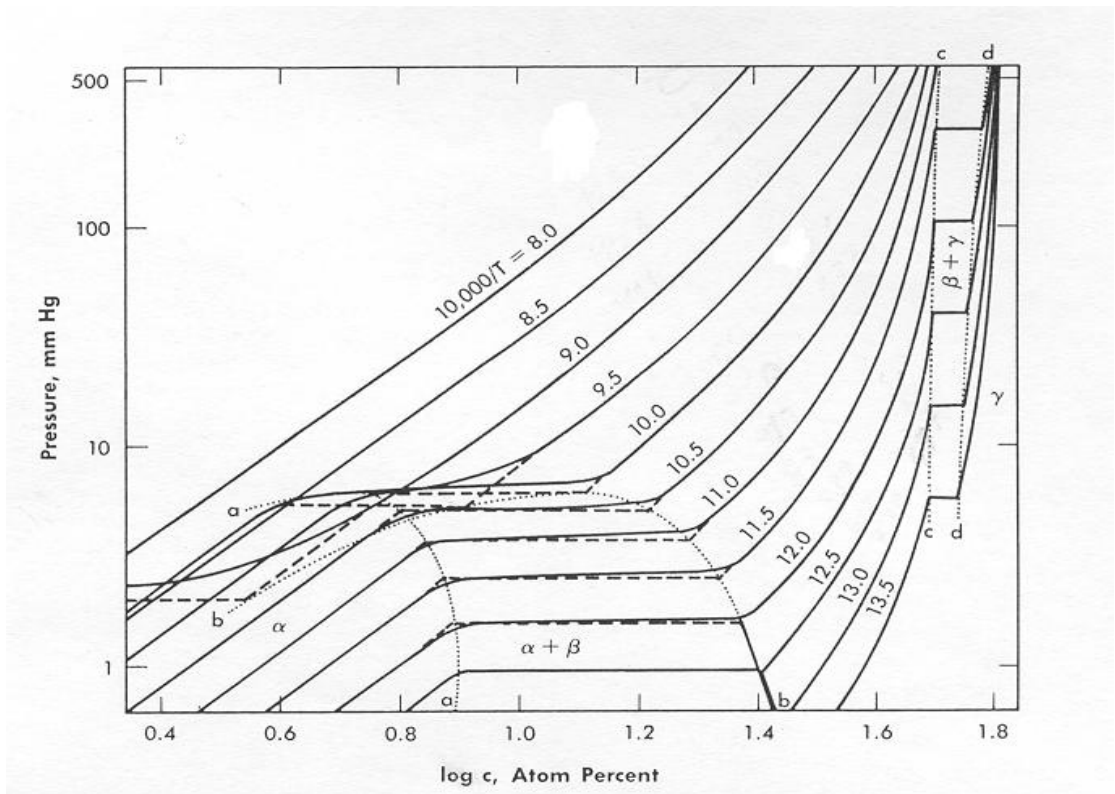


Figure 2.23. PCT diagram of TiH₂ (Mueller et al., 1968)

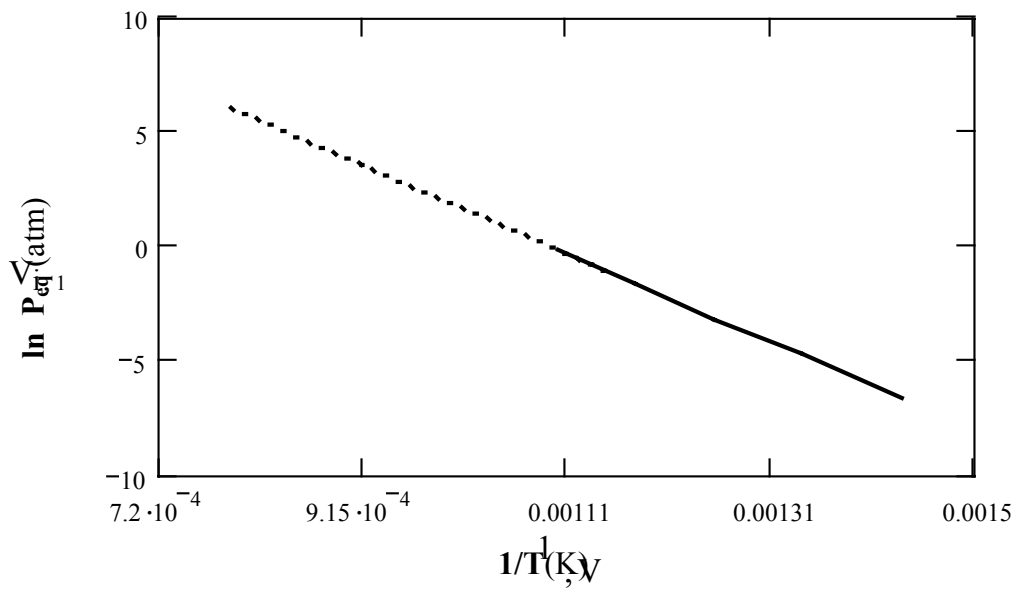


Figure 2.24. Variation of P_{eq} with temperature Data is shown by solid line and extrapolation is shown by dash line (Adapted from Mueller, 1968 and Sandroc, 1999)

Then activated adsorption develops on the surface. Hydrogen releases from the adsorbed layer into the media and form true solution.

Ransley and Talbot (1955) indicate that diffusion of hydrogen up to 200°C is practically undetectable. They also mentioned that the diffusion rate of hydrogen in Al increases with temperature and reaches 2×10^{-3} cm²/sec at the melting point, i.e. 660 °C.

Eichenauer and co-workers (1961) have determined the diffusion coefficient of hydrogen in solid Al as:

$$D = 0.11 \cdot e^{\left(\frac{-9780}{R \cdot T} \right)} \quad (2.19)$$

where R is the gas constant in calories and T is the absolute temperature.

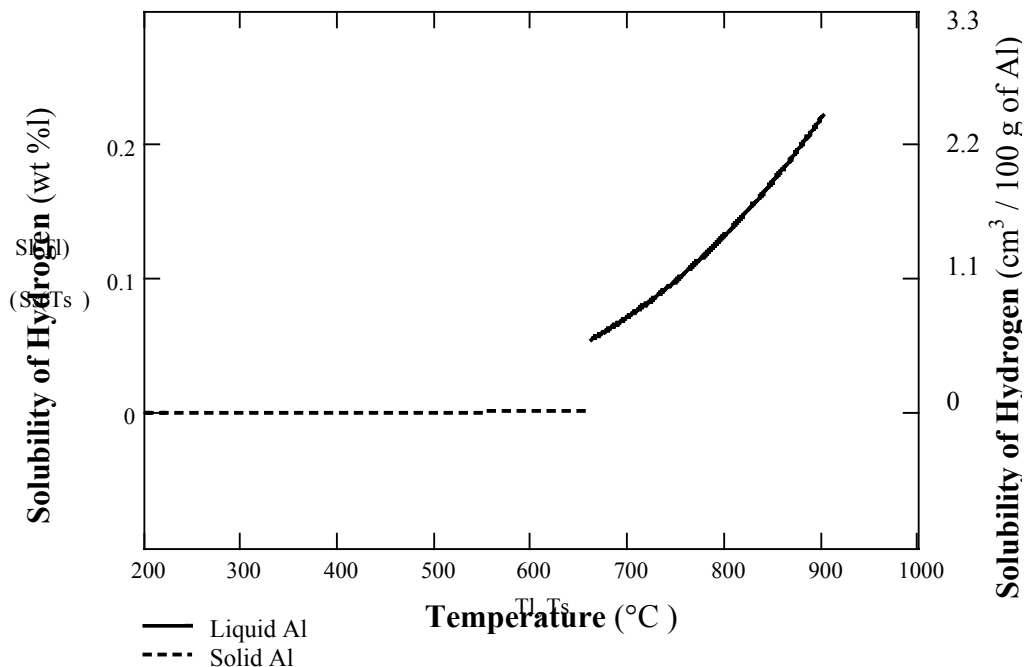


Figure 2.25. Solubility of hydrogen in solid and liquid Al (Adapted from Ransley and Neufeld, 1947/1948 and Eichenauer and co-workers, 1961)

2.4.3. Al-Ti System

Comprehensive study on Al-Ti systems has been carried out by Murray (1987) and equilibrium phase diagram of this binary system is given in Fig. 2.26. Similar diagrams have been proposed by Schuster et al. (1990), Kaltenbach et al. (1989) and Kattner et al. (1992). It is observed from the proposed phase diagrams that there are at least four different important intermetallics formed by these metals: Al₃Ti, Al₂Ti, AlTi, AlTi₃.

α -Ti has almost 5 wt % (i.e. 10 at. %) of Al solubility at 500°C. AlTi₃, i.e. α_2 phase, AlTi, i.e. γ phase, (Ohnuma et al., 2000) are the most widely examined phases in the system. Al₃Ti intermetallic, which is defined as a very brittle phase by Fu et al. (2000), has acicular shape (Wu et al, 2000) when precipitates in a matrix of Al. High Al content portion of the system is shown in Fig. 2. 27.

Al-Ti intermetallics may form in many ways. Commonly, formation is observed during casting of Al-Ti mixtures. Casting is used to obtain α_2 phase (AlTi₃), and γ phase (AlTi) by starting elemental materials in the related amounts (Cao et al., 2002; Chu et al., 2003; Romankov et al., 2002). Moreover, mechanical alloying is another process during which Al-Ti intermetallics form. Moon et al (1998, 1999) and Fadeeva et al. (1998) used ball mill to obtain Al-Ti intermetallics.

It is reported by various authors that Al-Ti intermetallics may form according to following exothermic reactions (Gaus et al., 2000; Travitzky et al., 2003; Tjong et al., 2003; Horvitz et al., 2002)



For the formation of Al₃Ti, Peng et al. (1997) suggested a mechanism. According to this mechanism, first Al reacts with TiO₂ to form Al₂O₃ and leave Ti in its elemental

form. During this reaction, temperature increases extremely, possibly up to 2000°C and simultaneously Ti dissolves into the Al matrix. Subsequently, Al-Ti solution solidifies and phases form according to phase diagram, firstly Al_3Ti forms into the liquid. Below 665°C, Al_3Ti needles precipitate in the structure. Moreover, when cooled fast some amount of Al_2Ti phase may be observed. Gaus et al. (2000) and Mackowiak (1959) indicate that reaction between Al and TiO_2 is very complicated and there are many intermediate steps. Fig. 2.28 is taken from Feng et al. (2000) and shows the microstructure of the Al and TiO_2 after internal reaction.

Hydrogen absorption/desorption capabilities of Al-Ti intermetallics have been investigated within a few years. Hashi et al. (2002) showed that AlTi_3 powder is converted to amorphous AlTi_3H_x alloy at room temperature under H_2 atmosphere in 48 hours. They also indicate that the amount of hydrogen in Al-Ti alloy decreases with increasing Al content of the intermetallic. Another important conclusion drawn by Hashi et al. (2002) is that AlTi , Al_2Ti and Al_3Ti could not absorb hydrogen at the specified absorption conditions.

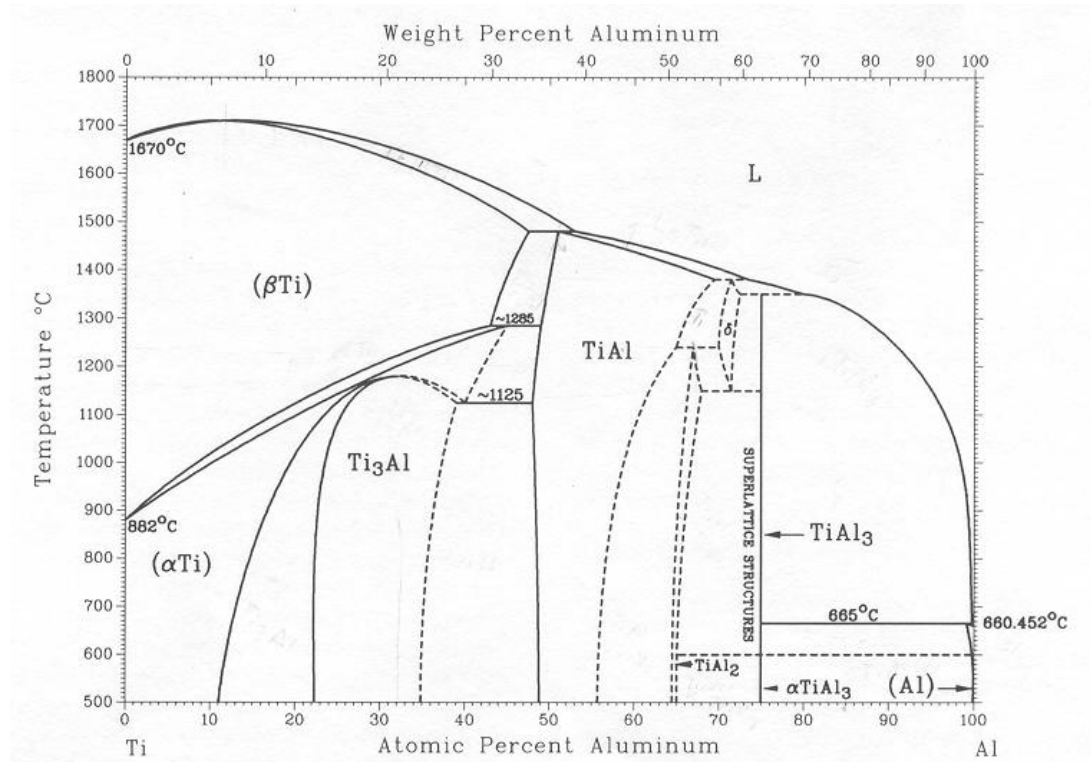


Figure 2.26. Al-Ti Phase Diagram (Muray, 1987)

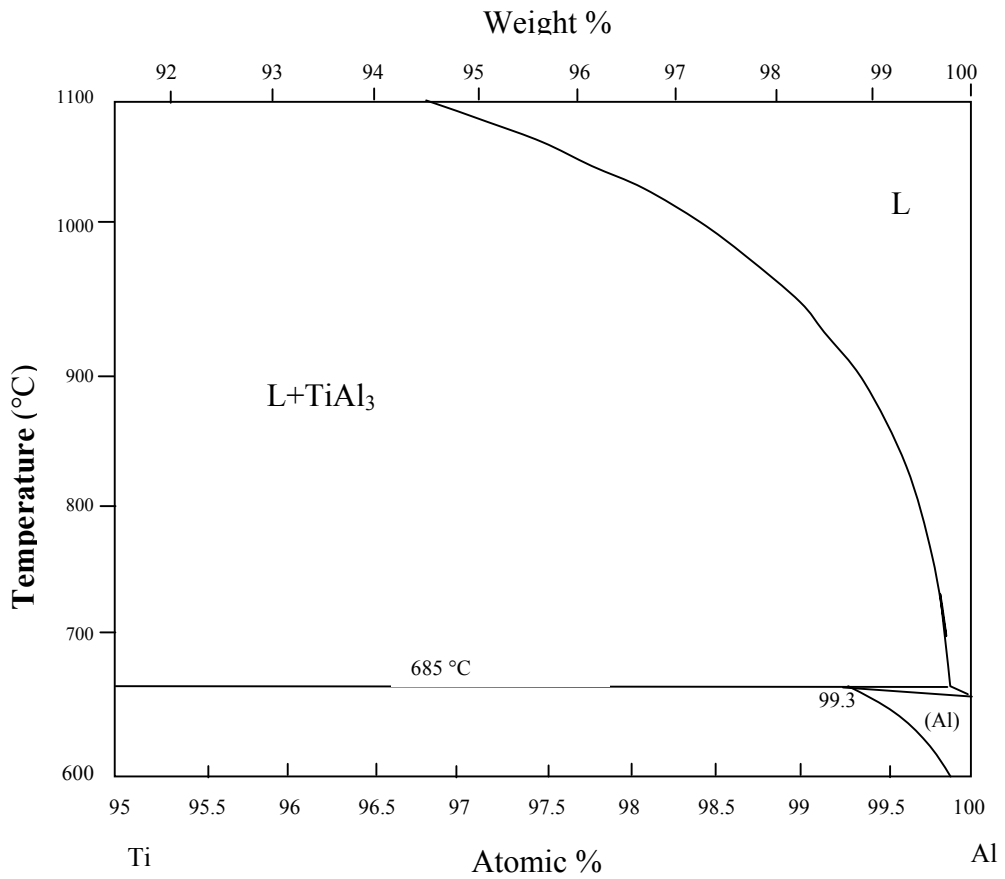


Figure 2. 27. Ti-Al phase diagram in Al rich region (Muray ,1987)

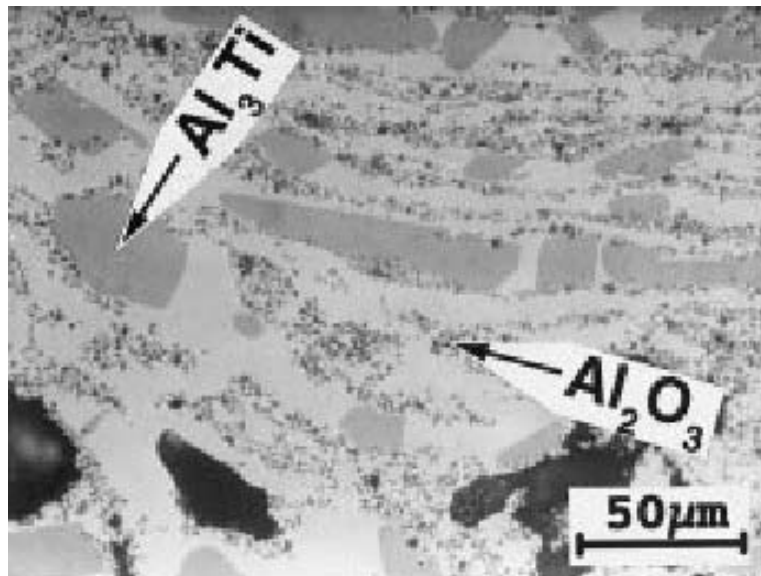


Figure 2.28. Microstructure of Al rich Al-Ti systems. (Feng et al., 2000). Al₃Ti blocks and agglomerated Al₂O₃ particles can be observed in Al matrix

CHAPTER III

EXPERIMENTAL PROCEDURE

3.1. MATERIALS

Pure aluminium (Al) powders were used as base metal. Powders are rounded and spherical in shape as given in Fig. 3.1. Particle size distribution of the Al powder was measured by a particle size analyzer* and result is given in Fig. 3.2. This indicates an average particle size of approximately 37 μm .

Coarse (as-received) and fine (milled) TiH_2 were used in the experiments as foaming agent, Fig. 3.3. Particle size distribution of TiH_2 powders is given in Fig. 3.4. Average particle size is approximately 20 μm for as-received TiH_2 . Milled powder has an average particle size of 3 μm , certain fraction of which (<24%) is agglomerated at approximately 100 μm .

Titanium dioxide (TiO_2) particles were used as stabilizing agent. TiO_2 particles were less than 1 μm , and in highly agglomerated condition, Fig.3.5. Particle size distribution of TiO_2 powders given in Fig. 3.6 also shows that the particles were highly agglomerated with clusters of 140 μm .

3.2. MILLING OF TiH_2

As-received powders were mechanically milled in a ball mill for 24 hours to obtain fine TiH_2 particles. Fig. 3.7 shows the ball mill system in a milling

* Particle size distribution of all powders used in this study was measured by a light scatter type particle size analyzer. Ethyl alcohol was used as dispersion medium, light source HeNe type. Average values given above refer to De Brouckere Mean Diameter, i.e. volume moment mean.

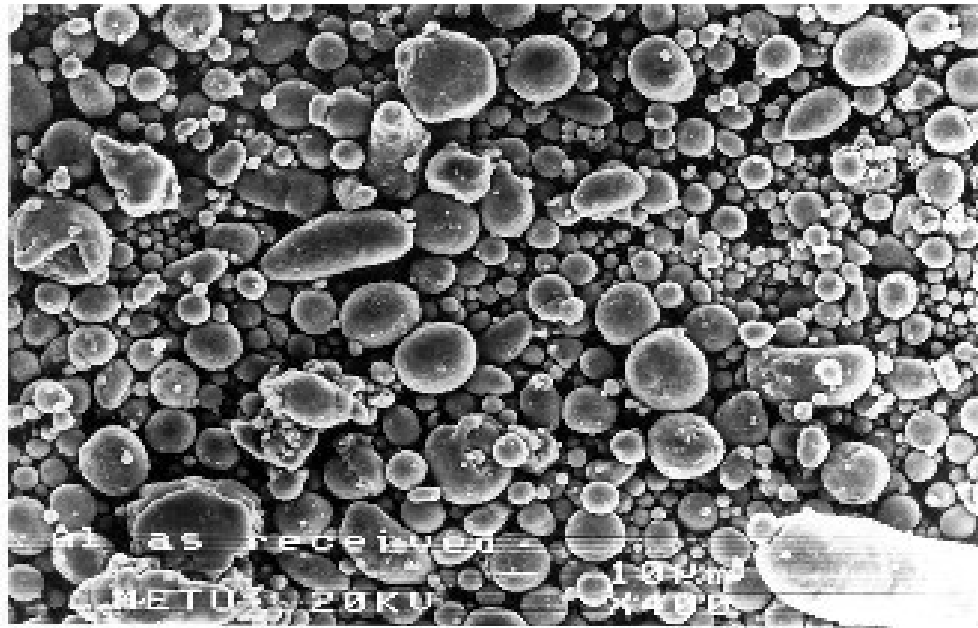


Figure 3.1. Structure of Al powders. Note that Al particles are rounded and mostly spherical in shape

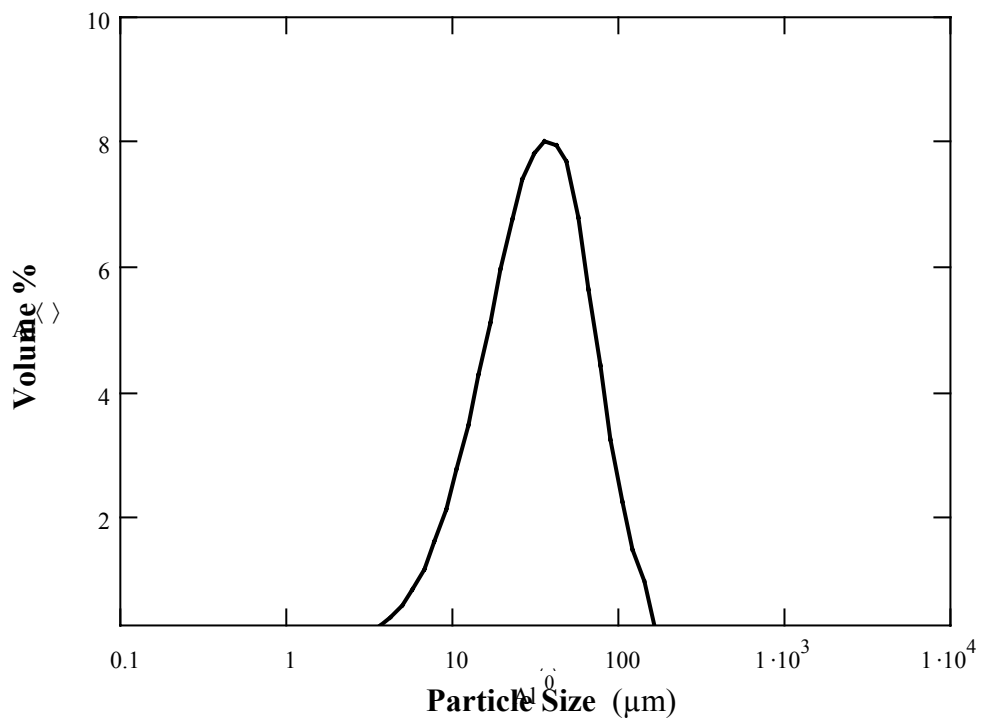


Figure 3.2. Particle size distribution of Al powders. Note that average particles size is $\approx 37 \mu\text{m}$.

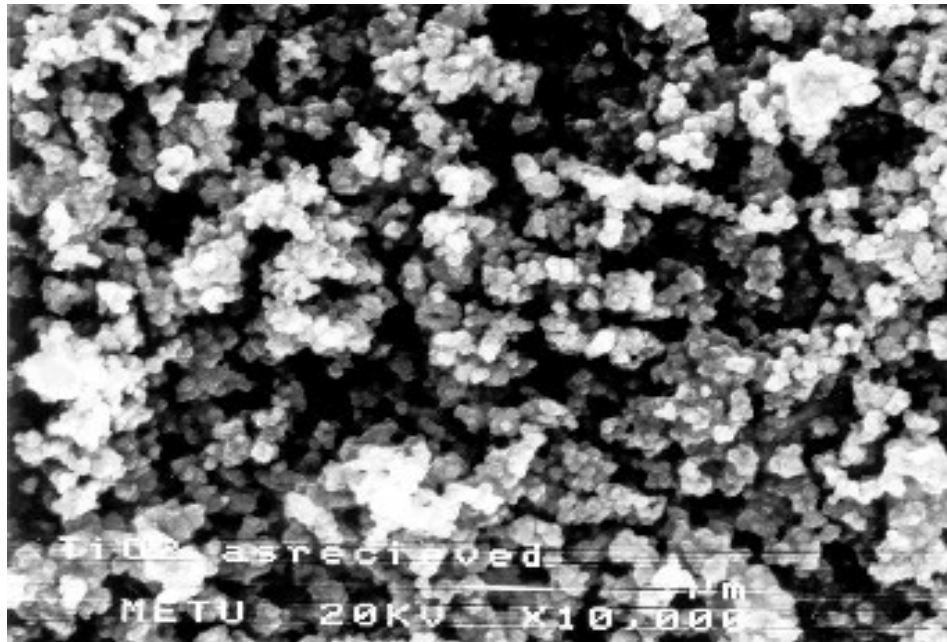


Figure 3.5. Structure of TiO₂ powders. Note that particles are small, in the order of 100nm, but highly agglomerated.

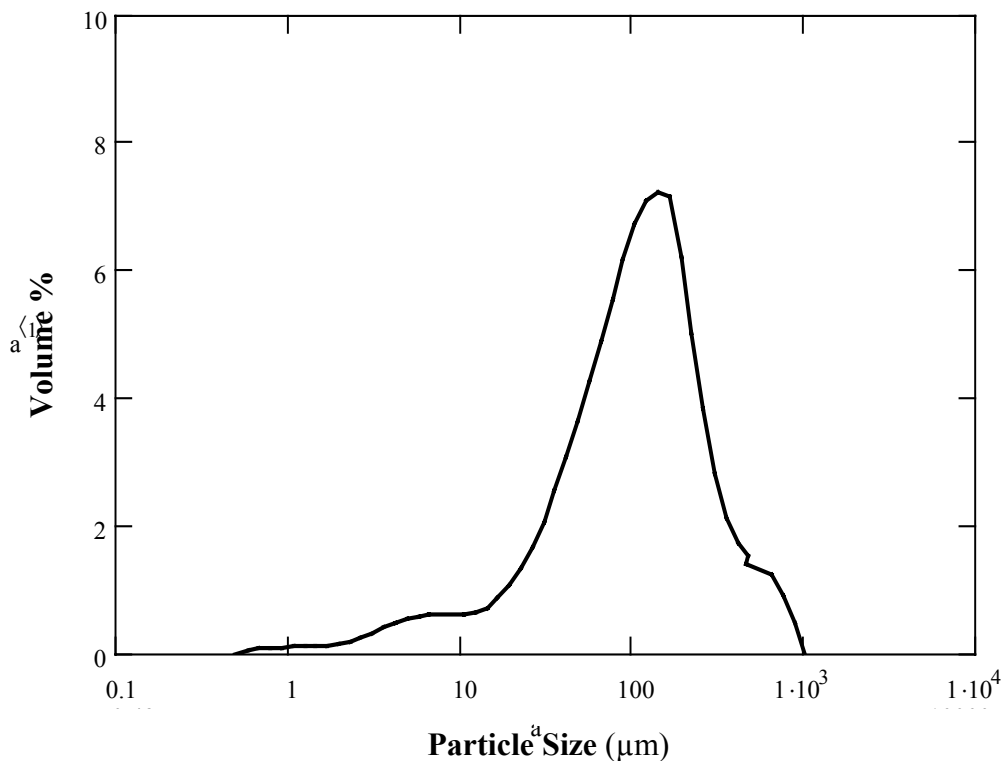


Figure 3.6. Particle size distribution of TiO₂. Distribution shows that particles are highly agglomerated with clusters of $\approx 140\mu\text{m}$.

operation. The mill has an inner diameter of 4 cm and operated at 200 rpm. Steel balls of 6 mm in diameter with 10:1 ball-to-powder ratio was used to mill 3 gm of TiH_2 powder with 1 wt % graphite.

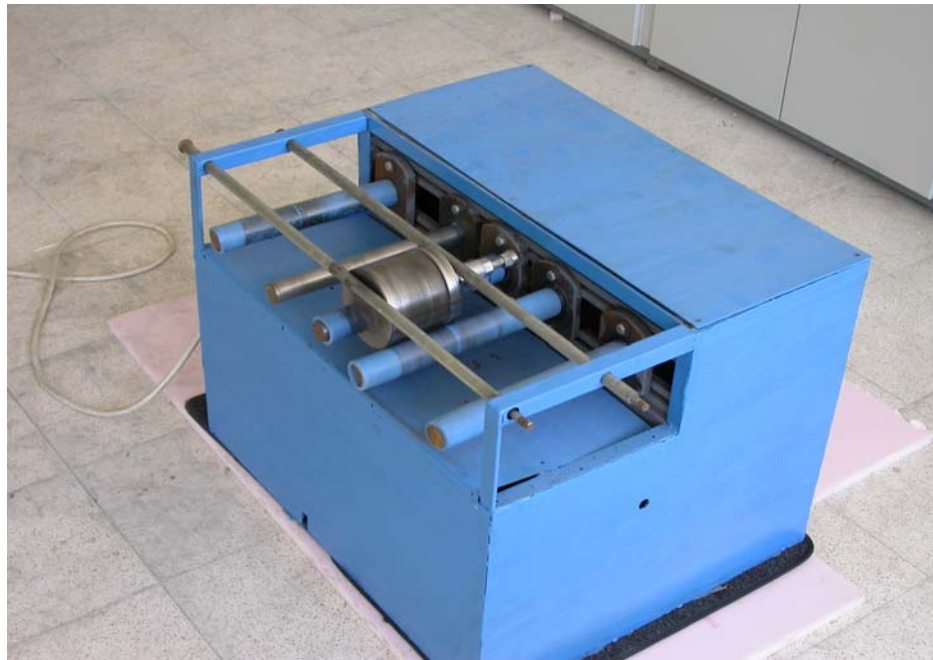


Figure 3.7. Ball mill used in milling of TiH_2 powder.

3.3. MIXING OF POWDERS

Dry mixing of powders was achieved via shaker. Shaker contains two arms with many holders by which the mixing chamber can be attached to it. A plastic bottle with 600cm^3 of volume was used as a mixing chamber. 10 grams of powder mixture was mixed in each batch. 1 hour of mixing with ball-to-powder (B/P) ratio of 1:2 was applied. Steel balls of 6 mm diameter were used in mixing operation. Mixing conditions were selected such that powders did not damage during process, i.e. particle size and shape did not change.

3.4. CONSOLIDATION OF POWDER MIXTURES

Powder mixtures were consolidated via a swagger. For this purpose, previously mixed 10 grams of powder mixture was enclosed into copper tube of 22 mm

diameter with 1 mm thickness. Two sides of copper tube were closed by copper plugs, Fig. 3.8. By this way, powder flow from ends of the tube was prevented. This initial structure was compacted by swagger.

Swaging was carried out in 5 steps: The steps involve decreasing the diameter to 19.75 mm, 15 mm, 11 mm, 8.8 mm and finally to 6 mm. Copper sleeve around the consolidated structure was removed after swaging is complete. Most compacts were hot swaged for which a furnace maintained at 400°C was used. Compacts were returned to furnace after each pass and maintained there for 10 minutes.

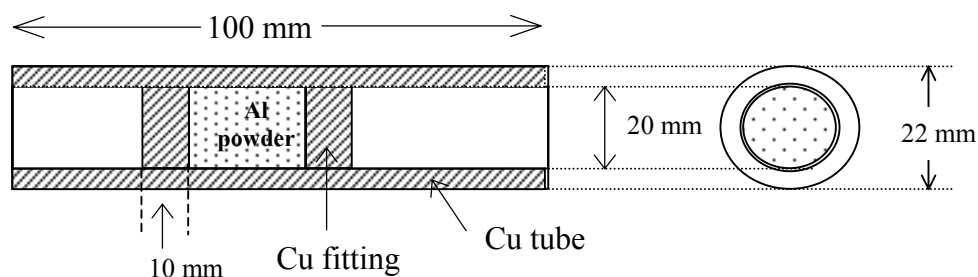


Figure 3.8. Schematic drawing of sample holder used for swaging, see text for details.

3.5. FOAMING OF COMPACT SYSTEMS

Foamable precursors approximately 6 mm in diameter and 10 mm in length were prepared for foaming. Foaming was carried out at temperatures 675°C-800°C and for 1-25 minute. For each system and temperature-time combination, two samples were foamed to see the reproducibility of the foaming process. To use in foaming experiments, a tube furnace was constructed. Photograph and schematic drawing of the furnace is given in Figs 3.9 and 3.10 respectively. The tube is mullite with an internal diameter of 50 mm with 700 mm in length. Both ends of the tube were closed by rubber corks.

The tube is used in connection with a stainless steel mould where the foaming experiments are carried out, see Fig. 3.9. The mould was in the form of steel tube



Figure 3.9. Furnace used in the foaming experiments.

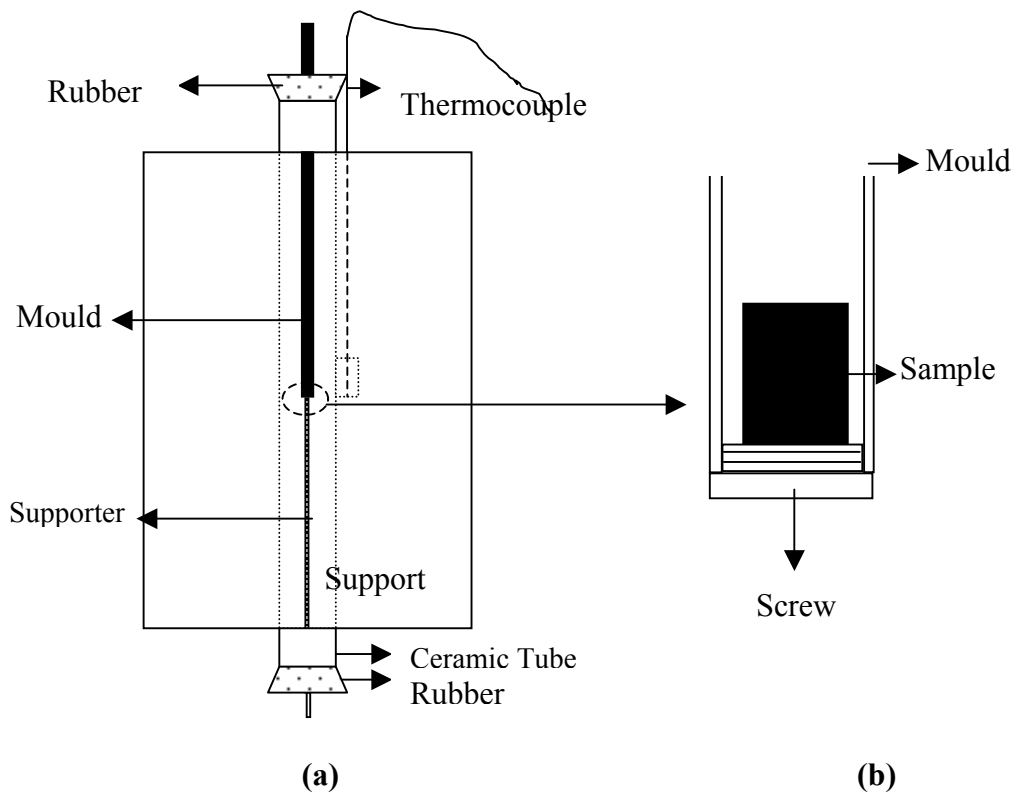


Figure 3.10. Schematic drawing of the furnace and the mould. Kanthal wire, which is not shown in the (a), was wound onto the ceramic tube as heating coil. Enlarged view of the mould is given in (b).

with approximately 8 mm inner diameter and 550 mm in length, the end of which could be closed with a suitable sized screw. The sample is placed at the bottom of the tube just above the screw. The mould passes through the upper cork the height of which is adjusted such that the sample resides at the hot zone. The tube is supported from below by a supporter.

Temperature of the furnace is followed by a thermocouple embedded in the hot zone in-between the heating elements and ceramic tube. The furnace temperature is controlled by $\pm 5^\circ\text{C}$ at the selected temperature by a programmable controller.

To ensure that the mould reaches the selected temperature, another thermocouple is inserted into the mould. As holder reaches the required temperature, i.e. foaming temperature, thermocouple was removed from the mould and sample was dropped into it. Thus, heating rate is quite fast. After foaming time is reached, the mould-tube was removed from the furnace and cooled by blowing air. Foamed samples were removed from the mould by removing the screw.

3.6. SAMPLE CHARACTERIZATION

To find the density of both consolidated and foamed samples, first the volume of the samples were measured by Archimedes principle. This requires that sample should be weighted in air and water.

$$F_{\text{bouncy}} = F_{\text{air}} - F_{\text{water}} \quad (3.1)$$

where F_{air} is the force due to gravity in air, F_{water} is the force due to gravity in water. Eq. 3.1 can be also written as :

$$F_{\text{bouncy}} = (m_h - m_s)g = V_c \cdot \rho_w \cdot g \quad (3.2)$$

or;

$$m_h - m_s = V_c - \rho_w \quad (3.3)$$

then ;

$$V_c = \frac{m_h - m_s}{\rho_w} \quad (3.4)$$

and

$$d_c = \frac{m_h}{V_c} \quad (3.5)$$

where m_h and m_s are the masses of the sample in air and water respectively, ρ_w is the density of water at that temperature and V_c is the volume of the sample.

CHAPTER IV

RESULTS AND DISCUSSION

4.1. FOAMING SYSTEMS

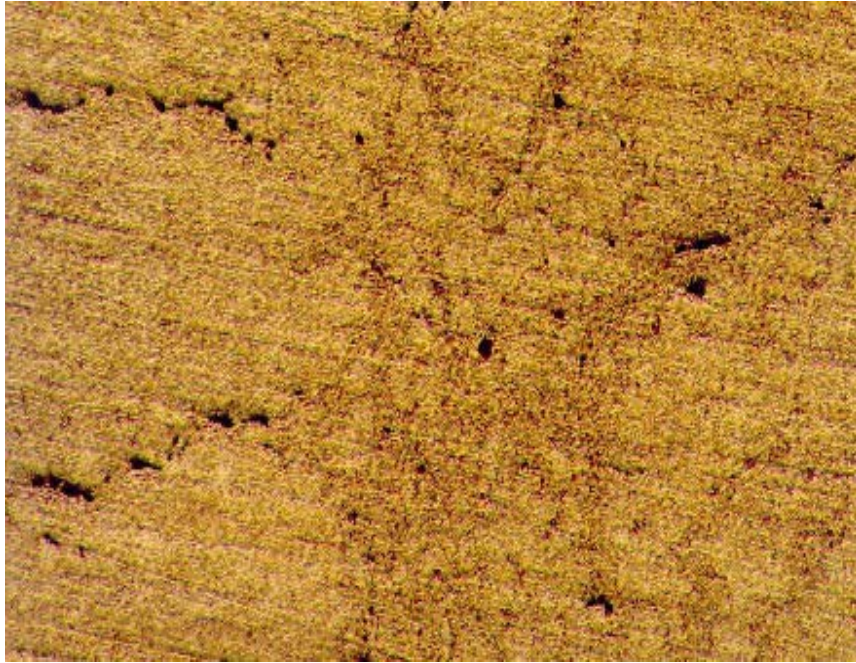
Two Al systems were studied. The first system is composed of Al as base metal and TiH₂ as foaming agent. The other system is TiO₂ stabilized and composed of Al (base metal), TiH₂ (foaming agent) and TiO₂ (stabilizing agent). In both systems, TiH₂ was used in two forms: coarse (20 μ m) and fine (3 μ m). Compositions and other details of the foaming systems are given in Table 4.1.

Table 4.1. Systems used for foaming experiments

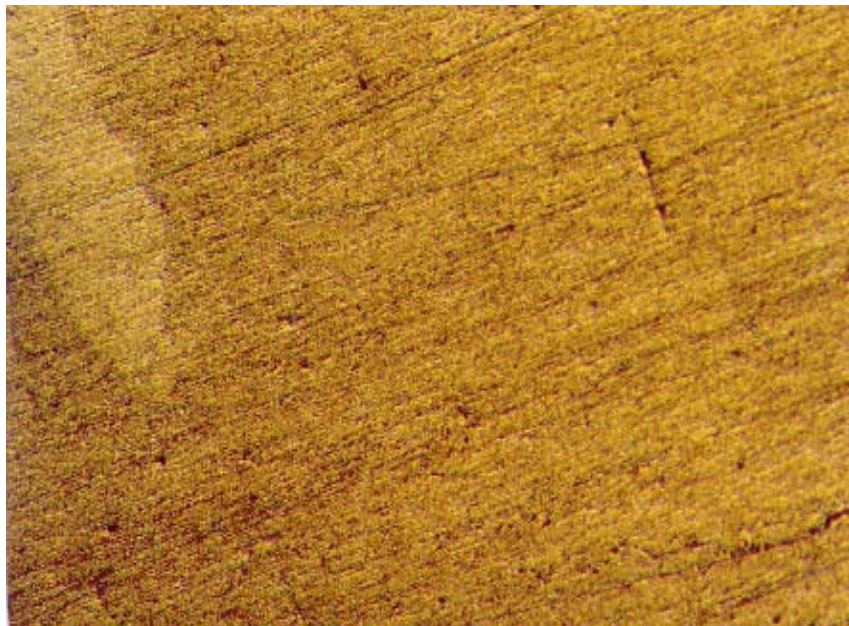
Composition				Foaming Conditions	
System	Base metal	TiH ₂ powder	TiO ₂ powder	Foaming Durations (minute)	Foaming Temperatures (°C)
Pure Al	Al	0.6 wt % coarse	-	1-25	675 & 725
	Al	0.6 wt % fine	-	1-25	675 & 725
TiO ₂ stabilized	Al	0.6 wt % coarse	5 wt %	1-5	750 & 800
	Al	0.6 wt % fine	5 wt %	1-5	750 & 800

4.2. CHARACTERIZATION OF SWAGED POWDER COMPACTS

Structures of the cold swaged and hot swaged samples are given in Fig. 4.1 and Fig. 4.2 for transverse and longitudinal sections respectively. Pores are seen in the cold swaged sample, which are relatively high in concentration at the center.



(a) Cold Swaged



(b) Hot Swaged (400°C)

Figure 4.1. Cold swaged and hot swaged view of pure Al system (X50). The structures in both systems are in transverse direction. Note that cold swaged sample contains high amount of pores.



(a) Cold Swaged



(b) Hot Swaged (400°C)

Figure 4.2. Cold swaged and hot swaged view of pure Al system (X50). The structures in both systems are in longitudinal direction. In the cold swaged sample pores are elongated along swaging direction.

Moreover, pores are elongated along the swaging direction. On the other hand, in hot swaged sample, pores are rare. Thus, hot swaging yields a more compact structure than cold swaging. In fact the measuring after hot swaging of pure Al powder yielded a value of $2.6971 \pm 0.0095 \text{ g/cm}^3$. This is very close to the full density, i.e. 2.6981 g/cm^3 (Straumanis and Ejima, 1960). Densities were also measured for each individual samples before foaming. There were variations in there values obtained, which may be due to small size of the sample as well as other uncertainties. Densities obtained are plotted against volume expansion regardless of composition, foaming temperature and time and are given in Fig. 4.3. It is seen clearly that there is a correlation between the amount of foaming and the density after consolidation. Thus, for a successful foaming, successful consolidation with values close to theoretical density is a critical step. This observation is consistent with the work of Duarte et al. (2000)

It can be concluded that hot swaging as a technique of compaction yields density values close to full density and therefore quite suitable as a method of processing for foaming. Moreover, it is verified that high level of compaction is the primary requirement for high amount of foaming.

Typical macrostructures in hot swaged pure Al samples are given Fig. 4.4. Size difference between coarse and fine TiH_2 is clearly observed, when Fig. 4.4(a) and 4.4(b) are compared. Overall TiH_2 distribution is quite uniform in pure Al systems for coarse as well as for fine of TiH_2 addition.

Similarly, Fig. 4.6 shows macrostructures of TiO_2 stabilized system. In these macrostructures the distribution of TiH_2 is uniform as before, but some localized cloud-like regions, with a size of $10\mu\text{m}$, are observed. Fig. 4.7 shows a view from the TiO_2 stabilized system, in the longitudinal direction. Elongation of the grains along swaging direction (upwards in the picture) and accumulation of the TiO_2 powders are clearly observed. Structure indicates that TiO_2 powders are squeezed between the Al grains. Point analysis of these regions showed that they contain Ti and O, which

indicate that they are agglomerated TiO_2 powders probably distributed into a cloud like morphology as a result of swaging.

Microstructural examination showed that TiH_2 particle might fracture during swaging. An example is given in Fig. 4.5. Similar observations were reported by Öztürk et al. (1994) where hard phase embedded into soft metal fracture into pieces when heavily deformed.

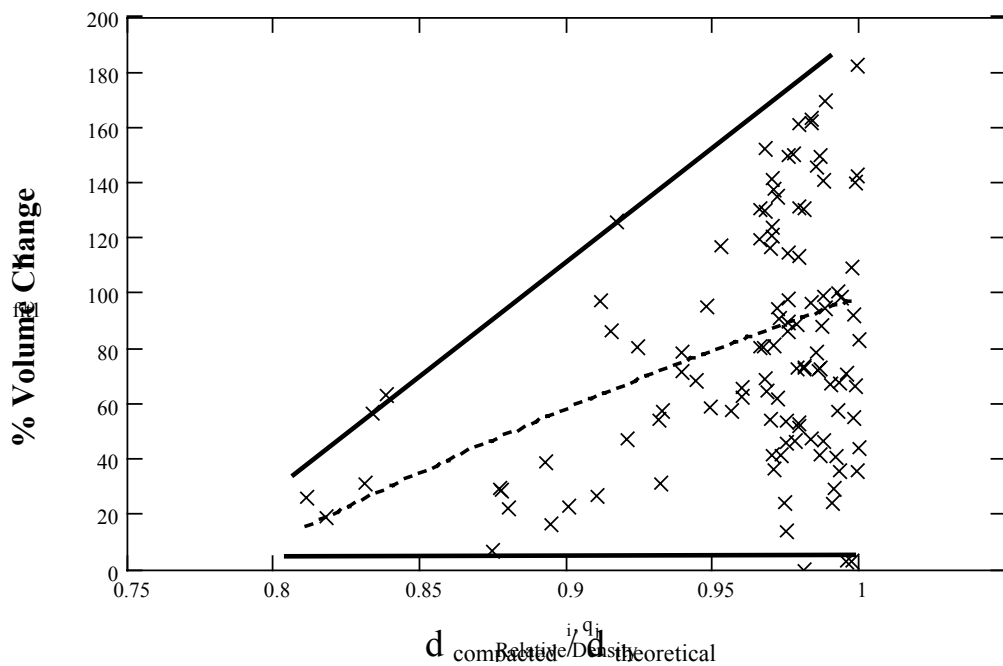
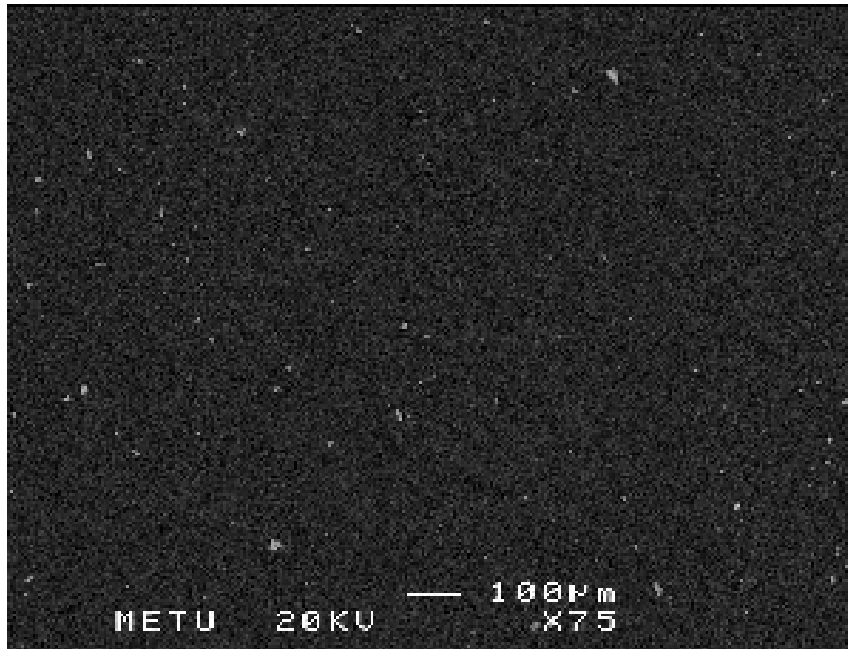


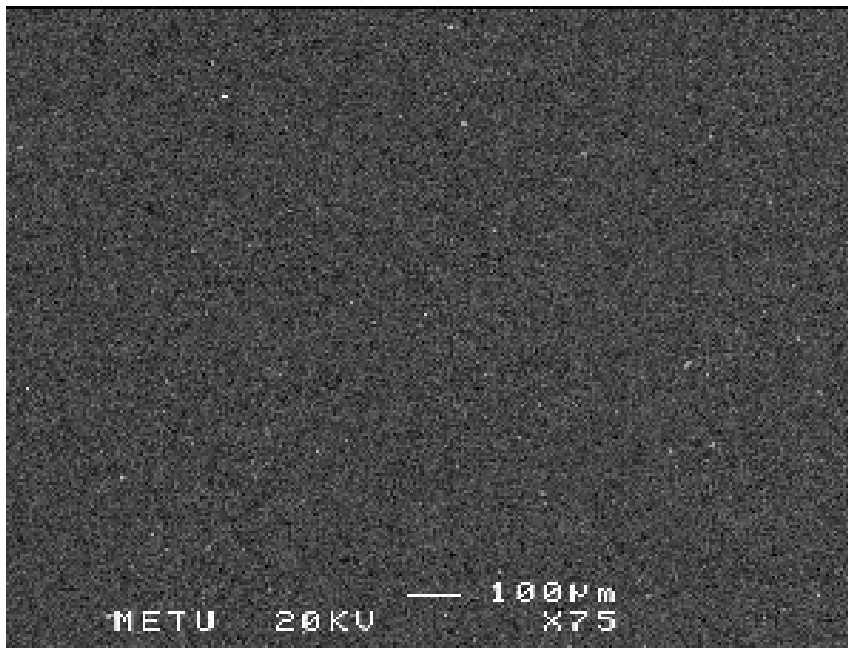
Figure 4.3. Swaged density versus volume expansion in foaming. Note that volume expansion obtainable after foaming tends to increase with increase in the density of the swaged sample. Boundaries show the possible density - % volume change range for pure Al and Al-5 wt % TiO_2 .

4.3. FOAMING OF PURE ALUMINIUM

Fig. 4.8 shows the % volume change of samples foamed at 675°C for coarse TiH_2 addition in which the data are shown by points and the curve is the trend line. It is observed that the amount maximum foaming is approximately 160 %. Fig. 4.9 show the % volume change of samples foamed at 675°C for fine TiH_2 addition. It is observed that maximum amount of foaming is approximately 90 %.



(a)



(b)

Figure 4.4. Structure of hot swaged pure Al samples. (a) with coarse TiH_2 (b) with fine TiH_2 . Structures refer to transverse section of the samples and obtained in back-scattered mode. TiH_2 particles appear as bright spots or regions. In both systems TiH_2 particles are uniformly distributed.

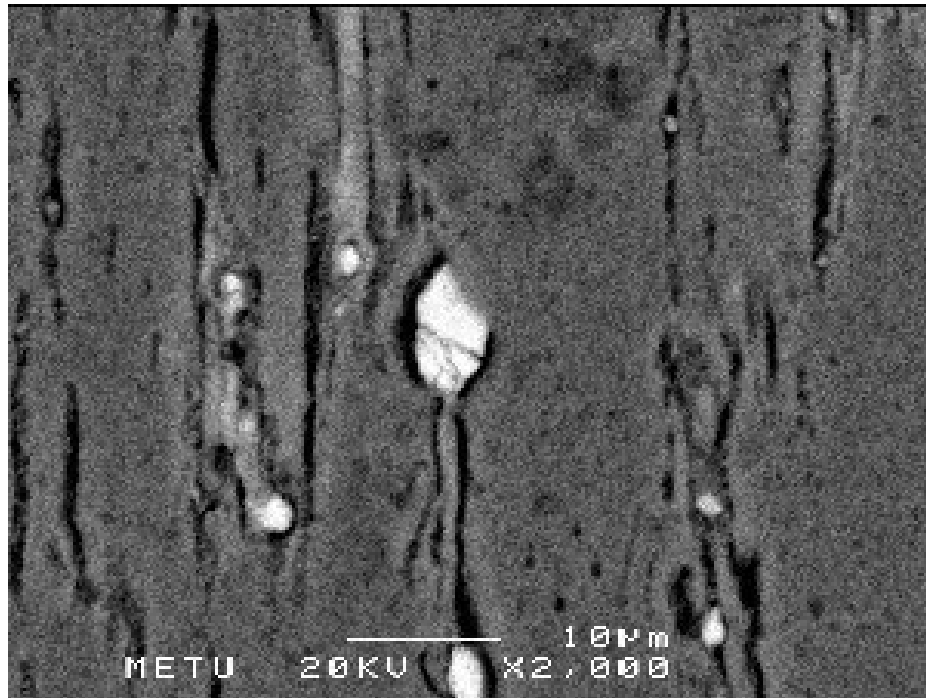
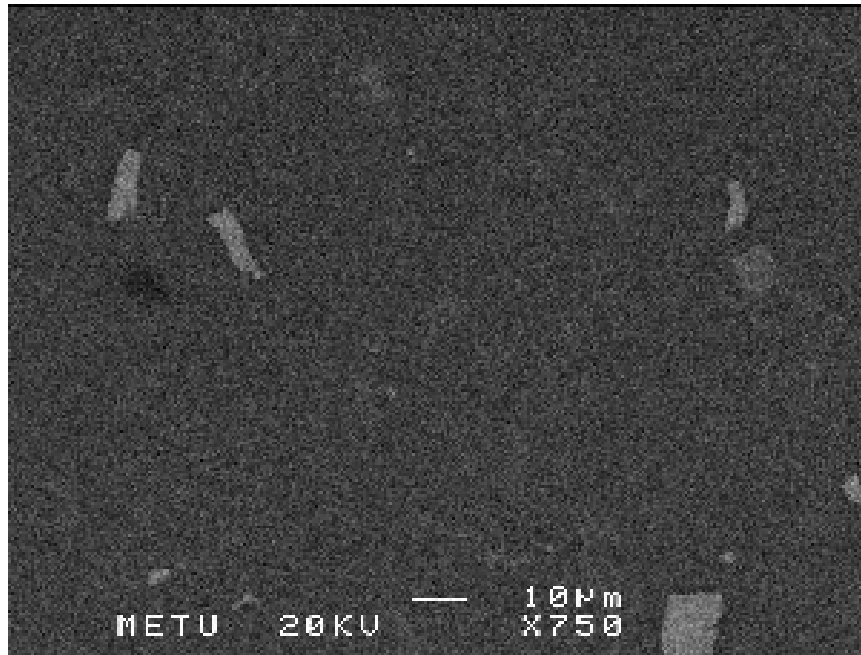


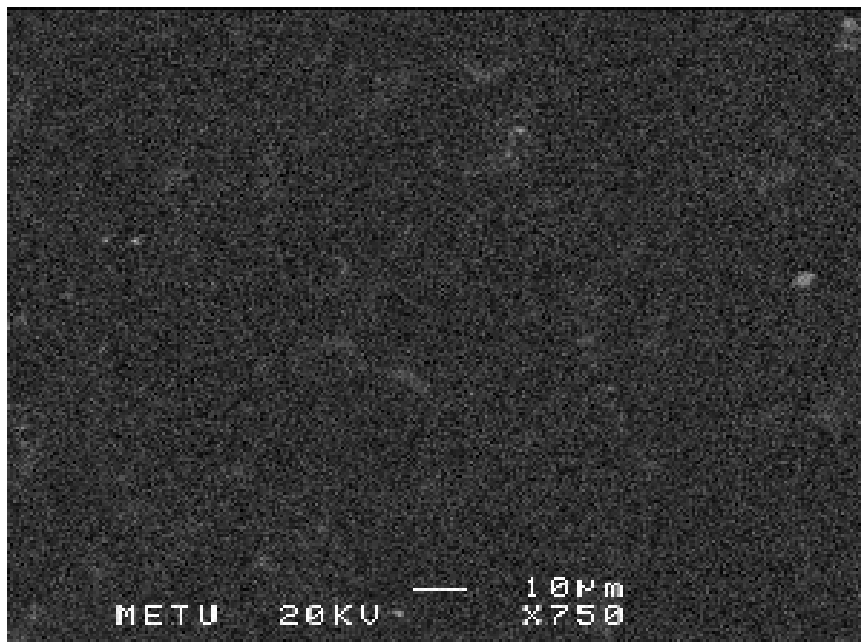
Figure 4.5. Structure of hot swaged oxide stabilized Al. Note cracking of TiH_2 particle.

The related macrostructures are given in Figs 4.10, 4.11. It can be seen that in both fine and coarse TiH_2 added samples, only pore initiation is observed within 3 minutes in the upward direction, i.e. perpendicular to swaging direction. For coarse TiH_2 added system, foaming effectively occurs after 4 minute and pore coalescence and gas loss through top of the sample are observed after 5 minute. In the case of fine TiH_2 addition, pore growth is not observed up to 5 minute.

Results of the % volume change of samples foamed at 725°C are given in Figs 4.12, 4.13. Graphs indicate that maximum amount of foaming is reached within 2 minutes with foaming amount of approximately 180 % for both coarse and fine TiH_2 added systems. Macrostructural observations given in Figs 4.14 and 4.15 indicate that foaming suddenly occurs after 1 minute. After 2 minute of foaming, however, foaming ends up with some pore coalescence and gas loss. It is interesting to see that in fine TiH_2 addition, pores are smaller than those with coarse TiH_2 addition, although both samples have some pore coalescence.



(a)



(b)

Figure 4.6. Structure of hot swaged oxide stabilized Al samples. (a) with coarse TiH_2 and (b) with fine TiH_2 . The structures refer to transverse section and obtained in back-scattered mode.

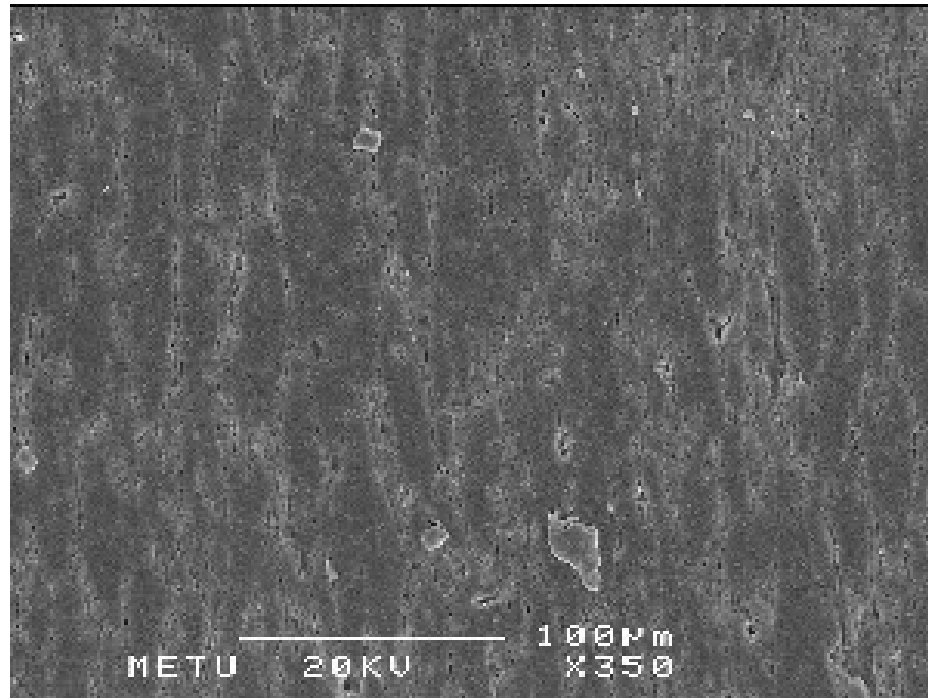


Figure 4.7. Structure of hot swaged oxide stabilized Al samples in longitudinal section. Note that Al grains are elongated and that TiO₂ (bright diffuse regions) in agglomerated form are entrapped within grains.

It can be concluded from the experiments that foaming is temperature dependent for pure Al in some extent. Moreover kinetic is also temperature dependent, i.e. maximum obtainable foaming amount is reached in a shorter duration at high foaming temperatures.

Experiments indicate that the size of TiH₂ particle affects the amount of foaming especially at low foaming temperatures. Macrostructural observations showed that as-swaged samples contain very coarse TiH₂ particles as given in Fig. 4.4, whereas foamed structures, given in Fig. 4.16, contain only 10-15 µm scale "TiH₂" particles. It is possible that small particles could not form bubbles and thus remain in the structure in between the pores but large ones could produce gas bubbles and therefore entrapped inside the bubble.

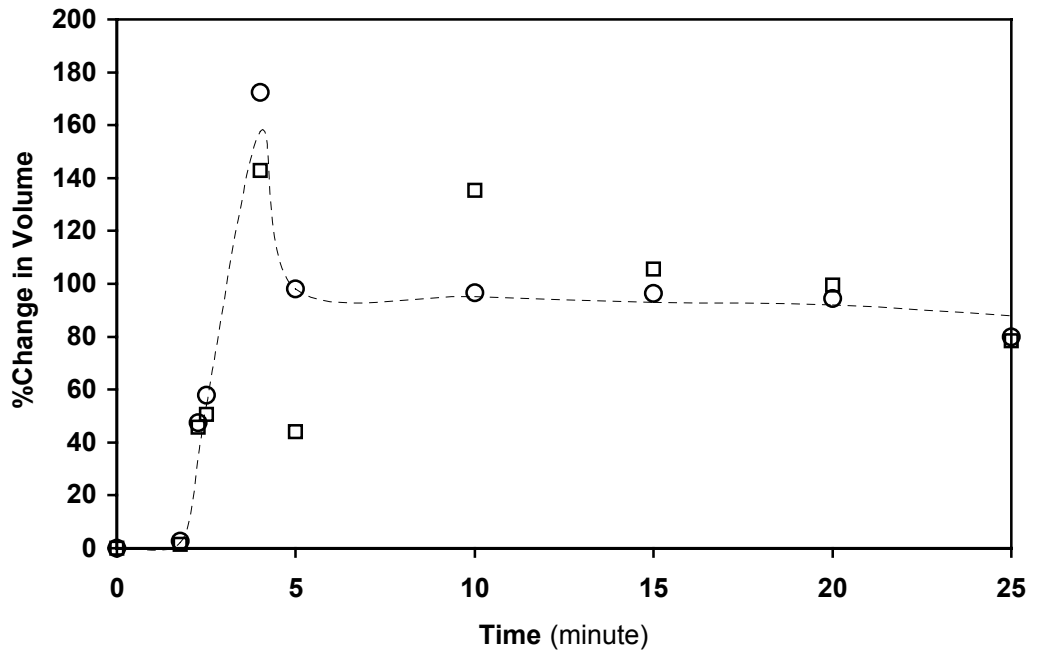


Figure 4.8. Foaming of pure Al with 0.6wt % coarse TiH₂ at 675°C.

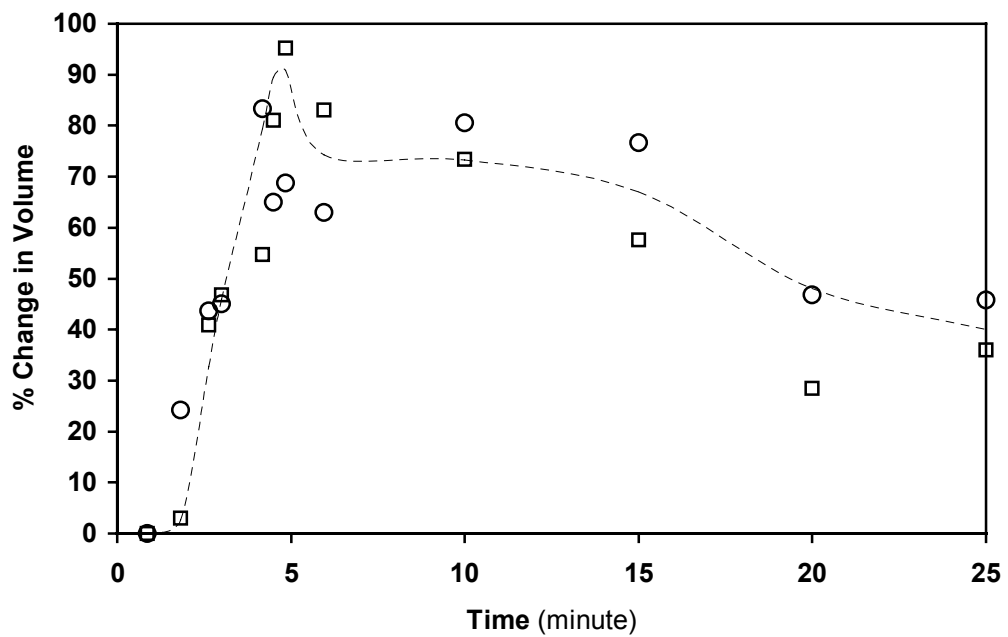


Figure 4.9. Foaming of pure Al with 0.6 wt % fine TiH₂ at 675°C.



(a) 1 minute



(b) 2 minute



(c) 3 minute



(d) 4 minute



(e) 5 minute



(f) 15 minute

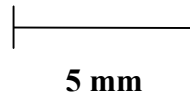


Figure 4.10. Macrostructures of pure Al foamed with coarse TiH_2 at 675°C . Note that pores initially form parallel to longitudinal direction. Note also that pore coalescence after 4 minutes.

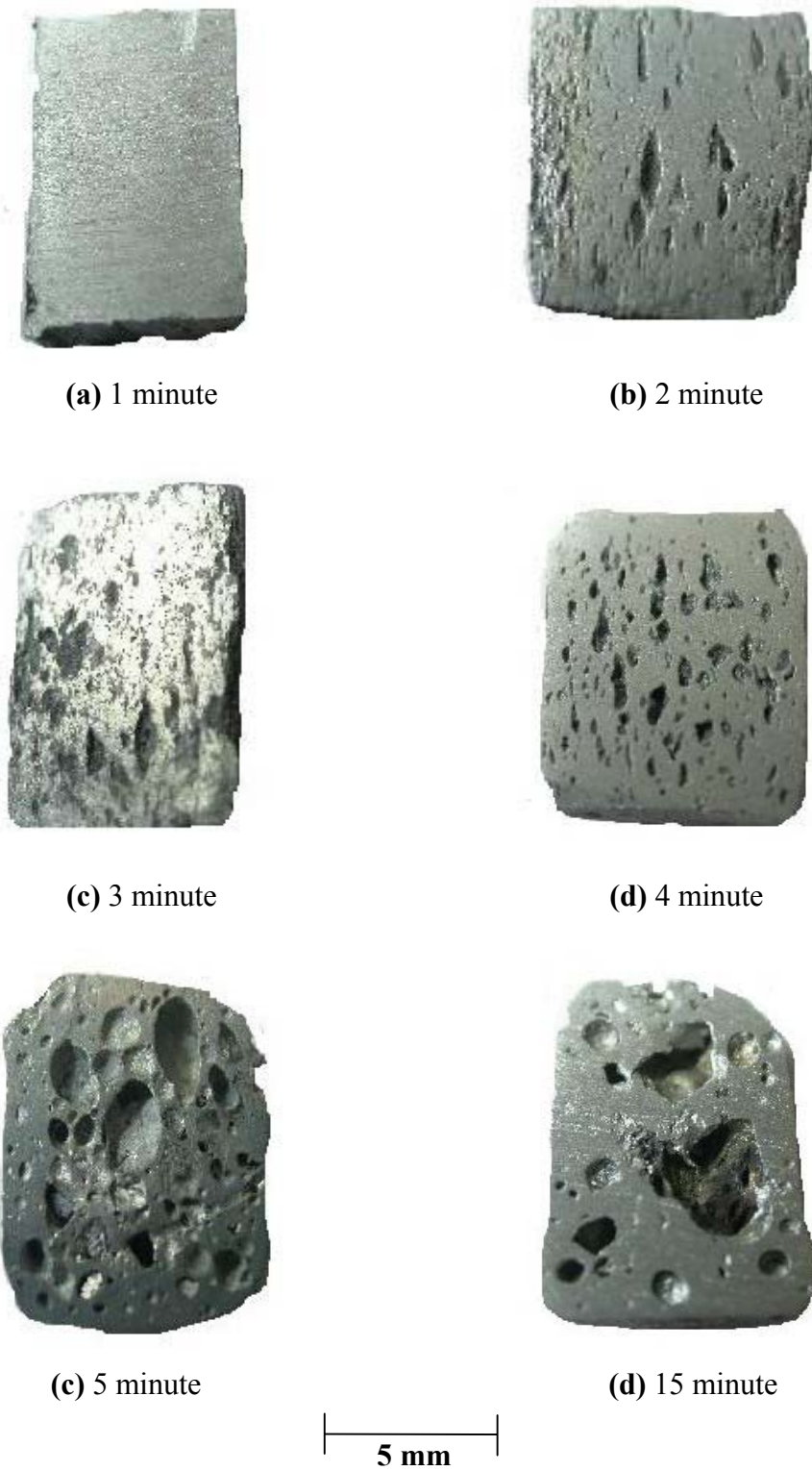


Figure 4.11. Macrostructures of pure Al foamed with fine TiH_2 at 675°C . Note that acceptable macrostructure is achieved after 4 minutes.

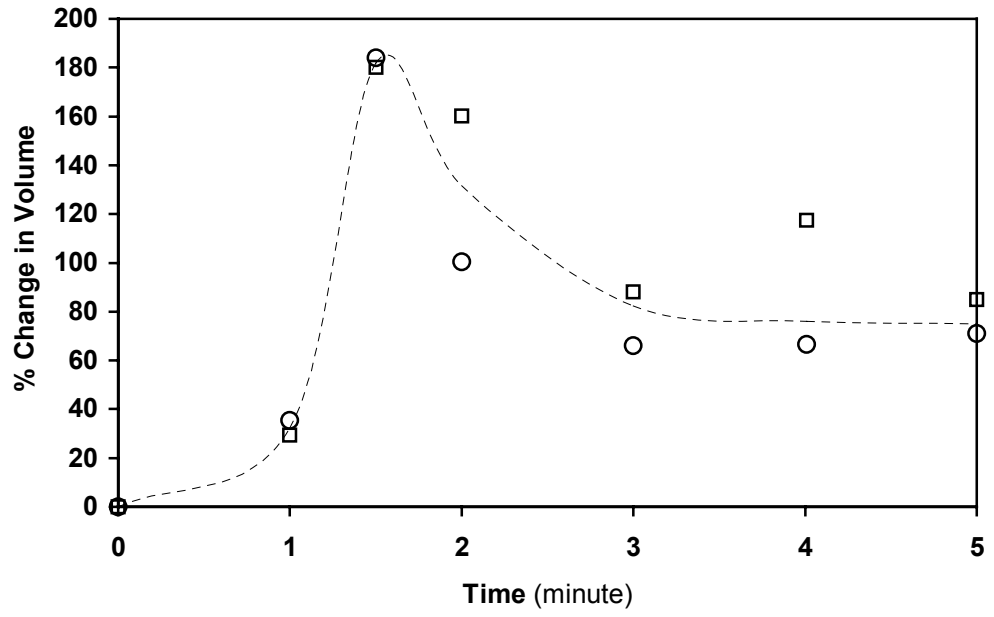


Figure 4.12. Foaming of pure Al with 0.6 wt % coarse TiH₂ at 725°C.

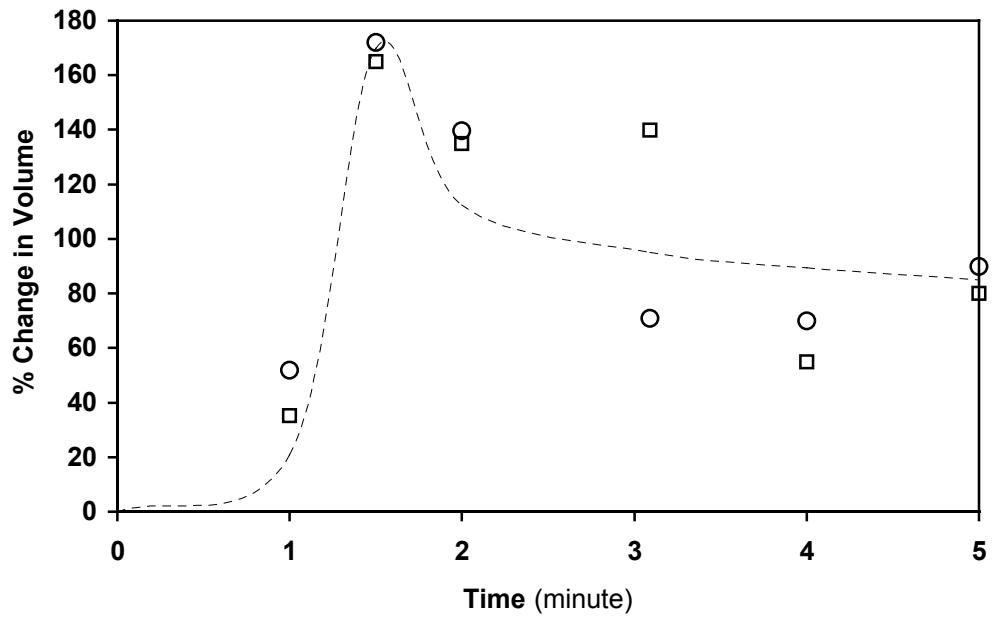


Figure 4.13. Foaming of pure Al with 0.6 wt % fine TiH₂ at 725°C.



(a) 1 minute



(b) 1.5 minute



(c) 2 minute



(d) 3 minute



(e) 4 minute

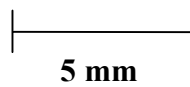


Figure 4.14. Macrostructures of pure Al foamed with coarse TiH_2 at 725°C . Note that acceptable macrostructure is achieved after 1.5 minutes of foaming whereas the system collapses then.



(a) 1 minute



(b) 1.5 minute



(c) 2 minute



(d) 3 minute



(e) 4 minute

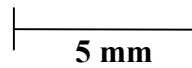
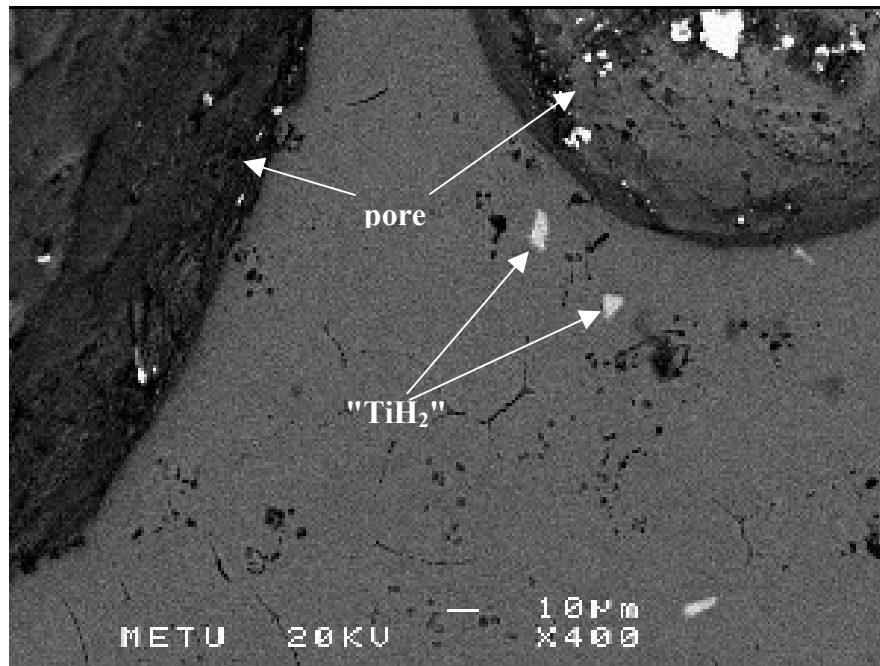
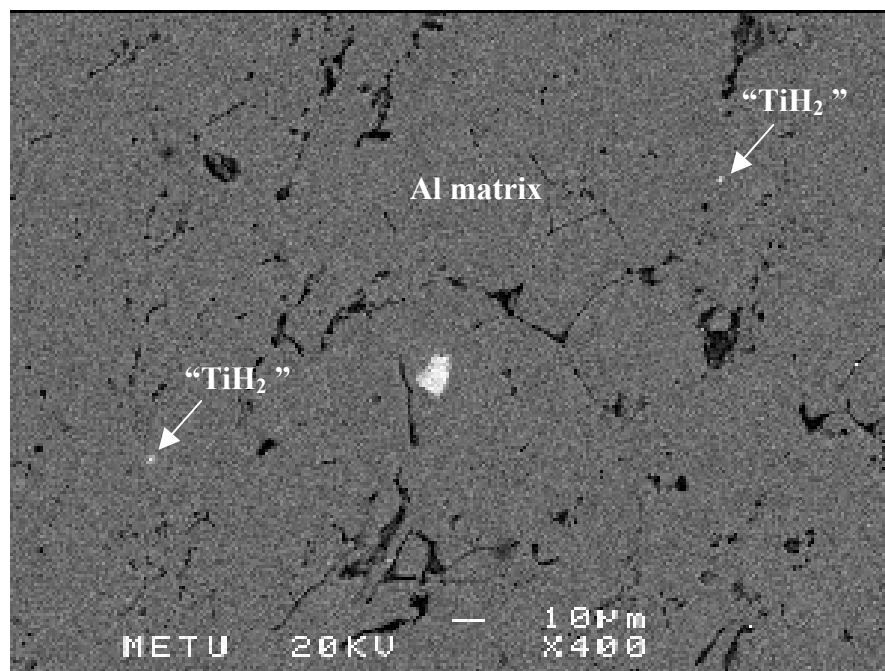


Figure 4.15. Macrostructures of pure Al foamed with fine TiH_2 at 725°C . Note that pore coalescence occurs after 1.5 minutes with some coalescence and gas loss.



(a)



(b)

Figure 4.16. Structure of pure Al foamed with coarse TiH_2 at 675°C . (a) shows coarse " TiH_2 " particles ($12\mu\text{m}$) close to a pore ; (b) shows presence of fine " TiH_2 " particles in the same sample

4.4. A MODEL FOR FOAMING OF PURE ALUMINIUM

In foaming of pure Al by TiH₂ decomposition, three physical parameters characterize the foaming system: pressure inside the gas bubble (P_{in}), pressure against the gas bubble (P_{ext}), and equilibrium pressure of hydrogen over the TiH₂ (P_{eq}). Equations given for these parameters in section 2.3 and 2.4 are repeated below.

P_{ext} is the pressure necessary to maintain the bubble with a diameter r . The quantity depends on the pressure due to surface tension P_s , hydrostatic pressure caused by the weight of the liquid P_h , and atmospheric pressure P_a :

$$P_{ext} = P_a + P_h + P_s \quad (4.1)$$

where $P_s = 2\gamma/r$, $P_h = \rho gh$, $P_a = 1\text{atm}$

here, γ is surface tension, r is the radius of the bubble, ρ is the density of the aluminium, g is the gravitational acceleration and h is the height of the liquid aluminium over the bubble.

P_{in} is the pressure generated by hydrogen gas released by TiH₂ enclosed to a pore of radius r . P_{in} depends on the quantity of hydrogen, n_{H_2} and temperature.

$$P_{in} = \frac{3 n_{(H_2)} \cdot R \cdot T}{4\pi r^3} \quad (4.2)$$

P_{eq} is the equilibrium pressure of hydrogen, above which hydrogen release stops. As it is indicated by Mueller (1968), it is a function of temperature and for TiH₂ it can be written as:

$$\ln P_{eq} = \frac{-19821}{T} + 21.671 \quad (4.3)$$

Relations between these parameters determine the pore initiation and its growth.

4.4.1. Pore Initiation / Critical Particle Size of Foaming Agent

Bubble nucleation is the starting point of the foaming process thus should be considered first. Fig. 4.17 gives the schematic variation P_{ext} with the diameter of the pore. Since at the nucleation stage pore diameter is equal to particle size, this is also the particle diameter. P_{ext} is quite large at small values of particle/pore sizes. P_{eq} is also shown on the figure. For a given temperature, P_{eq} is constant therefore it appears as a horizontal line. For TiH_2 to release its hydrogen, pressure over the hydride should less or equal to P_{eq} . Thus, where $P_{\text{ext}} > P_{\text{eq}}$ hydrogen is not released so no pores are formed. For pore to nucleate $P_{\text{ext}} \leq P_{\text{eq}}$ and where $P_{\text{ext}} = P_{\text{eq}}$, intersection point in Fig. 4.17, is the critical particle size, d_n , for pore nucleation. Thus, for a given temperature only particles larger than d_n can release their hydrogen to form bubble.

Ignoring hydrostatic pressure and atmospheric pressure, P_{ext} can be written as:

$$P_{\text{ext}} = P_s = \frac{2\gamma}{r} \quad (4.4)$$

where γ is the surface tension and r is the pore radius.

By ignoring the effect of temperature on surface tension, d_n values are calculated for various values of surface tension. Values assigned varied form 0.45-3.6 N/m of which 0.90 N/m may be considered typical for pure Al. Results are shown in Fig. 4.18 and tabulated in Table 4.2, which referred to 675°C. It is observed that the effect of surface tension is quite pronounced on d_n .

Critical particle sizes were obtained for 675 °C and 725°C for the real Al system. For this, the real value of Al surface tension and its dependence on temperature is used. Results are given in Fig. 4.19. Graph indicates that P_{ext} curves at 675°C and 725°C are almost the same, indicating that the change of surface tension is of little concern within this temperature range. Critical particle size for pore initiation is, however, a strong function of temperature due to its effect on P_{eq} . Temperature dependency of d_n for pure Al system is given in Fig. 4.20.

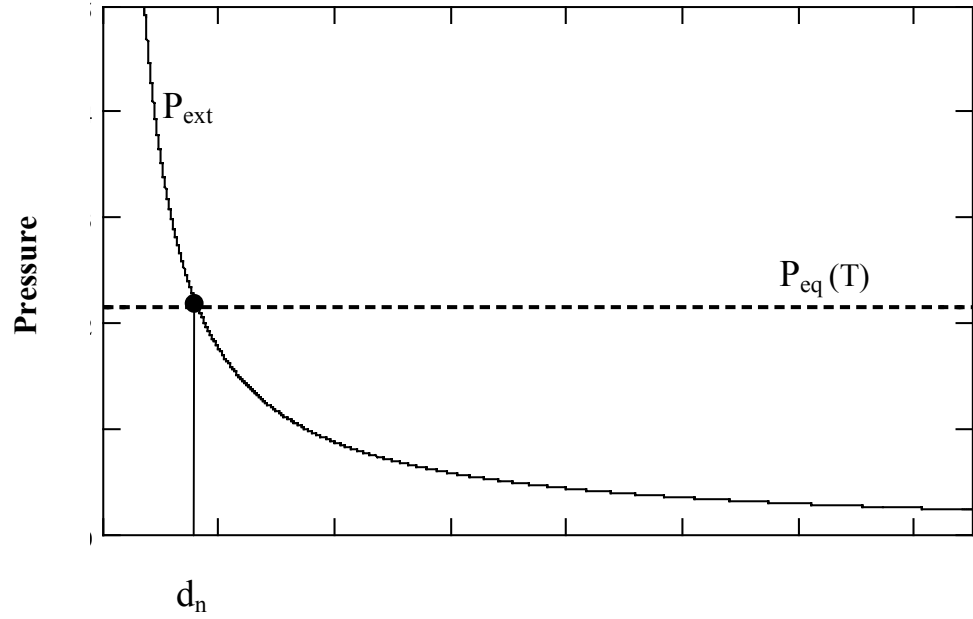


Figure 4.17. Schematic variation of P_{ext} and P_{eq} with pore size. P_{eq} is constant at a given temperature. Intersection point is called as critical particle size (d_n).

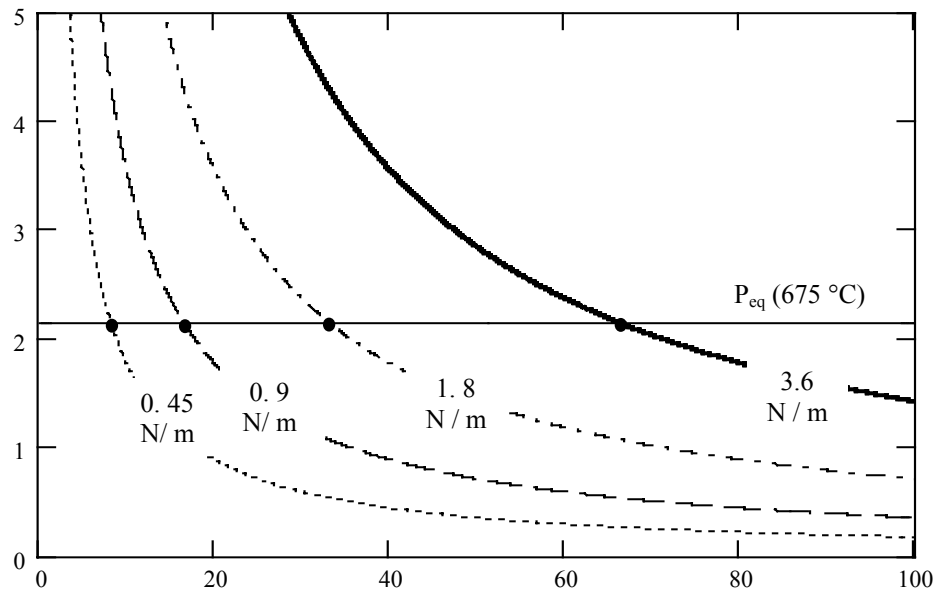


Figure 4.18. Critical particle sizes (d_n) for pure Al for different values of surface tension. The values are calculated for foaming at 675 °C. Note that with lower values of surface tension, minimum size of TiH_2 particle that can nucleate bubbles decreases.

Table 4.2. Critical particle sizes (d_n) for different surface tension values at 675 °C

Surface Tension (N/m)	0.45	0.90	1.80	3.6
d_n (μm)	8.2	16.5	33.1	66.2

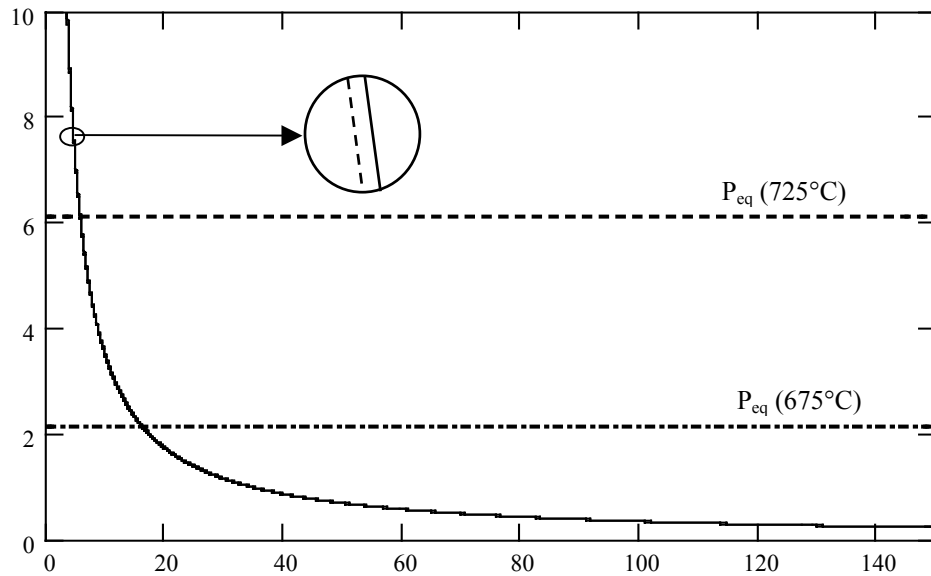


Figure 4.19. Critical particle sizes (d_n) of pure Al systems for 675°C (dashed curve) and 725°C (continuous curve). Note that P_{ext} are almost the same for 675°C and 725°C.

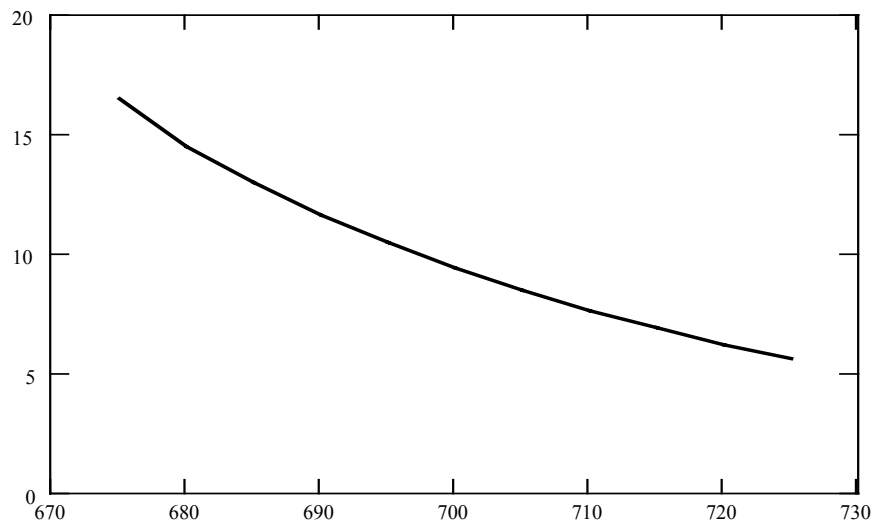


Figure 4.20. Critical particle sizes (d_n) of pure Al system for different temperatures. Note that critical particle size decreases as the temperature increases.

4.4.2. Equilibrium* Pore Size

With reference to Fig. 4.17, equilibrium pore size may be defined by introducing a new parameter P_{in} , in addition to the existing parameters P_{ext} and P_{eq} . P_{in} is the pressure generated by released hydrogen. The value of P_{in} depends on the mole of hydrogen released, the size of the pore and temperature.

For various levels of hydrogen release, the variation of P_{in} are superimposed on Fig. 4.17 and are given in Fig. 4.21. Note that P_{in} and P_{ext} yields an intersecting point where $P_{in}=P_{ext}$ which is the equilibrium pore size for the relevant level of hydrogen release.

When foaming agent releases a trace amount of hydrogen the pore nucleates, point A in Fig. 4.21. As more hydrogen is released the point move on the P_{ext} curve in the direction of arrow and reaches B when 50% hydrogen is released. When all hydrogen is released the point moves to C. This, i.e. point C, is defined as the equilibrium pore size, D_{eq} .

By using the available data, equilibrium pore sizes were calculated for 675 and 725°C. Fig. 4.22 shows the effect of particle sizes on the equilibrium pore size. At 675°C, it is seen that the use of 20 μm TiH_2 leads to the formation of 1.1 mm pores. Two fold increase in the particle size, i.e. 40 μm yields pores that are three times larger, i.e. roughly 3.3 mm, Fig. 4.21(a), Table 4.3. At 725°C, the values are similar (slightly higher) indicating that particle size is more important parameter than foaming temperature.

4.4.3. Comparison with Experiments

Predictions given above are collected together in a diagram given in Fig. 4.23. It is seen that equilibrium pore sizes are determined by particle size of foaming agent and does not seem to be affected much by the temperature. The values predicted are approximately 1160 μm and 1200 μm for foaming agent sizes of 20 μm at 675° C and 725° C respectively. Minimum sizes of foaming agent that nucleate bubbles are

* Here the term refers to mechanical equilibrium where $P_{ext} = P_{in}$.

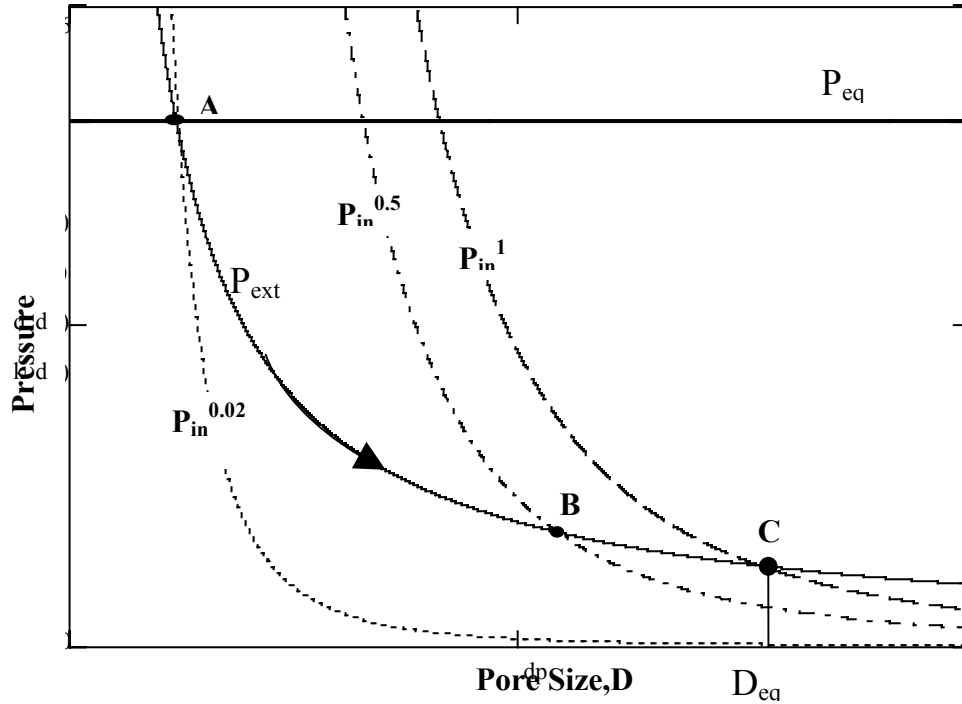
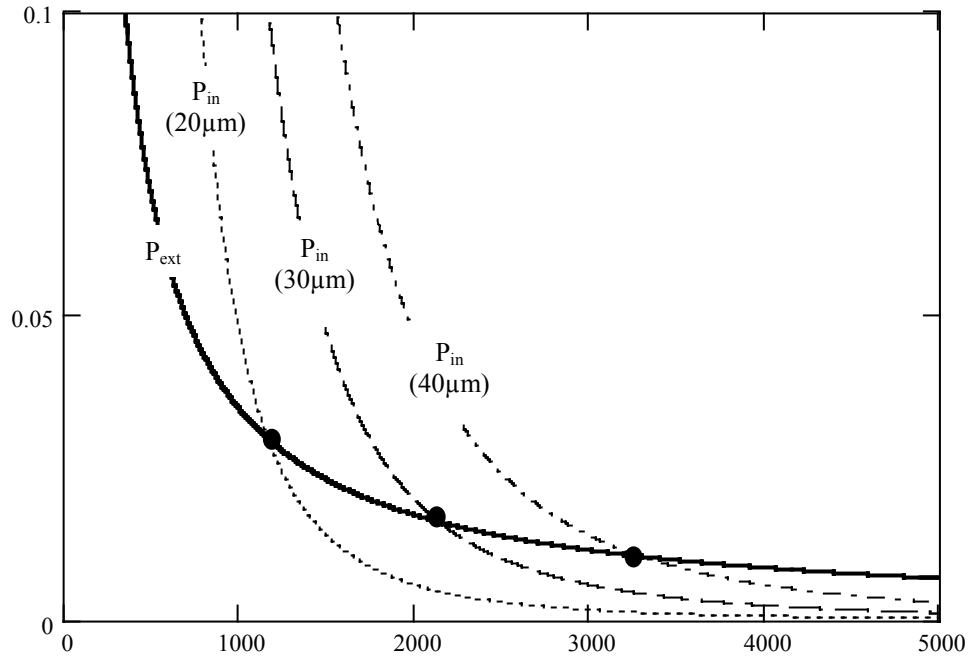


Figure 4.21. Variation of P_{in} and P_{ext} with pore size. In the graph P_{eq} is also shown. Superscript in P_{in} shows the fraction of hydrogen released by TiH_2 . Note that D_{eq} is defined as the intersection of P_{ext} with P_{in}^1 .

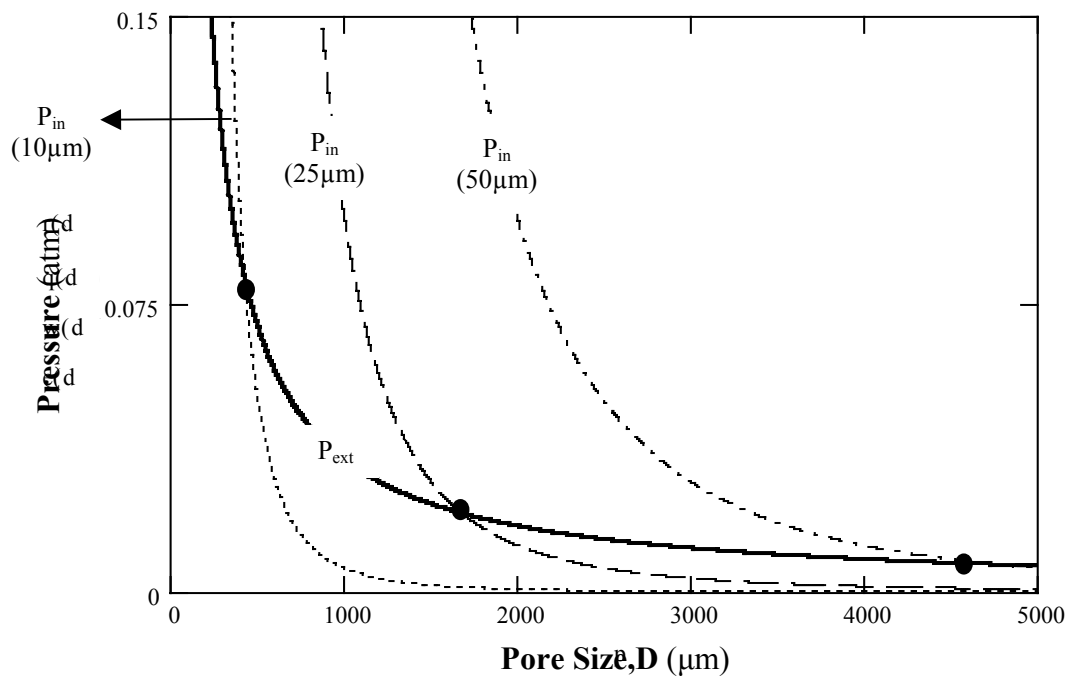
also shown on the diagram, which is determined by foaming temperature. The size, d_n has a value of $16 \mu m$ for $675^\circ C$. The value for $725^\circ C$ is $6 \mu m$.

Predictions made above may be compared with experiments. However, before this comparison, it should be pointed out that the values predicted above are obtained by assuming that $P_{ext} = P_s$, i.e. external pressure on the bubble is solely determined by surface tension, i.e. the effect of hydrostatic, (P_h) and atmospheric pressures (P_a) on P_{ext} are ignored. In reality, $P_{ext} = P_s + P_h + P_a$ as given in Section 2.3. When P_a and P_h are included, P_{ext} changes. The relative contribution of P_a and P_h (at a depth of 1 cm) to P_{ext} are given in Table 4.4 which refers to a surface tension value of $0.86 N/m$.

As given in Table 4.4, contribution of the hydrostatic pressure, P_h , to P_{ext} is very small for all sizes of pores. Atmospheric pressure P_a is also not important for small sizes., but becomes quite important for pore sizes larger than $5-10 \mu m$.



(a) 675°C



(b) 725°C

Figure 4.22. Equilibrium pore sizes (D_{eq}) for various sizes of TiH_2 . (a) For 675°C and (b) for 725°C. Note that equilibrium pore size increase with increase in TiH_2 particle size.

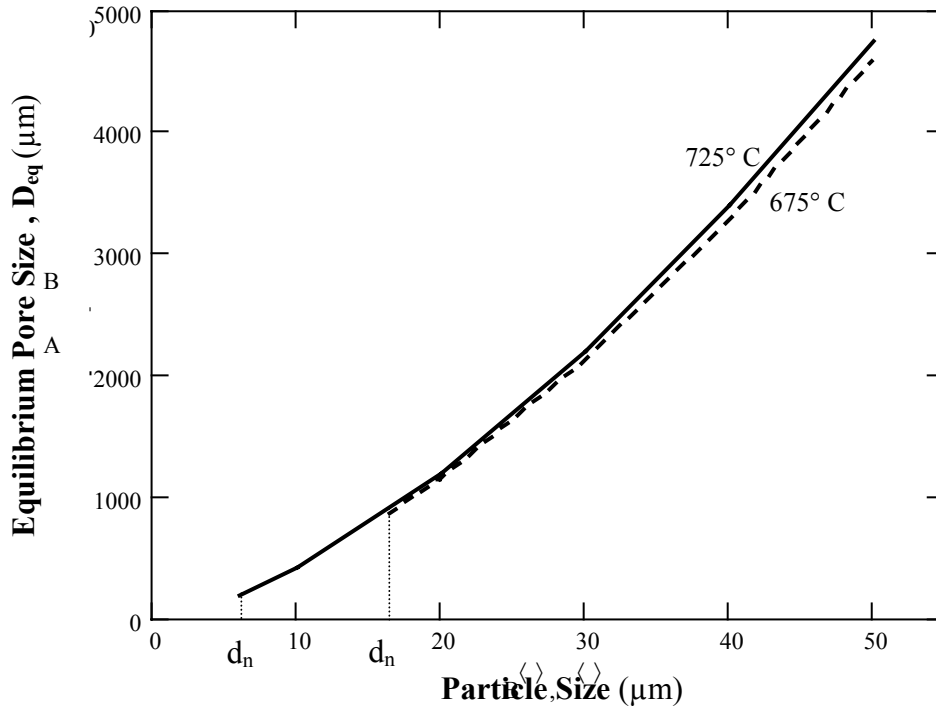


Figure 4.23. Variation of equilibrium pore size (D_{eq}) with TiH_2 particle size. Critical particle sizes for pore initiation are also indicated.

With the inclusion of P_s and P_a , d_n , particle size for pore initiation and D_{eq} equilibrium pore sizes were reevaluated for specific cases. Results are given in Table 4.5. Hydrostatic pressure, as would be expected, produces little change in critical particle size and in pore size. This is true even at a depth of 50 cm.

Table 4.3. Equilibrium pore sizes (D_{eq}) calculated for pure Al with foaming agent TiH_2 of different sizes

Temperature	675° C					725° C				
Particle Size (μm)	16	20	30	40	50	6	20	30	40	50
D_{eq} (μm)	871	1163	2136	3289	4596	187	1198	2200	3390	4740

Table 4.4. Pressure acting on a pore size of diameter D , i.e. P_{ext} . Relative contribution of hydrostatic (P_h) and atmospheric (P_a) and that required by surface tension (P_s) are given as percentages. Hydrostatic pressure refers to Al liquid at a depth of 1 cm.

Pore Size, D (μm)	P_{ext} (atm)	% P_h	% P_a	% P_s
1	34.95	0.007	2.86	97.13
5	7.79	0.033	12.83	87.13
10	4.40	0.058	22.74	77.20
20	2.70	0.095	37.04	62.87
30	2.13	0.120	46.86	53.02
40	1.85	0.139	54.02	45.85
50	1.68	0.153	59.47	40.38

Table 4.5. Effect of hydrostatic pressure (P_h) and atmospheric pressure (P_a) on critical particle size and equilibrium pore size at 675°C and 725°C. Equilibrium pore sizes refer to 40 μm TiH_2 .

	675°C		725°C	
	Critical Particle Size (μm)	Eq. Pore Size (μm)	Critical Particle Size (μm)	Eq. Pore Size (μm)
Only P_s	16.0	3289	6.0	3390
$P_s + P_a$	30.4	709	6.7	722
$P_s + P_a + P_h$ (1 cm depth)	30.4	709	6.7	722
$P_s + P_a + P_h$ (10 cm depth)	31.0	703	6.7	716
$P_s + P_a + P_h$ (50 cm depth)	34.2	682	6.9	694

It can be seen from data in Table 4.5 that with the inclusion of atmospheric pressure there is an increase in critical particle size. For instance, at 675°C the size becomes 30.4 μm instead of previous value of 16.0 μm . The effect at 725°C however is not as pronounced, the value is in the neighborhood of 6 μm at both cases.

In terms of critical particle size for bubble nucleation, the model implies that TiH_2 particles smaller than certain size should not participate in the foaming process. Although detailed analysis has not been carried out, there are signs that this could be the case. Thus, as reported above in foamed samples, 10-15 μm TiH_2 particles appear in the matrix in-between the pores, whereas larger particles (e.g. 30-50 μm), despite their presence in the swaged sample, are not present at such locations. This observation made at 675°C thus is in agreement with model that predicts critical sizes of 16-30 μm .

In terms of equilibrium pores size, Table 4.5 show that the inclusion of atmospheric pressure P_a results in a sharp decrease of equilibrium pores sizes at both temperatures. For instance, at 725°C the pore size, which had a value of 3390 μm has now have a value of 722 μm .

Thus, the model predicts that for foaming agent with sizes in between 16.0 μm and 50 μm produce pores in the range 1- 4 mm diameter. This is in the same order as those observed in the foamed samples (1-3 mm) and comparable with values reported in the literature

In conclusion, it can be stated that if the aim is to produce fine size pores, two requirements must be met. One is the use of fine size foaming agent. The other is the use of higher foaming temperature. For instance according to the model to obtain Al foam of 50 μm pore size, foaming agent TiH_2 should have a size of 3.2 μm and the temperature should be in the neighborhood of 800 °C.

4.5. FOAMING OF TiO₂ STABILIZED SYSTEM

TiO₂ stabilized systems were selected such that they would have similar viscosities with those of pure aluminum. As discussed in Section 2.3 by solid addition the viscosity of liquid can be adjusted to desired value. Fig.4.24 shows the temperature dependency of viscosity at various level of solid addition. Selected viscosity data are given in Table 4.6.

With 5% TiO₂ addition (solid content of 3.5 vol. %), viscosities similar to pure Al system can be obtained at temperatures around 750°C. Based on this approach, foaming experiments were carried out at 750°C and 800°C.

Volume expansion data of TiO₂ stabilized system are given in Figs 4.25 and 4.26 for 750°C in which the data are shown by points and the curve is the trend line. The degree of foaming achieved is in the range 120-140 %. These values are comparable with pure Al (90-180%). Volume expansion at 750°C is greater when fine TiH₂ was used. Foaming at 800°C leads to better expansion with values up to 160%, given in Figs 4.29 and 4.30.

Evolution of macrostructure during foaming is given in Figs 4.27-28 and 4.31-32 at specific time intervals. Comparing these with those of pure Al, i.e. Figs 4.10-11 and 4.14-15, indicate that foaming is faster in the current systems. This is probably due to the use of higher temperature of foaming. However, in terms of pore size and distribution, all samples are similar. In conclusion, the use of fine TiH₂ and the high temperature of foaming did not lead to formation of fine pores contrary to what was concluded in the section above.

Macrostructure of foamed samples are given in Figs 4.33-4.34. The structures are very different from those observed in pure Al system. As seen in the figures, the structure contain substantial amount of "bright" regions.

A typical example is that given in Fig. 4.33(a) that refer to a white particle. Point analysis taken from the inner part of this bright region indicates Ti, i.e. "TiH₂".

Note that there is a layer of reduced contrast covering the Ti rich region. Point analysis was carried out in this surrounding layer. The approximate composition was the 67 % Al and 33 % of Ti, indicating that it is Al₂Ti intermetallic. Thus, TiH₂ or by releasing its hydrogen Ti reacts with Al giving the Al₂Ti intermetallics. Intermetallics covering TiH₂ or Ti particles are a common feature of macrostructure at 750°C.

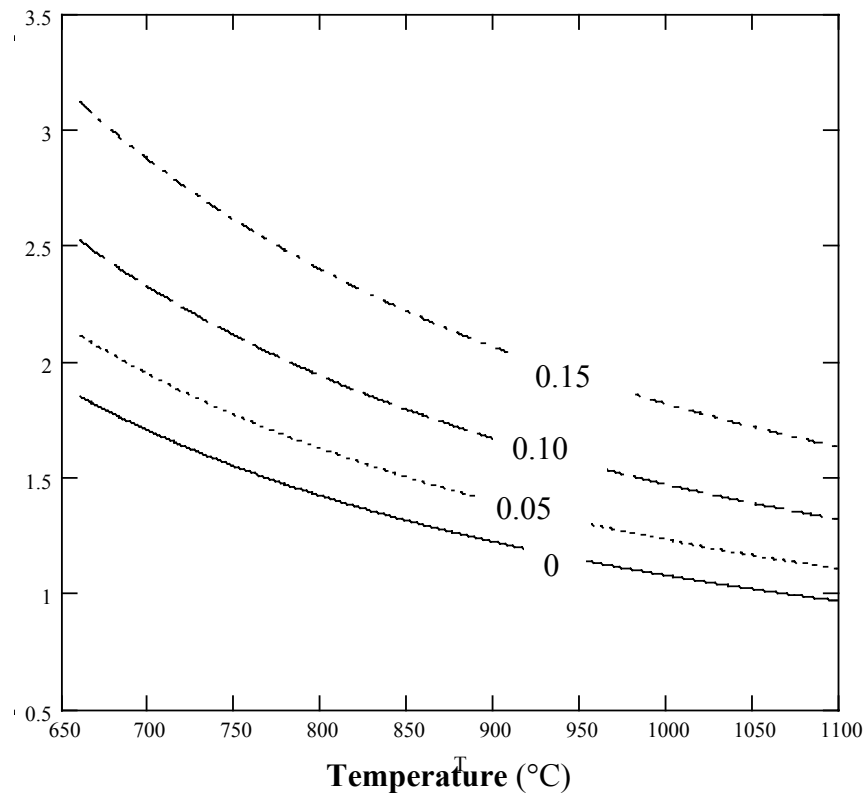


Figure 4.24. Temperature dependence of Al viscosity at various level of solid addition. The values given on the lines represents the volume fraction of the solid in the liquid Al.

Table 4.6. Viscosity of the Al systems at different foaming temperatures.

Temperature (°C)	Viscosity without solid content (mPa·s)	Viscosity with initial solid content 5wt % TiO ₂ , i.e. 3.5 vol. % (mPa·s)
675	1.79	-
725	1.62	-
750	1.55	1.69
800	1.42	1.55

Fig. 4.34 refers to TiO₂ stabilized system at 800°C after 5 minute of foaming. Note the presence of white needles in the structure. Similar formation has been reported in the literature and has been attributed to internal reaction between Ti or TiO₂ and Al. White regions are quite dominant in the structure and are roughly make up 15 % of the total volume.

Thus, unlike pure Al, internal reactions are a dominating feature of TiO₂ stabilized system especially at high temperatures. In the experiments, solid fraction introduced into the system was 5%. However, due to internal reactions, the solid fraction would be more than this value. Ti will react with Al giving Ti-Al intermetallics. Moreover, as given in Section 2.4, Al would react with TiO₂ giving alumina and additional Ti-Al intermetallics.

Assuming that all TiO₂ (5 wt %) would react with Al; Ti content of the system would increase by 3 % Ti (the total content 3.5% Ti, the amount of TiH₂ is 0.5%). Assuming that intermetallic formed as a result of this reaction is Al₃Ti, the weight fraction is approximately 37 wt%, Fig. 2.27. Using density value of 3.3 gr/cm³ this corresponds to a volume fraction of 33 %.

Thus solid content which is initially only 3.5 vol.% increases as a result of internal reaction and can reach a value as high as 33%. When this change occurs however is not known. It is possible that foaming occurs i.e. TiH₂ releases its hydrogen before the internal reactions. If this is the case, increased viscosity would affect only later stages of foaming, i.e. the growth rate of pores to equilibrium pore size may be reduced. This may also affect coalescence of pores in the positive manner.

If the internal reactions occur before hydrogen release then stabilized system would have much higher viscosity. With 33% solid content viscosity of aluminum is approximately 7.3 mPa·s at 750°C. This is 4 times the value aimed for the current system.

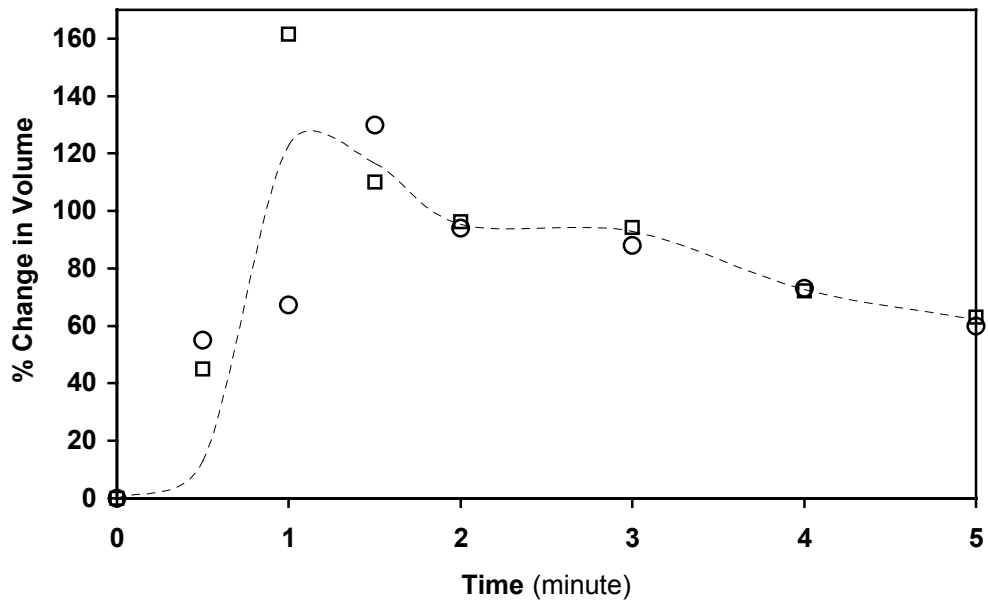


Figure 4.25. Foaming of TiO₂ stabilized Al with 0.6 wt % coarse TiH₂ at 750°C. Amount of oxide addition is 5 wt %.

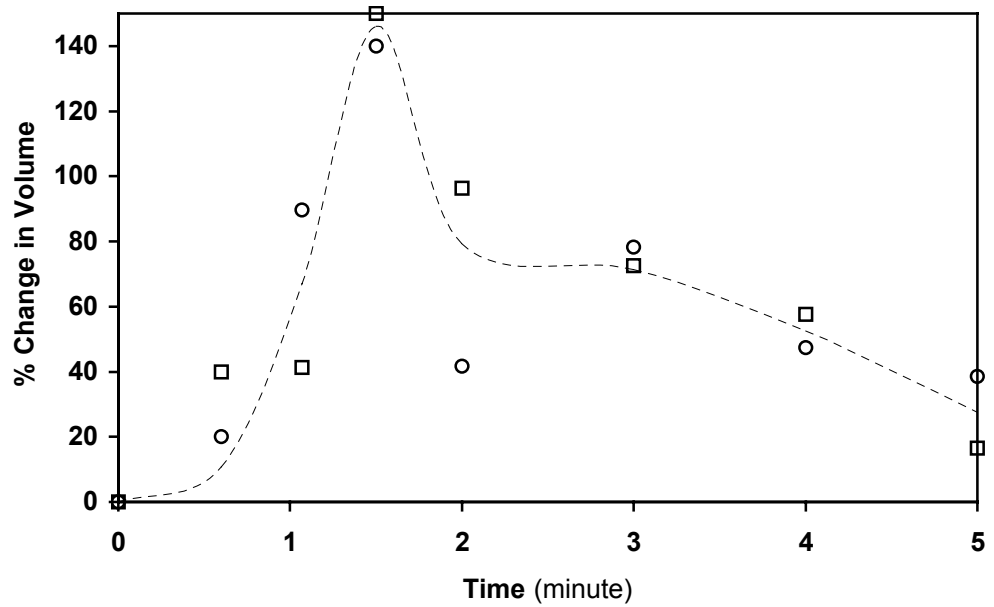


Figure 4.26. Foaming of TiO₂ stabilized Al with 0.6 wt % fine TiH₂ at 750°C. Amount of oxide addition is 5 wt %.

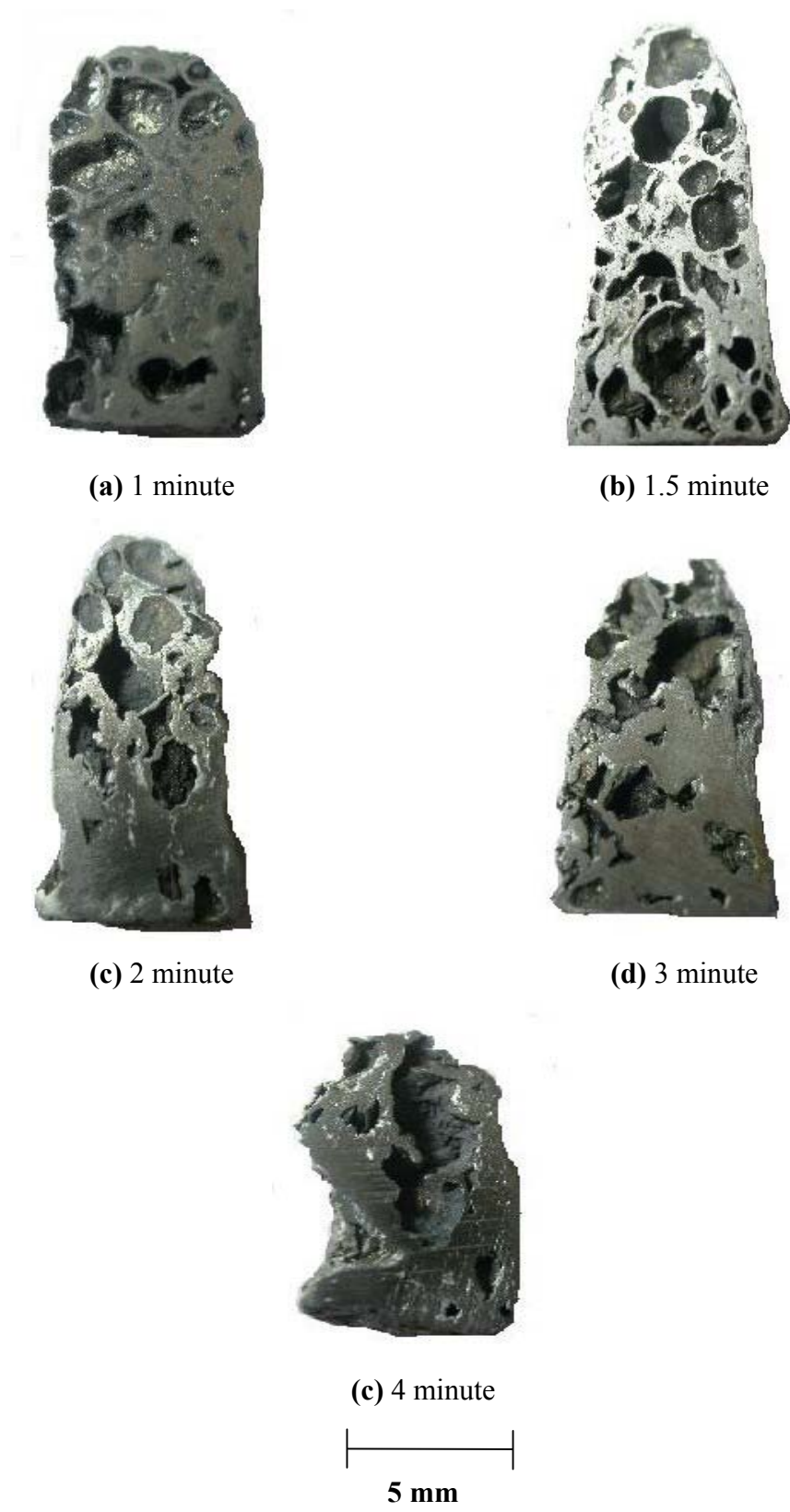


Figure 4.27. Macrostructures of TiO_2 stabilized Al foamed with coarse TiH_2 at 750°C . Note pore coalescence after 1.5 minute.



(a) 1 minute



(b) 1.5 minute



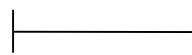
(c) 2 minute



(d) 3 minute



(e) 4 minute



5 mm

Figure 4.28. Macrostructures of TiO_2 stabilized Al foamed with fine TiH_2 at 750°C . Note pore coalescence after 1.5 minute.

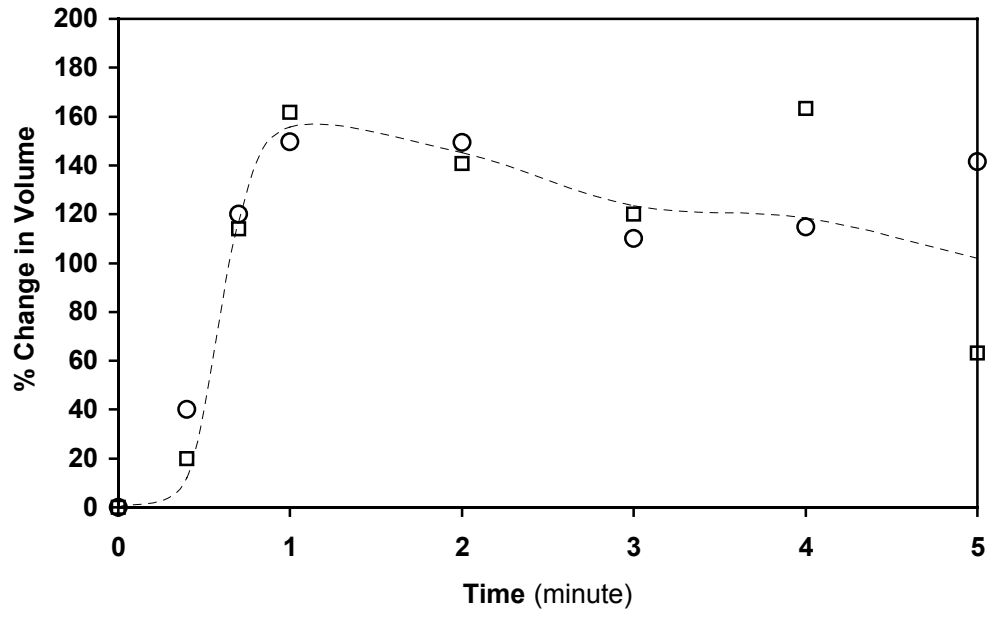


Figure 4.29. Foaming of oxide stabilized Al with 0.6 wt % coarse TiH_2 at 800°C . Amount of oxide addition is 5 wt %.

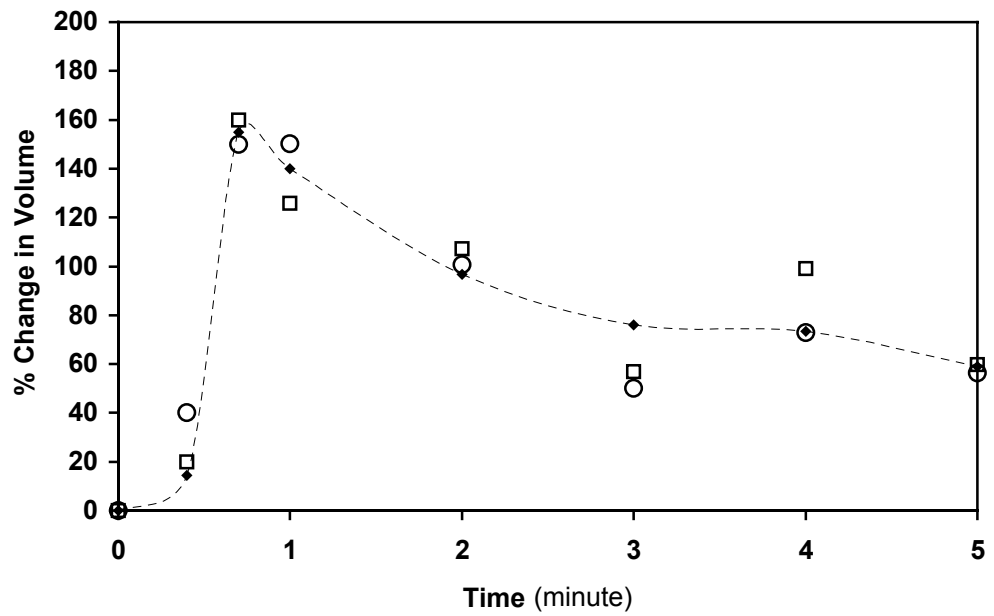


Figure 4.30. Foaming of TiO_2 added Al with 0.6 wt % fine TiH_2 at 800°C . Amount of oxide addition is 5 wt %.



(a) 40 seconds



(b) 1 minute



(c) 2 minute



(d) 3 minute



(e) 4 minute

5 mm

Figure 4.31. Macrostructures of TiO_2 stabilized Al foamed with coarse TiH_2 at 800°C . Note pore coalescence after 1 minute.



(a) 40 seconds



(b) 1 minute



(c) 2 minute



(d) 3 minute



(e) 4 minute

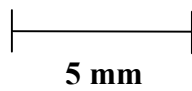
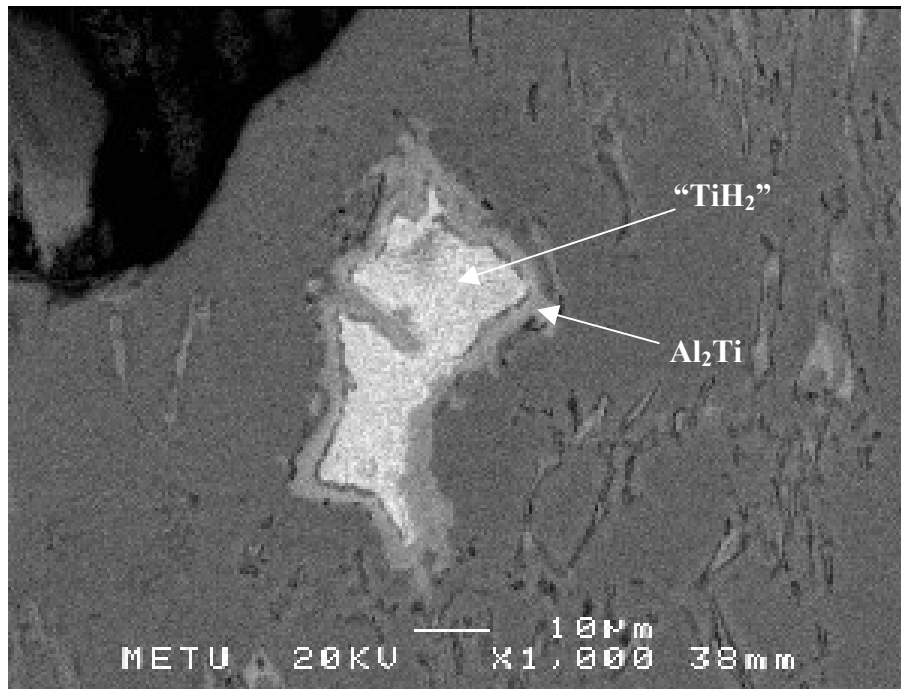
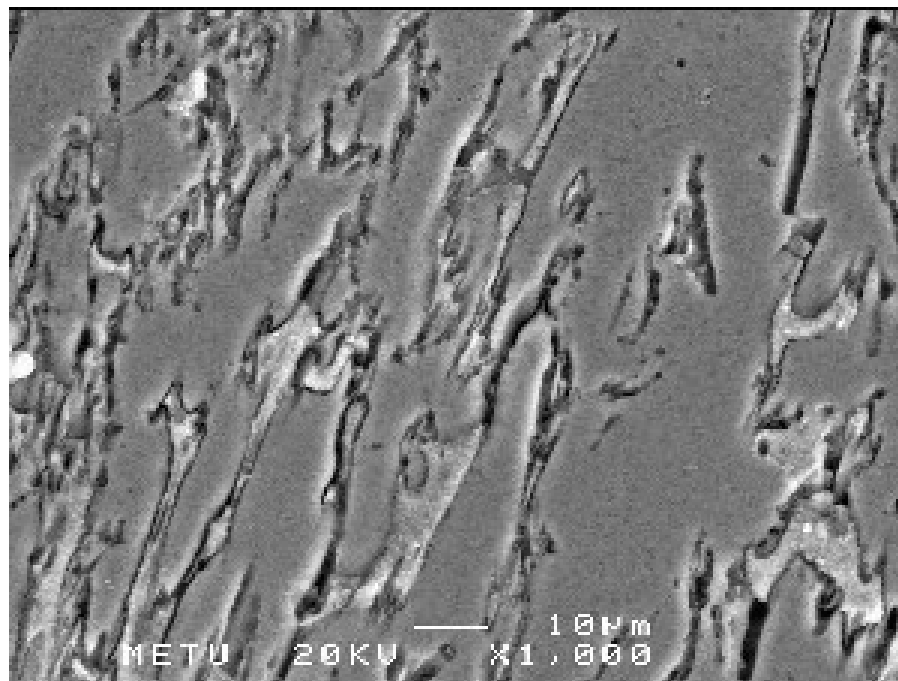


Figure 4.32. Macrostructures of TiO_2 stabilized Al foamed with fine TiH_2 at 800°C . Note gas loss and pore coalescence after 1 minute.

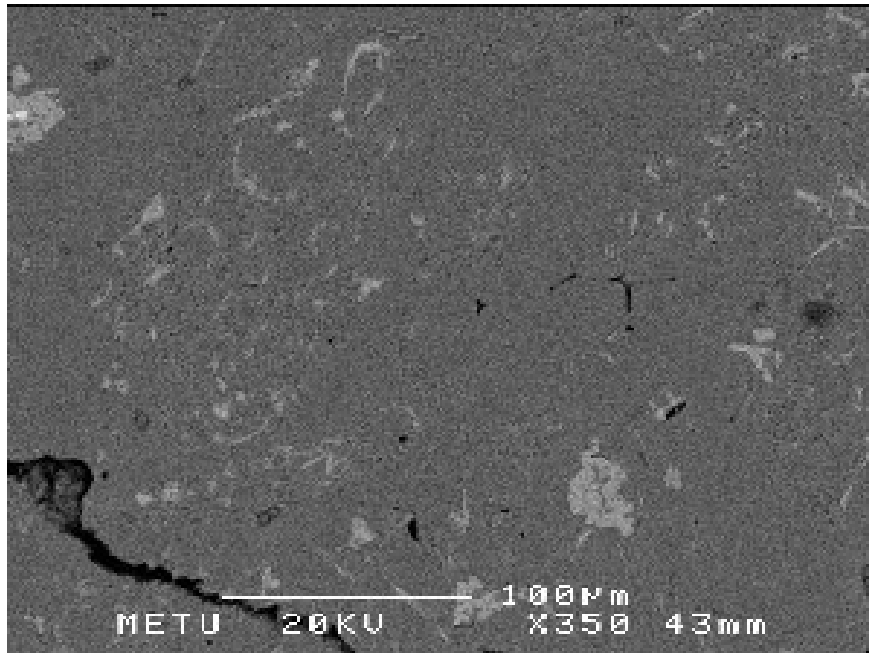


(a)

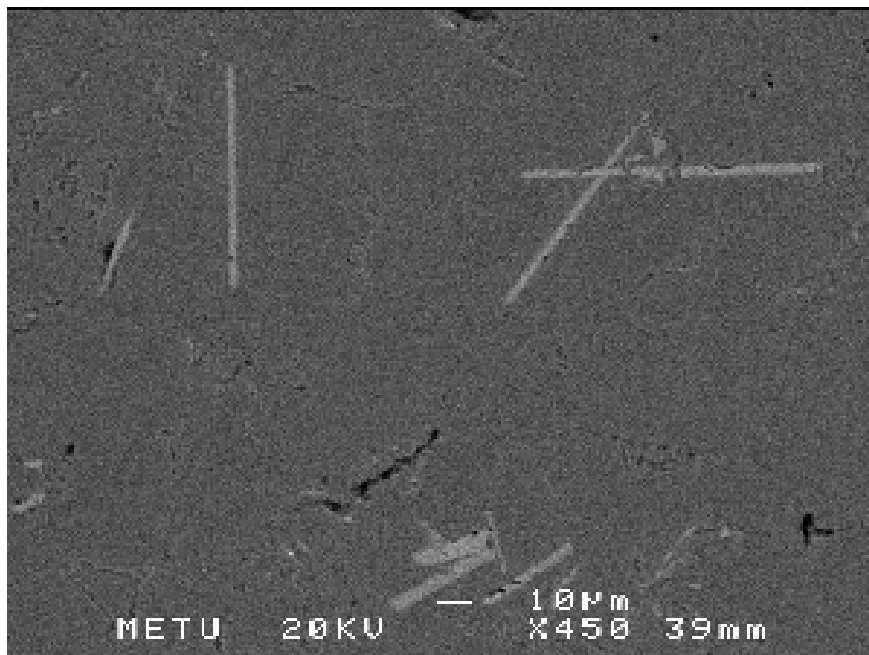


(b)

Figure 4.33. Structure in Al-5 wt % TiO₂ foamed at 750°. (a) coarse “TiH₂” particles in the structure. Note the gray region covering particle has composition of Al₂Ti. (b) formations at a finer scale.



(a)



(b)

Figure 4.34. Structure in Al-5 wt % TiO₂ foamed at 800°C. Note Al-Ti intermetallics in the form needles and plates at (b).

CHAPTER V

CONCLUSION

Pure aluminium and TiO_2 stabilized aluminium foams were produced by powder metallurgy technique with the use of fine and coarse TiH_2 particles. Compaction of powders was carried out by hot swaging at 400°C . Foaming of pure aluminium were carried out at temperatures near to solidification point of aluminium. To obtain similar viscosities with pure system, TiO_2 added systems were foamed at higher temperatures.

Hot swaging as a technique of compaction yields density values close to full density and therefore it is quite suitable as a method of compaction for foaming. Moreover, it is verified that high level of compaction is the primary requirement for high amount of foaming.

For pure systems the amount of foaming up to 180 % is obtained. The kinetic and amount of foaming is found to be temperature dependent. At low temperatures, the amount of foaming is low for fine TiH_2 addition.

A model is developed for foaming of pure aluminium. Equilibrium pressure of hydrogen in TiH_2 decomposition is the basis for the model which enables the prediction of pore initiation and equilibrium pore size.

Using the model and excluding atmospheric pressure critical particle sizes have been found as $16\mu\text{m}$ and $6\mu\text{m}$ for 675 and 725°C respectively. Atmospheric pressure is crucial on pore initiation whereas effect of liquid metal depth is negligible.

The model shows that equilibrium pore size depends directly on TiH_2 size. For foaming agent with sizes in between 16 μm and 50 μm , pores in the range 1- 4 mm diameter are produced. This is in the same order as those observed in the foamed samples (1-3 mm) and comparable with values reported in the literature. Model indicates that if the aim is to produce fine sized pores, two requirements must be met: use of fine size foaming agent and use of high foaming temperature.

For oxide added systems amount of foaming up to 160% is obtained. The amount of foaming and kinetic of foaming are found to be temperature dependent. Unlike pure Al, internal reactions are a dominating feature of TiO_2 stabilized system. Thus, solid content which is initially only 3.5 vol.% increases as a result of internal reaction between Al-Ti and Al- TiO_2 and can reach a value as high as 33%. This corresponds to four fold increase in viscosity.

REFERENCES

- Adamson A.W., 1976, 'Physical Chemistry of Surfaces', (Wiley Interscience Publication)
- Andrade, E. N. Phil. Mag., (1934), vol.17, 698
- Angarska J.K., Manev E.D., Colloids and Surfaces A: Physicochemical and Engineering Aspects, 190, (2001), 117-127
- Anson J.P., Drew R.A.L. Gruzelski J.E., Metallurgical & Materials Transactions B, vol. 30B, (1999), 1027-1031
- Banhart J., Baumeister J., Journal of Materials Science, 33, (1998), 1431-1440
- Banhart J., Brinkers W., Journal of Materials Science Letters, Vol.18, (1999), 617-619
- Banhart J., JOM, 52(12), (2000), 22-27
- Banhart J., Progress in Materials Science, 46,(2001) ,559-632
- Battezzati L., Greer A.L., Acta Materialia, vol.37, No.7, (1989), 1791-1802
- Baumeister J., Banhart J., Weber M., Günther B., 1992, 'Proceedings of International Symposium on Advanced Materials for Lightweight Structures'
- Baumgartner F., Duarte I., J.Banhart, Advanced Engineering Materials, 2, No.4, (2000), 168-174
- Bende W.U., Fuhe G., 1992, in 'Advances in Powder Metallurgy and Particulate Materials, vol. 6 ', (Metal Powder Industries Federation, Princeton, NJ)
- Bikerman J. J., 1973, Foams, (Springer-Verlag)
- Bram M., Stiller C., Advanced Engineering Materials, 2, No.4, (2000), 196 -199
- Bretznajder S., 1971, 'Prediction of Transport and Other Physical Properties of Fluids ', International Series of Monog. in Chem. Eng. Vol. 11, (Pergamon Press, New York)

- Cao W.B., Kirihara S., Miyamoto Y., Matsuura K., Kudoh M., *Intermetallics*, (2002), 879-885
- Chou K., Song M., *Scripta Materialia*, 46, (2002), 379-382
- Chu M.S., Wu S.K., *Acta Materialia*, 51, (2003), 3109-3120
- Cox S.J., Bradley G., Weaire D., *The European Physical Journal Applied Physics*, 2001
- Cymat Technical Manual for Stabilized Aluminium Foam, 2002
- Davies G.J., Zhen S., *Journal of Materials Science*, 18, (1983), 1899-1911
- Degischer H.P. and Kriszt B., 2002, ' Handbook of Cellular Metals: Production, Processing, Applications ' (Wiley -VCH Weinheim)
- Duarte I., Banhart J., *Acta Materialia*, 48, (2000), 2349-2362
- Eichenauer W., Hattenbach K., Pebler Z., *Z.Metallk.*, 52 ,(1961) ,682-684
- Eisenmann M., 1998, in ' Metal Powder technologies and Applications, ASM Handbook Vol. 7 ', (ASM International, Materials Park OH), 1031-1042
- Elbir S., Yilmaz S., Toksoy A.K., Hall I.W., Guden M., (2001), unpublished study
- Elliott J.C., US Patent 2751 289 (1956)
- Fedeeva V.I., Leonov A.V., Szewczak E., Matyja H., *Materials Science and Engineering A242*, (1998), 230-234
- Feng C.F., Froyen L., *Composites: Part A*, 31, (2000), 385-390
- Frischmann W., European Patent Application EP 0666129,1995
- Fu Y., Shi R., Zhang J., Sun J., Hu G., *Intermetallics*, 8, (2000), 1251-1256
- Fuganti A., Lorenzo L., Hanssen G.A., Langseth M., *Advanced Engineering Materials*, 2,No.4,(2000), 200-204
- Fusheng H., Jianning W., Hefa C., Junchang G., *Journal of Materials Processing Technology*, 138, (2003), 505-507
- Garcia-Cordovilla C., Louis E., Pamies A., *Journal of Materials Science*, vo.21, (1986), 2787-2789
- Gaus S., Hermer M.P., Chan H.M., Caram H.S., Bruhn J., Claussen N., *Journal of American Ceramic Society*, 83, 7, (2000), 1606-1612

- Gaus S., Hermer M.P, Chan H.M., Caram H.S., Claussen N., Journal of American Ceramic Society, 83, 7, (2000), 1599-1605
- Gebhardt E., Becker M., Dorner S., Aluminium, 31, (1955), 315-385
- Gergely V., Clyne B., Advanced Engineering Materials, 2, No.4, (2000), 175-178
- Gibson L.J., Ashby M.F., 1997, ' Cellular Solids, 2nd Edition ', (Cambridge University Press)
- Goumiri L., Joud J.C., Acta Materialia, 30, (1982), 1397
- Güvendiren M., Baybour E., Öztürk T., International Journal of Hydrogen Energy, 2003
- Hashi K., Ishikawa K., Suzuki K., Aoki K., Journal of Alloys and Compounds, 330-332, (2002), 547-550
- Haydn N.G .W., Advanced Engineering Materials, 4, No.10, (2002), 726-733
- Helfen L., Baumbach T., Stanzick H., Banhart J., A. Elmoutaoukkil, P. Cloetens, Advanced Engineering Materials, 4, No.10, (2002), 808-813
- Hirai, M ISIJ, vol.33, (1993), 281-258
- Horn K.R., 1967, 'Aluminium Vol.1: Properties, Physical Metallurgy and Phase Diagrams ', (American Society for Metals, Ohio)
- Horvitz D., Gotman I., Gutmanas E.Y., Claussen N., Journal of the European Ceramic Society, 22, (2002), 947-954
- Kaltenbach K., Gama S., Pinatti D.G., Schulze K., Z Metallkde, 80, (1989), 511
- Kattner R.U., Lin J.C., Chang Y.A., Metallurgical Transactions A, 23A, (1992), 2081
- Kennedy A.R., Scripta Materialia, 47, (2002), 763-767
- Kennedy A.R., Materials Science and Engineering, A357, (2003), 258-263
- Körner C., Singer R.F., Advanced Engineering Materials, 2, No.4, (2000), 159-165
- Korol'kov A. M., 1963, ' Casting Properties of Metals and Alloys', (Consultants Bureau)
- Kumar K., Nikolov A.D., Wasan D.T. Journal of Colloid and Interface Science, 256, (2002), 194-199
- Lehmhus D., Banhart J., Rodriguez M.A., Materials Science and Technology, vol.18,

- (2002), 1-6
- Leitlmeier D., Degischer H.P., Flankl H.J., *Advanced Engineering Materials*, 4, No.10, (2002), 735-740
- Ma L., Song Z., He D., *Scripta Materialia*, vol.41, no. 7, (1999), 785-789
- Ma L., Song Z., *Scripta Materialia*, Vol.39, no.11, (1998), 1523-1528
- Mackowiak J., Shreir L.L., *Journal of Less Common Materials*, 1, (1959),456-466
- Miyoshi T., Itoh M., Akiyama S., Kitahara A., *Advanced Engineering Materials*, 2, No.4, (2000), 179-183
- Moon K.I., Lee K.S., *Journal of Alloys and Compounds*, 264, (1998), 258-266
- Moon K.I., Lee K.S., *Journal of Alloys and Compounds*, 291, (1999), 312-321
- Mueller W.M., Blackledge J.P., Libowitz G.G., 1968, 'Metal Hydrides', (Academy Press Inc., London)
- Murray J.L., 1987, 'Phase Diagrams of Binary Titanium Alloys' (ASM International, OH)
- Nieh T.G., Kinney J.H., Wadsworth J., Ladd A.J.C., *Scripta Materialia*, vol.38, No.10, (1998), 1487-1494
- Ohnuma I., Fujita Y., Mitsui H., Ishikawa K., Kainuma R., Ishida K., *Acta Materialia*, 48, (2000) , 3113-3123
- Öztürk T., Mirmesdagh J., Ediz T., *Materials Science and Engineering*, 1994
- Palm M., Zhang L.C., Stein F., Sauthoff G., *Intermetallics*, 10, (2002), 523-540
- Park C., Nutt S.R., *Materials Science and Engineering*, A297, (2001), 62-68
- Park S., Hur B., Kim S., Ahn D., Ha D., 2002, in '65th World Foundry Congress Proceedings ', 515-522.
- Peng H.X., Wang D.Z., Geng L., Yao C.K., Mao J.F., *Scripta Materialia*, Vol.37, No.2, (1997), 199-204
- Ransley C.E., Neufeld H., *Journal of Inst. Metals*, 74, (1947/1948), 599-620
- Ransley C., Tablot D., *Z. Metallkunde*, 46, No.5, (1955)
- Richardson F. D., 1974, 'Physical Chemistry of Melts in Metallurgy', (Academic Press)

- Romankov S.E., Suleeva S., Volkova T.V., Ermakov E., *Crystal Engineering*, 5, (2002), 255-263
- Sandrock G., *Journal of Alloys and Compounds*, 293-295, (1999), 877-888
 Saravanan et al., *Scripta Mater.*, 44, (2001), 965-970
- Schuster J.C., Ipser H., *Metallkde Z*, 81, (1990), 389
- Shimoji M., 1977 'Liquid Metals: An Introduction to the Physics and Chemistry of Metals in the Liquid State', (Academic Press)
- Simancik F., Minarikova N., Culak S., Kovacik J., 1999, in 'Metal Foams and Porous Structures', Verlag MIT Publishing, Bremen.
- Simone A.E., Gibson L.J., *Journal of Materials Science*, 32, (1997), 451-457
- Simone A.E., L.J. Gibson, *Acta Materialia*, vol. 46, No: 9, (1998), 3109-3123
- Sokolskaya L.I., 1961, 'Gases in Light Metals', (Pergamon Press, London)
- Song Z., Ma L., Wu Z., He D., *Journal of Materials Science*, 35, (2000), 15-20
- Sosnik A., US Patent 2434 775, 1948
- Straumanis M.E., Ejima T., *Z. Physik Chem.*, 23, (1960), 440-448
- Swars H., German Patent Application 36 19 360, 1987
- Thornton P.H., Magee C.L., *Metallurgical Transactions A*, Vol.6A, (1975), 1975-1801
- Tjong S.C., Tam K.F., Wu S.Q., *Composites Science and Technology*, 63, (2003), 89-97
- Travitzky N., Gotman I., Claussen N., *Materials Science Letters*, 57, (2003), 3422-3426
- Türkdoğan E.T., 1983, 'Physicochemical Properties of Molten Slags and Glasses', (The Metal Society, London)
- Van Lander M., 1967, 'Metallurgy of Aluminium Alloys', (Chapman & Hall)
- Wu J.M., Zheng S.L., Li Z.Z., *Materials Science and Engineering A289*, (2000), 246-254
- Wübben Th., Stanzick H., Banhart J., Odenbach S., (2002), will be published in *Journal of Physics C: Solid State Physics*

- Yamada Y., Shimojima K., Sakaguchi Y., Mabuchi M., Nakamura M., Asahina T., Mukai T., Kanahashi H., Higashi K., *Advanced Engineering Materials* , 2, No.4 , (2000) ,184-187
- Yamada Y., Shimojima K., Sakaguchi Y., Mabuchi M., Nakamura M., Asahina T., Mukai T., Kanahashi H., Higashi K., *Journal of Materials Science Letters*, 18, (1999), 1477-1480
- Yamada Y., Shimojima K., Sakaguchi Y., Mabuchi M., Nakamura M., Asahina T., Mukai T., Kanahashi H., Higashi K., *Materials Science and Engineering*, A272, (1999), 455-458
- Yamada Y., Shimojima K., Sakaguchi Y., Mabuchi M., Nakamura M., Asahina T., Mukai T., Kanahashi H., Higashi K., *Materials Science and Engineering*, A280, (2000), 225-228
- Yash P.K., *Advanced Engineering Materials*, 3, No.9, (2001), 702-705
- Yu C.J., Eifert H.H., Banhart J., Baumeister J., *Advanced Materials and Processes*, 11, (1998), 45-47
- Zhao Y.Y., Sun D.X., *Scripta Materialia*, 44, (2001), 105-110

APPENDIX A

FOAMING OF ALUMINIUM WITH AND WITHOUT TiO₂ ADDITION¹

S.Tan and T.Öztürk

Department of Metallurgical and Materials Engineering
Middle East Technical University
06531, Ankara, Turkey

A study was carried out into the formation of aluminium foams via powder processing route. Aluminum powder compacts both in pure form and Al-5%TiO₂ were foamed at temperatures ranging from 675 to 800°C. Foaming agent TiH₂ was mixed with powders typically with 0.6 wt % in two different sizes. Experiments have shown that foaming in excess of 120 % is possible both with pure Al as well as in Al-TiO₂. It is found that with coarse TiH₂, with and without TiO₂, Al expands more, implying that there may be a certain size below which particles may not participate in the foaming process. It is further found that with the use of high temperature there are internal reactions between foaming agent and aluminium as well as between TiO₂ and Al. This is with the result that with TiO₂ added system foaming becomes more temperature dependant than the pure Al.

KEYWORDS: Aluminum foam, powder processing, foaming agent size, TiH₂, TiO₂, macrostructural control.

1.INTRODUCTION

In recent decades there has been much emphasis on lightweight materials and structures. Therefore metallic foams together with other cellular materials are becoming an important group of materials within themselves. In addition to their lightness, metallic foams have additional properties such as energy absorption, heat insulation etc.

Metallic foams can be produced with a variety of techniques [1]. Of these, foaming, based on powder processing is quite common [2]. This typically involves mixing of a suitable foaming agent with metallic powder, followed by compaction and finally foaming. Aluminium and its alloys due their already low density are particularly attractive for foaming. Foaming agent is normally titanium hydride (TiH₂) that decomposes at temperatures above 550 °C.

Foaming of aluminum in its pure form is not very common. Normally it is necessary to add some additives such as nitrides, carbides and oxides that act as stabilizing agent. These additives may be added as they are or may be formed in situ as is the case with Ca addition to form CaO [3]. In the case of alloys, such additions may not be necessary since, when foaming is carried out between solidus and liquidus, the solid fraction that remain in the system may act as stabilizing agent. As reported by Webben et al.[4], stabilizing agent contributes the foam stability by three possible

¹ Published in the Proceedings of 3rd Balkan Metallurgy Conference, 2003, pp.191-195.

mechanisms: by increasing viscosity, by decreasing surface tension, by delaying liquid film rupture. Various systems [5-8] have successfully been foamed e.g. AlSi, AlCuMgSi AlSiCu and AlMgSi. The current work uses TiH₂ in two different particle sizes and examines the foaming of aluminium with and without stabilizing agent, i.e. TiO₂. Emphasis is on structural changes that occur during foaming which may be important so as to exercise control over the process.

2. EXPERIMENTAL PROCEDURE

Powders used in this study were Al (27 μm) and TiO₂ (<1 μm). TiH₂ 44 μm in size, was used as foaming agent. To examine the effect of TiH₂ size on foaming, it was ground to below 5 μm via ball milling for 24 hours with ball to powder ratio 10:1.

Table 1: Systems for Foaming

System	Temperature of Foaming
Al - unmilled TiH ₂	675°C & 725°C
Al - 24 hrs milled TiH ₂	675°C & 725°C
Al - unmilled TiH ₂ - 5 wt % TiO ₂	750°C & 800°C
Al - 24 hrs milled TiH ₂ - 5wt % TiO ₂	750°C & 800°C

Metal powders of composition specified in Table 1 were dry mixed for one hour with a shaker (ball to powder ratio: 1/2). Powders were subsequently consolidated by hot swaging at 400°C. This temperature was selected based on desorption tests at which there was no noticeable hydrogen release from TiH₂. For swaging, mixed powders were enclosed into a copper tube of 22 mm in diameter and hot swaged down to 6.6 mm.

Swaged samples were cut into pieces approximately 10 mm in length for foaming experiments. Foaming was carried out in a preheated vertical tube furnace in which temperature were controlled with ± 5 °C. For pure systems, foaming temperatures were 675°C and 725°C, and with TiO₂ addition, 750°C and 800°C.

Volumes of sample before and after foaming were measured by Archimedes principle and the change was used as a measure of foaming.

3. RESULTS AND DISCUSSION

Typical macrostructures of as swaged powder compacts are shown in Figure 1. The micrographs were recorded in backscattered mode and therefore TiH₂ and TiO₂ where present appear bright. Structure as seen in longitudinal section indicate that swaging leads to a good consolidation of powders, Figure 1(a). Samples with TiO₂ addition when examined at transverse section shows a cloud like distribution, Figure 1(b). Thus, TiO₂ which had extremely fine size (< 1 μm) could not be homogeneously distributed among Al powders. Agglomerated TiO₂ particles enclosed within Al powders, see Figure 1(a), are distributed into the cloud like morphology given in Figure 1(b) as a result of swaging deformation.

Structural examination on as swaged samples showed that there are instances of particle cracking in consolidated samples, Figure 1(c). Thus, there is some degree of TiH₂ size reduction during swaging, especially for coarse TiH₂ addition. Such observations have also been reported in other similarly deformed heterogeneous systems [9]. With coarse TiH₂ addition, swaged samples show a distribution of TiH₂ sizes up to 50 μm. With fine TiH₂ additions, the sizes are normally in the order of 2-3 μm and occasionally can reach sizes up to 10 μm.

Results of foaming experiments for pure aluminium carried out at 675°C and 725°C are given in Figure 2(a) and (b) respectively. A value of approximately 120 % foaming is achieved at both temperature.

An example of foamed structure is given in Figure 3 ,where region in between the pores show a well-defined solidification structure with embedded bright “TiH₂” particles. Whether these particles are TiH₂ or Ti, i.e. they released their hydrogen, could not be determined. It is interesting to note that “TiH₂” particles observed in-between the pores are not as large as those observed in the original swaged samples. A careful examination on the sizes of “TiH₂” showed that although there were few exceptions, the particles were mostly of sizes close to or less than 10-15 μm.

At 725°C, there is clear indication of internal reaction between the host and added particles. Figure 4 shows originally TiH₂ particle feeding a pore at one of its edge, partially transformed, verified by local elemental analysis, into Al₂Ti.

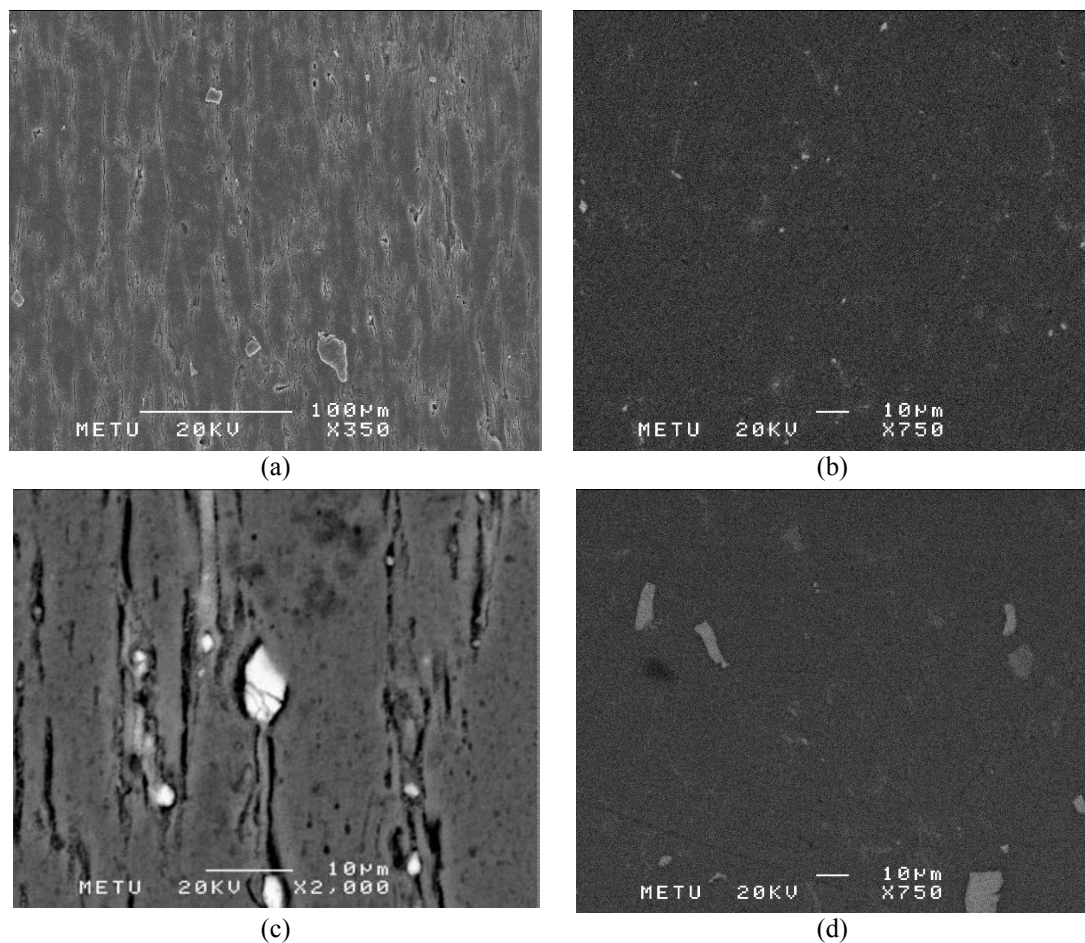
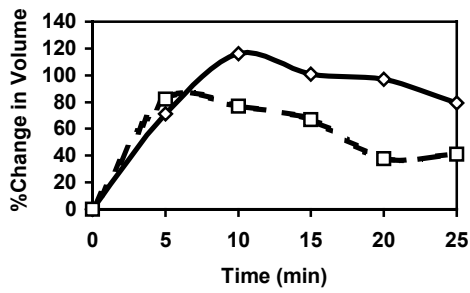
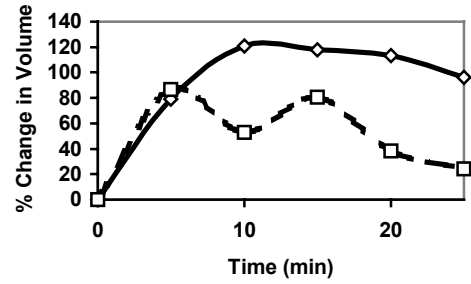


Figure 1. Macrostructures of Al-5 wt% TiO₂ in swaged condition. Ti containing phases, i.e. TiO₂ and foaming agent TiH₂ appear bright. (a) and (c) refer to longitudinal , (b) and (d) refer to transverse cross-section. Note cracking of TiH₂ in (c)



(a) 675°C



(b) 725°C

Figure 2. Foaming in Al containing either coarse (solid) or fine (dotted) TiH₂, see text for details. a) at 675 °C and b) at 725 °C

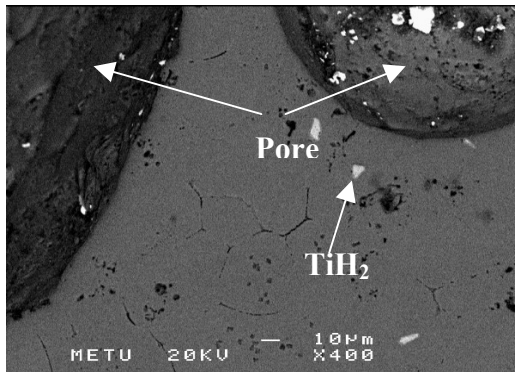


Figure 3. Structure of Al, foamed at 675 °C. Note Ti rich particles close and away from pores

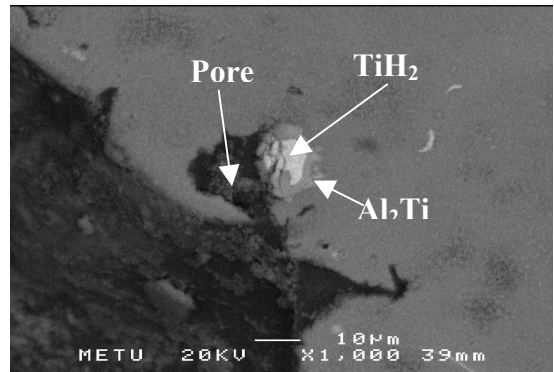
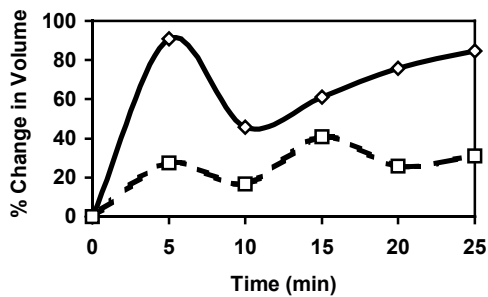
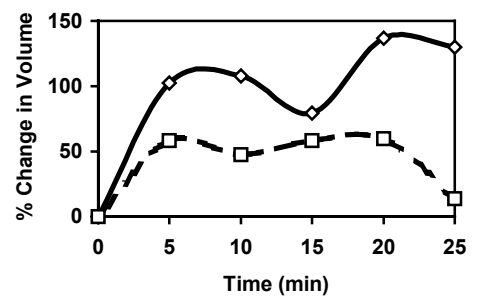


Figure 4. Structure of Al, foamed at 725 °C. Note Ti rich particle at a bay of a pore.



(a) 750°C



(b) 800°C

Figure 5. Foaming in Al - 5wt% TiO₂ containing either coarse (solid) or fine (dotted) TiH₂, see text for detail. a) at 750 °C and b) at 800 °C

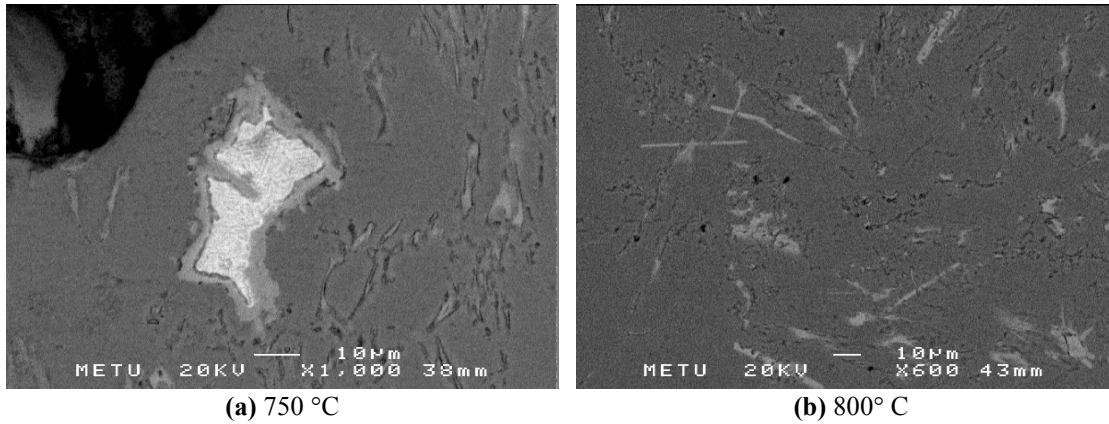


Figure 6. Structure in Al-5wt% TiO₂. a) 750 °C . Note gray(intermetallic) region enveloping bright Ti particle. b) 800 °C, note that all particles appear gray

Samples with TiO₂ addition required much higher temperatures for foaming. Thus, foaming experiments were carried out at 750 and 800°C. Results are reported in Figure 5. Unlike the case of pure Al reported above, the temperature of foaming produces a pronounced effect on the degree of foaming achieved.

Structural examination showed that there are pronounced internal reactions at these temperatures; particles of originally TiH₂ or TiO₂ compositions were partially or totally transformed into intermetallics of Al and Ti. An example of partial transformation is given in Figure 6 that refers to 750°C and that of complete transformation at 800°C in Figure 6(b).

In samples foamed at both 750 and 800°C, there is no clear evidence for the presence of TiO₂. This is also probably due to internal reaction between Al and TiO₂. It is well known that the two constituents react with each other starting from approximately 600°C giving rise to formation of TiO and Al₂O₃. According to Feng and Froyen [10] at temperatures above 700°C TiO further reacts with Al producing the same Al₃Ti. Thus TiO₂ added system is much more complex than that of pure aluminium. These complex internal reactions changes the solid content of the system and thus its viscosity in a manner that is dependent on temperature (as well as on time). This is probably the reason for the temperature dependant behavior of TiO₂ added systems in foaming

4.CONCLUSION

With the current investigation into foaming of Al with the use of TiH₂ the following can be concluded;

- 1- TiH₂ particles of less than a certain size do not seem to participate in the foaming process. The existence of such critical particle size require further investigation.
- 2- Especially at high temperatures, foaming agent and Al matrix react with each other giving rise to the formation of high melting point intermetallics. The formation of such intermetallics modifies the viscosity of the liquid and thus may affect the foaming process.
- 3- With respect to selection of additives, The possibility of internal reaction between the additive and the host, , should be taken into account which can lead to greater volume fraction of solid content and thus greater viscosity than that aimed for, as is the case with TiO₂ .

REFERENCES

- 1.J.Banhart , JOM, 52(12),(2000), pp.22-27
- 2.I.Duarte, J.Banhart, Acta Materialia ,48,(2000),pp.2349-2362

- 3.Song Z., Ma L.Wu Z., He D. Journal of Materials Science, 35 , (2000), pp.15-20
- 4.Th.Wübben, H.Stanzick, J.Banhart, S.Odenbach , J.Phys. C: Solid State Phys 2002
- 5.V.Gergely, B.Clyne, Advanced Engineering Materials, No: 4 , 2, (2000),pp.175-178
- 6.F.Baumgartner,I.Duarte, J.Banhart , Advanced Engineering Materials,2, No.4,(2000),pp168-174
- 7.J.Banhart, J.Baumeister , Journal of Materials Science , 33, (1998) ,pp.1431-1440
- 8.D.Lehmhus, J.Banhart , Materials Science Technology , Vol.18 , (2002)
- 9.T.Öztürk, J.Mirmesdagh, T.Ediz, Materials Science and Engineering A, vol.175, (1994),pp.125-129
- 10.C.F. Feng , L. Froyen , Composites: Part A , 31,(2000), pp.385-390

APPENDIX B

MILLING AND SEDIMENTAL SIEVING OF TiH₂ POWDERS

1. INTRODUCTION

TiH₂ is a material that is used in foaming of aluminium. TiH₂ with particle size close to 44 µm is commercially available. It is indicated in Cymat technical manual (2002) that foaming of aluminium by using this coarse powder results in aluminium foams with pores up to 25 mm. In order to obtain foams with fine pore, it is necessary to use fine TiH₂ powders. As it is stated by Mueller (1968), due to existence of hydrogen, TiH₂ suffer from brittle fracture upon mechanical milling. Milling of TiH₂ seems to be an efficient way to obtain fine TiH₂ powders. However, this concept was not investigated previously.

Shanefield (1996) states that sol-gel and slip preparation are widely used in ceramic technology to obtain end-use products. According to Zeng (2001), these techniques are also useful in order to obtain composite made out of ceramic powders. As it is pointed out by Reodeghiero (1998), homogeneity of the powder mixtures obtained in sol-gel and suspension preparation is the primary advantage of techniques. It is stated in the literature that fine powders and suitable liquid medium are necessary to obtain powder suspensions.

Suspension characteristic of TiH₂ powders was not investigated previously. On the other hand, suspension of TiO₂ powder, in liquid organic systems was widely studied (Zupancic et al., 1997; Murakata et al., 1998; Mizutani et al., 1994). These studies may be thought relevant to suspension of TiH₂ because it is possible that TiH₂ may be covered by an oxide layer. Water was not considered because it is known that TiH₂ decomposes if it contacts with water.

In this study, milling behavior of TiH₂ was investigated. It was aimed to obtain TiH₂ powders with particle size near to 1 µm. In order to mix aluminium and fine scale TiH₂ uniformly, suspension characteristics of TiH₂ was investigated. In addition, it is examined whether sedimentation is a suitable technique to separate coarse and fine TiH₂ powders.

2. MILLING OF TiH₂

TiH₂ powders with particle size less than 44 µm were used. 5 gram of as-received powder was attritor milled for 2, 4 or 8 hours at a rate of 500 rpm. Milling was carried out in 10 ml of 99.95 % pure ethanol. Ball-to powder ratio (B/P) of 24:1 was used in all milling operations.

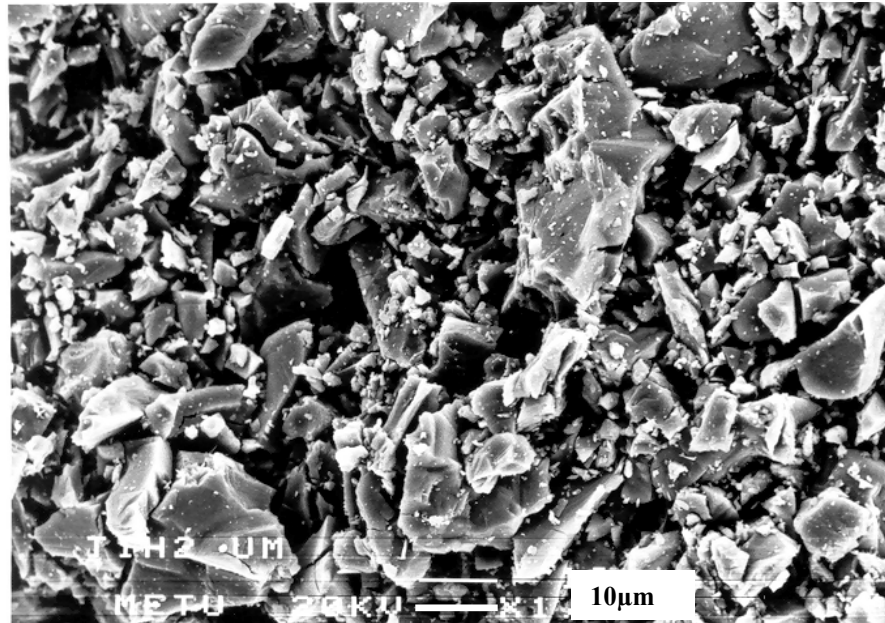
Effect of milling on TiH₂ particle size is given in Fig. 1. The structural refinement is clearly observed. As received powders contain particles in the order of 10 µm, Fig. 1(a). They also have particles in the order of 1 µm. On the other hand, in 4 hours milled TiH₂ powders, particle size is less than 5 µm, Fig. 1 (b). Thus it is concluded that attritor milling is quite a suitable method to refine TiH₂.

3. SUSPENSION OF TiH₂

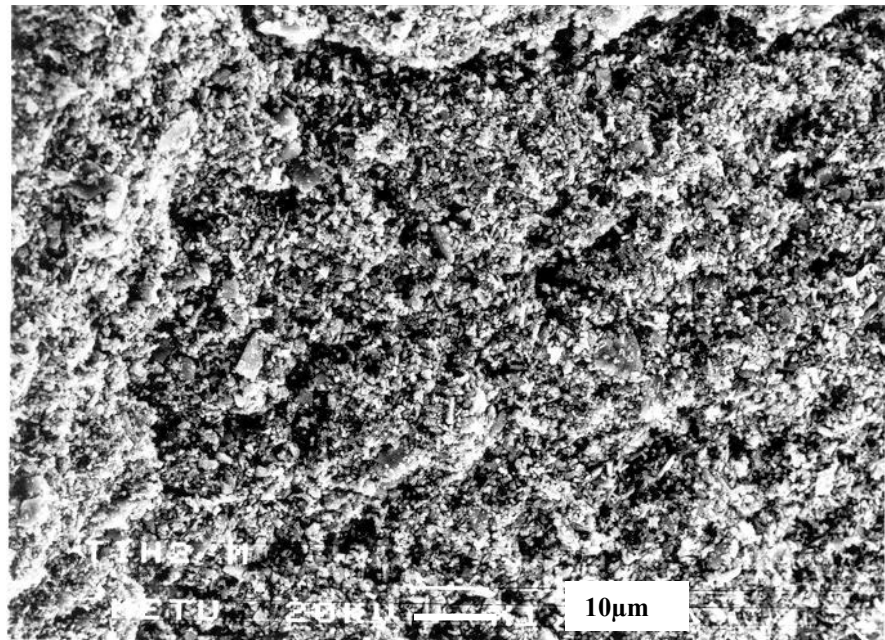
Sedimentation tests are carried out for milled TiH₂ powders. Powders were 8 hours milled. A medium of suspension Ethanol, MIBK (Methyl Isobutly Ketone), MIBK: Ethanol (3:1), MIBK:n-Butanol (3:1)

were used. The tests were carried out in a glass tube with a diameter of 1.43 cm and a length of 10 cm. For each test, 0.68 gram of powder was used. This corresponds to a height of 2 mm at the glass tube.

For sedimentation tests, 0.68 grams of dried powder were mixed with 10 ml of the liquid. This gives a total height of 65 mm at the glass tube. After 15 minute of vigorous hand mixing of the powder-solvent mixture, the glass tube was left at rest for various periods of time.



(a)



(b)

Figure 1. Effect of milling on TiH_2 particle size. (a) As received TiH_2 . Note that presence of fine as well as coarse (several tens of microns) particles. (b) TiH_2 after 4 hours of milling. Note that particles are less than $5 \mu\text{m}$.

While at rest, some fraction of powder sediments and two regions were observed: clarification zone and sediment zone. Clarification zone is a region in which there is no powder, but only liquid. Sediment zone is the rest of the column in which TiH_2 powders exist. Fig.2 shows a schematic representation of various zones observed during the test. At the end of the test, sediment height, i.e. the sum of suspended and sedimented heights, was measured. Sedimented height refers to a column height of 2 mm, i.e. dry height of powders.

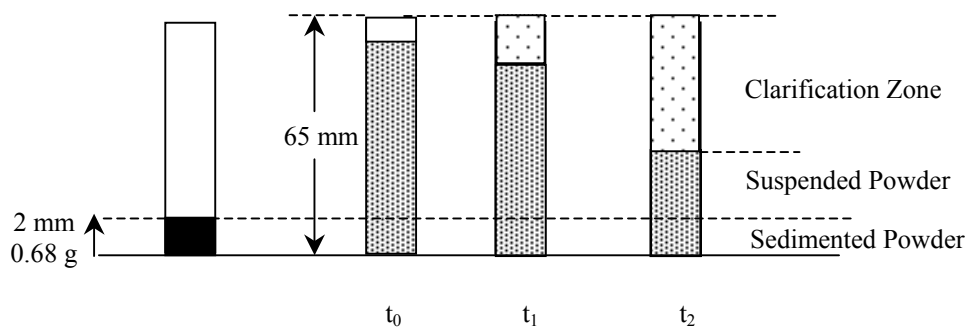


Figure 2. Sedimentation test. Note that t_0 represents the start of the test and $t_0 < t_1 < t_2$

The sedimentation tests indicate that for 8 hours milled TiH_2 powders, sedimentation rate is the lowest in MIBK: Ethanol (3:1) mixture, Fig. 3. In MIBK: Ethanol (3:1) mixture, sediment height is more than 40 mm after 5 hours whereas in other systems it drops to very low values (<10 mm) within 4 hours. MIBK-alcohol mixtures have a synergetic effect on suspension of TiH_2 . It is found that effect of ethanol is more pronounced than n-butanol.

Whether or not the experiments are repeatable a separate tests were carried out with suspended powders. Powders suspended in MIBK: Ethanol (3:1) were separated (suspended region see Fig. 2) and collected into a humidity free chamber. When 0.68 g of suspended powder was obtained, the sedimentation test was repeated in MIBK: Ethanol (3:1) mixture. It was found that these powders although suspended previously could not suspend in the solvent. Thus sedimentation tests are not easily reproducible.

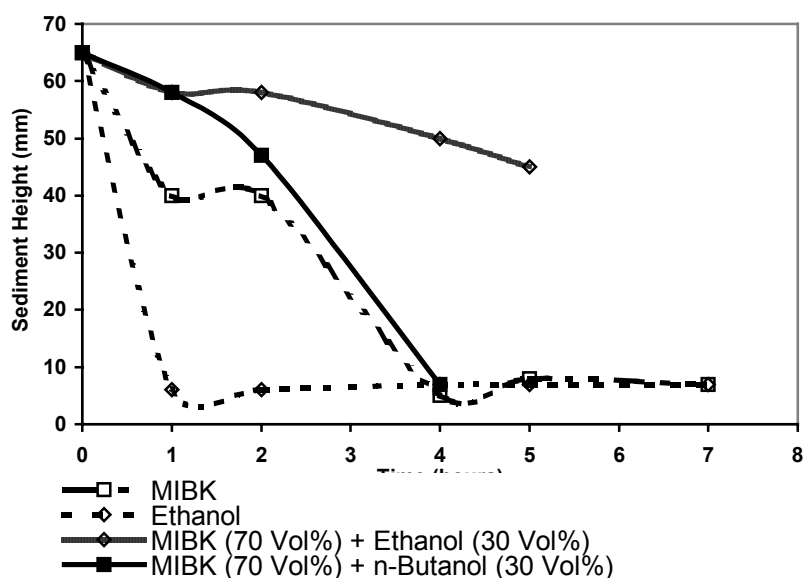


Figure 3. Sedimentation characteristics of 8 hours ethanol milled TiH_2 powder in different organic solvents. Sediment height is the sum of suspended and sedimented heights. Note that with MIBK: Ethanol (3:1) sedimentation rate is the lowest.

3.SEDIMENTAL SIEVING OF TiH₂

To examine if the sedimentation is a suitable technique to separate coarse and fine TiH₂ powders, as received, 2,4 and 8 hours milled TiH₂ powders were suspended into MIBK: Ethanol (3:1) mixture for 2 hours. Suspended and sedimented powders were removed from each other and dried at 100°C for further examinations.

Microstructures of suspended and sedimented powders are given in Fig. 4. It is seen that suspended powder are very fine (micron) as compared to sedimented fraction for as received powder, compare Fig. 4 (a) and (b). Thus, clear separation is achieved for as received powder. The case of milled powders were less successful, Fig. 4 (c) and (d). Although the suspended powder appear to be less in size the difference is not as clear as was the case with as received powders.

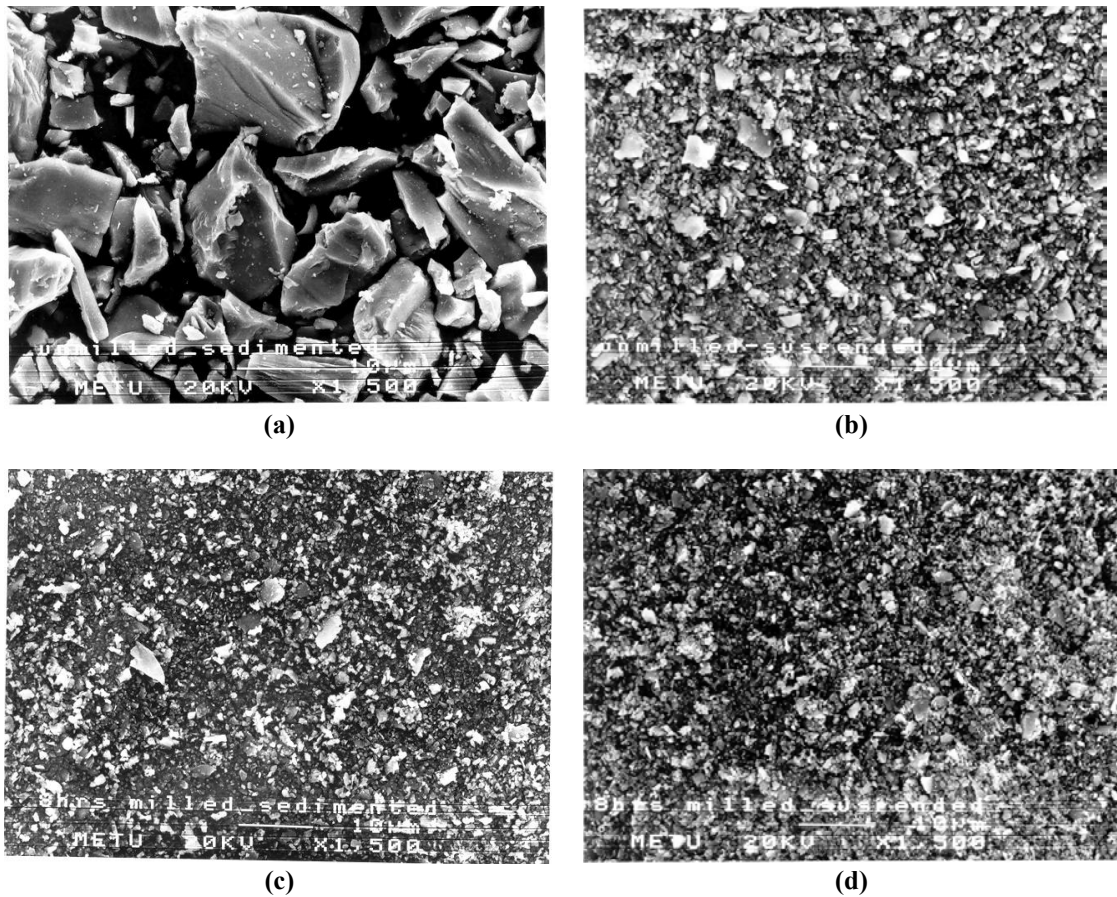


Figure 4. Comparison of the sedimented and suspended powders. (a) and (b) are sedimented and suspended powders of as-received TiH₂ respectively; (c) and (d) are sedimented and suspended powders of 8 hours milled TiH₂ respectively. Note that for as-received TiH₂ powders, there is a sharp difference between particle sizes of suspended and sedimented powders. Thus, suspension can be used to separate fine and coarse powders for as received powders. On the other hand, for 8 hours milled powders there is not a size difference between suspended and sedimented powders. Thus, the separation technique cannot be used for them.

REFERENCES

- Cymat Technical Manual for Stabilized Aluminium Foam, 2002
- Mizutani N., Ogihara T., Kondo M., Ikeda M., Shinozaki, Journal of Materials Science, 29, (1994), 366-372
- Mueller W.M., Blackledge J.P., Libowitz G.G., 1968, 'Metal Hydrides', (Academy Press Inc., London)
- Murakata T., Yamamoto R., Yoshida Y., Hinohara M., Ogata T., Sato S., Journal of Chemical Engineering of Japan, vol. 31, No.1, (1998), 21-28
- Rodeghiero E.D., Moore B.C., Wolkenberg B.S., Wuthenow M., Tse O.K., Giannelis E.P., Materials Science and Engineering A244 (1998), 11-21
- Shanefield D.J., 1996, Organic Additives & Ceramic Processing 2nd Edition, Kluwer Academic Publishers.
- Zeng Y., Jiang D., 2001, Ceramics International, , vol.27, pp. 597-602.
- Zupancic A., Lapasin R., Zumer M., Progress in Organic Coatings, 30 (1997) , 67-78

